

# Micius quantum experiments in space

Chao-Yang Lu<sup>1</sup>, Yuan Cao<sup>1</sup>, Cheng-Zhi Peng<sup>1</sup>, and Jian-Wei Pan<sup>1\*</sup>

*Hefei National Laboratory for Physical Sciences at Microscale and Department of Modern Physics, University of Science and Technology of China, Hefei, Anhui 230026, China*  
*and CAS Center for Excellence and Synergetic Innovation Center in Quantum Information and Quantum Physics, University of Science and Technology of China, Shanghai, 201315, China*

 (published 6 July 2022)

Quantum theory has been successfully validated in numerous laboratory experiments. But would such a theory, which effectively describes the behavior of microscopic physical systems and its predicted phenomena such as quantum entanglement, still be applicable on large length scales? From a practical perspective, how can quantum key distribution (where the security of establishing secret keys between distant parties is ensured by the laws of quantum mechanics) be made technologically useful on a global scale? Owing to photon loss in optical fibers and terrestrial free space, the achievable distance using direct transmission of single photons has been limited to a few hundred kilometers. A promising route to testing quantum physics over long distances and in the relativistic regimes, and thus realizing flexible global-scale quantum networks, is via the use of satellites and space-based technologies, where a significant advantage is that the photon loss and turbulence predominantly occurs in the lower  $\sim 10$  km of the atmosphere, and most of the photons' transmission path in space is virtually in vacuum, with almost zero absorption and decoherence. Progress in free-space quantum experiments, with a focus on the fast-developing Micius satellite-based quantum communications, is reviewed. The perspective of space-ground integrated quantum networks and fundamental quantum optics experiments in space conceivable with satellites are discussed.

DOI: [10.1103/RevModPhys.94.035001](https://doi.org/10.1103/RevModPhys.94.035001)

## CONTENTS

I. Introduction	1	IX. Satellite-Based Quantum Experiments with Micius	23
II. Small-Scale Quantum Communications	3	A. Satellite-to-ground quantum key distribution	24
A. First proof-of-concept demonstrations	3	B. Satellite-based entanglement distribution	26
B. Early efforts toward longer distances	6	C. Entanglement-based quantum key distribution	28
1. Quantum key distribution	6	D. Ground-to-satellite quantum teleportation	29
2. Entanglement distribution	7	E. Satellite-relayed intercontinental quantum key distribution	30
3. Quantum teleportation	8	F. Probing gravity-induced decoherence	30
III. Challenges in Practical and Large-Scale Applications	9	X. Other Quantum Satellite Projects	32
A. Security loopholes	9	XI. Outlook	34
B. Long distances	9	A. Daytime quantum communications	34
IV. Quantum Repeater and Its Progress	9	B. Satellite-constellation-based quantum networks	35
V. Satellite-Based Free-Space Channels	11	C. Fundamental test of quantum physics at space scale	36
A. Analysis of space-ground links	12	Acknowledgments	40
B. Feasible channel parameters for the low-Earth-orbit satellite	13	References	40
VI. Ground-Based Feasibility Studies and Key Technologies	15		
A. Overcoming the effective atmospheric thickness	15		
B. Feasibility of satellite-to-ground one- and two-downlink channels and ground-to-satellite uplink channel	15		
C. Testing with moving and vibrating objects	16		
D. Time synchronization	16		
E. Polarization maintenance and compensation	17		
F. Other parallel ground-based free-space experiments	18		
VII. Development and Testing of the Satellite Payloads	18		
A. Payload design	19		
B. Testing the payload under various conditions	20		
VIII. Construction of Cooperative Ground Stations	21		

## I. INTRODUCTION

Privacy and security concerns have been rooted in human nature since ancient times. They underpin human dignity and are among the most important human rights. With the exponential growth of the Internet and the use of *e-commerce*, it is critically important to establish a secure global network. Cryptography, the use of codes and ciphers to protect secrets, began thousands of years ago. Traditional public-key cryptography has usually relied on the perceived computational intractability of certain mathematical functions. However, history has shown that many advances in classical cryptography were subsequently defeated by advances in code cracking. Thus, it was even suggested that “human ingenuity

\*pan@ustc.edu.cn

cannot concoct a cipher which human ingenuity cannot resolve” (Poe, 1841).

It might come as a surprise that the fundamental principle of quantum mechanics was exploited to solve this long-standing problem of information security, which mathematicians have struggled with for centuries. The first approach along these lines was proposed in the 1970s by Stephen Wiesner, who designed quantum banknotes using quantum two-state systems and conjugate encoding that would be impossible to counterfeit. The principal drawback of Wiesner’s idea was that it would require quantum information in superposition states to be held captive and kept coherent for long periods of time, which appears to be beyond our technological capabilities even today, some 50 years later. Inspired by Wiesner’s idea, in the 1980s Charles Bennett and Gilles Brassard put forward a feasible protocol of quantum key distribution (QKD) known as BB84 (Bennett and Brassard, 1984). This protocol permits two distant communicating parties to produce a common, random string of secret bits called a secret key. This key can then be used alongside the one-time pad encryption, which, as strictly proven by Shannon in 1949 (Shannon, 1949), is an unconditionally secure method to encrypt and decrypt a message.

A notable surge of interest in the international scientific and industrial community has recently propelled quantum cryptography into mainstream computer science and physics. Particularly after the invention of Shor’s quantum factoring algorithm in 1994, an important goal of the field is to transform the idea of QKD into a practically useful technology. While significant progress has been made on small-scale demonstrations (Bennett *et al.*, 1992; Bouwmeester *et al.*, 1997), the real challenge is to increase the communication range to large distances, eventually on a global scale. Because of photon loss in the channel, the range of secure QKD via direct transmission of single photons is limited to a few hundred kilometers; see Secs. II and III. Unlike classical bits, the quantum signal of QKD cannot be noiselessly amplified due to the implications of the quantum noncloning theorem (Wootters and Zurek, 1982), where the security of QKD is rooted (Gisin *et al.*, 2002).

One potential solution to this notorious scalability problem is via the use of quantum repeaters (Briegel *et al.*, 1998). However, the current state of quantum memories (Yang *et al.*, 2016) and quantum repeaters remains far beyond practical application in realistic long-distance quantum communications; see Sec. IV.

A more promising solution for global-scale QKD is to utilize satellites, which can conveniently connect two distant locations on Earth. An important advantage of satellite-based free-space quantum communications is that the photon loss induced by atmospheric absorption and scattering predominantly occurs only in the lower  $\sim 10$  km of the atmosphere, with about a 3 dB loss on a clear day. Most of the photon transmission is across a near-vacuum environment, with almost no absorption and decoherence. The loss caused by beam diffraction is approximately proportional to the square of the distance. By contrast, the losses in fiber channels are predominantly due to the absorption and scattering of the fiber medium, which is proportional to the exponent of the distance. Thus, for long communicating distances (typically hundreds

to thousands of kilometers) the satellite-to-ground free-space channels will have advantages over fiber-based channels in terms of channel losses; for more details, see Sec. V.

In addition to QKD, the use of quantum communication in space would be beneficial for the testing of fundamental principles of quantum physics on a large scale. The confirmation of the laws of physics is restricted by the boundaries of our experimental observations. For instance, quantum mechanics predicts that it is possible to observe quantum entanglement over any distance; however, it is necessary to confirm such a prediction and verify whether unexpected effects (such as the influence of gravitational fields) place some bounds on such distances (Pirandola *et al.*, 2019). New satellite-based laboratories in space would create vast platforms for fundamental experiments in quantum optics at distances that were previously inaccessible on the ground, such as long-range Bell tests (Bell, 1964) on human free will (Hall, 2010; BIG Bell Test Collaboration, 2018; Cao *et al.*, 2018) and the probing of the interaction of quantum mechanics with general relativity (Rideout *et al.*, 2012).

Owing to the low-gravity and ultrastable conditions in space, many experiments related to quantum physics that cannot be undertaken on the ground can be achieved in space. High-precision measurements on quantum systems, especially those involving matter waves, in the presence of a gravitational field could challenge our understanding of general relativity and quantum mechanics. Researchers from Germany, France, and the United States created Bose-Einstein condensate in space and conducted 110 experiments central to matter-wave interferometry as part of the sounding-rocket mission MAIUS-1 in 2017 (Becker *et al.*, 2018).

Exploiting the persistent free fall condition of a low Earth orbit, cold atom systems can take advantage of microgravity, which is high on the to-do list in next-generation experiments. The Cold Atom Lab was designed to provide the first ultracold quantum gas experiment aboard the International Space Station (ISS) utilizing an apparatus developed, assembled, and qualified by NASA’s Jet Propulsion Laboratory (JPL); this facility was successfully launched on May 21, 2018 (Ethan *et al.*, 2018), and has been installed on the ISS. Recently a proposal for the mission Space Atomic Gravity Explorer (SAGE) was presented to the European Space Agency. It has the scientific objective of investigating gravitational waves, dark matter, and other fundamental aspects of gravity while also investigating the connection between gravitational physics and quantum physics using new quantum sensors, namely, optical atomic clocks and atom interferometers based on ultracold strontium atoms (Tino *et al.*, 2019). The successful operation of the Laser Interferometer Space Antenna (LISA) Pathfinder (Armano *et al.*, 2016) has paved the way for the space optical LISA, which will observe gravitational waves at low frequencies, with a peak sensitivity in the range 1–10 mHz. In the SAGE proposal, the use of atomic sensors may allow for the observation of gravitational waves in the low frequency range ( $10^{-3}$  – 10 Hz). This proposal will complement LISA as an alternative technology and, more importantly, it will provide a measurement method in the range between those of LISA and the terrestrial detectors (Kolkowitz *et al.*, 2016).

Using satellite-based free-space channels can be regarded as extending the space scale of quantum experiments from

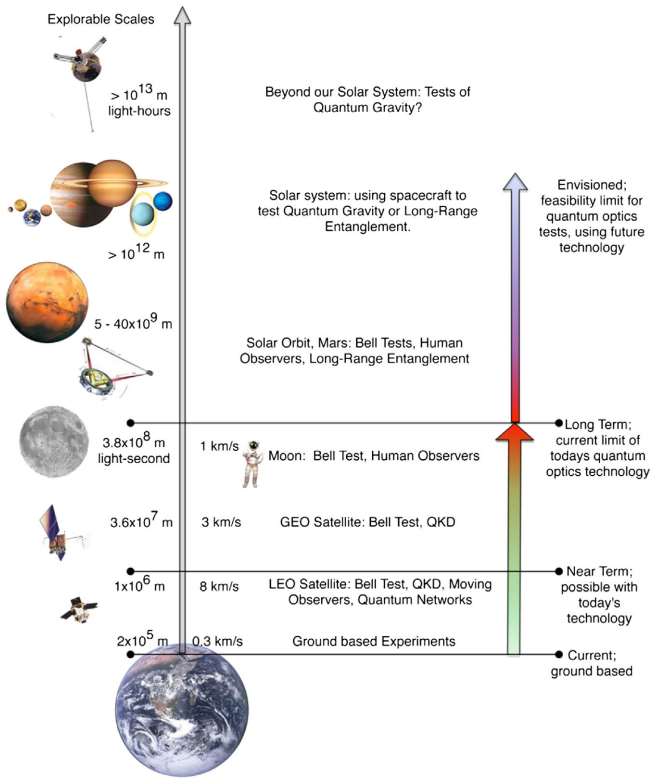


FIG. 1. Overview of the distance scales and the corresponding conceived quantum experiments. From Rideout *et al.*, 2012.

several meters to the magnitude of thousands of kilometers or more, as shown in Fig. 1 (Rideout *et al.*, 2012), which will allow us to explore the nature of the quantum world at increasingly large length scales. It is of great interest to carry out quantum experiments on such a large space scale in terms of fundamental scientific interest as well as practical applications.

The focus of this review is on the developments in satellite-based quantum communications and fundamental tests of quantum physics using the Micius satellite. This review begins by introducing early ideas (Rarity *et al.*, 2002; Hwang, 2003) and preliminary tests (Buttler, Hughes, Kwiat, Luther *et al.*, 1998; Kurtsiefer *et al.*, 2002; Aspelmeyer *et al.*, 2003). To envision a practically working low-Earth-orbit satellite with a feasible budget, serious numerical analysis and engineering considerations are put forward and summarized in Secs. III and V. Step-by-step ground-based feasibility studies (Peng *et al.*, 2005; Ursin *et al.*, 2007; Villoresi *et al.*, 2008; Jin *et al.*, 2010; Ma *et al.*, 2012; Yin *et al.*, 2012, 2013; Cao *et al.*, 2013; Nauerth *et al.*, 2013; Wang *et al.*, 2013) and developments of the key technologies required are reviewed in Sec. VI. For example, entanglement distribution over a terrestrial free-space channel with a length of 13 km was demonstrated by Peng *et al.* (2005), who proved that the entanglement can extend over distances greater than the effective atmospheric thickness. A bidirectional distribution of entangled photons (Yin *et al.*, 2012) was later performed over a distance of 102 km with an  $\sim 80$  dB effective channel loss, which was comparable to that of a two-downlink channel from a satellite to the ground. Finally, the full verification, in conditions of

rapid motion and random movement of satellites, attitude change, vibration, and a high-loss regime, addressing a wide range of parameters relevant to low-Earth-orbit satellites, has been carried out (Wang *et al.*, 2013). During these feasibility studies, the necessary toolbox for satellite-based long-distance quantum communications was gradually developed, including robust and compact quantum light sources, narrow beam divergence, time synchronization, and rapid acquiring, pointing, and tracking (APT) technologies, which are the key to the optimization of the link efficiency and to overcoming the atmospheric turbulence. This body of work was sufficient groundwork to permit the funding of the Micius satellite project for quantum experiments in the framework of the Chinese Academy of Sciences Strategic Priority Program.

The satellite, which is dedicated to quantum science experiments, named after the fourth century BCE Chinese philosopher Micius, was launched in China in August 2016. Within a year of the launch, the following three key milestones for a global-scale quantum communication network were achieved: (1) a satellite-to-ground decoy-state QKD with a kilohertz rate over a distance of up to 1200 km (Liao *et al.*, 2017a) and a satellite-replayed intercontinental key exchange (Liao *et al.*, 2018), (2) a satellite-based entanglement distribution to two locations on Earth separated by 1205 km and the subsequent Bell test (Yin *et al.*, 2017a), and (3) ground-to-satellite quantum teleportation (Ren *et al.*, 2017). These experiments established the possibility of effective link efficiencies through a satellite of 12–20 orders of magnitudes greater than direct transmission through optical fibers over a distance of  $\sim 1200$  km. A comprehensive survey and an analysis of these works are presented in Secs. VII–IX.

Meanwhile, with the success of the Micius satellite an international race related to quantum communication experiments in space is predicted to start. Many satellite projects designed for quantum communications have been approved and funded, such as the Quantum Encryption and Science Satellite (QEYSSat) project in Canada (Jennewein *et al.*, 2014), and the CubeSat Quantum Communications Mission (CQuCoM) undertaking by a joint research team (Oi *et al.*, 2017). Meanwhile, further studies of quantum physics in space, including matter waves in the presence of a gravitational field, are also being implemented or are in the planning stages; more details can be found in Sec. X.

This review ends with an outlook on the future work that needs to be done to eventually build a global-scale practical quantum network. Outstanding challenges include enabling daytime operation of QKD (Liao *et al.*, 2017c), increasing time and area coverage through the use of higher-orbit satellites, and constructing satellite constellations; these challenges are being considered and addressed by the ongoing research efforts in this emerging field.

## II. SMALL-SCALE QUANTUM COMMUNICATIONS

### A. First proof-of-concept demonstrations

Quantum superposition is one of the fundamental principles of quantum mechanics; this property distinguishes a quantum state from a classical one. In a classical two-value system, for example, a coin, we find it in either one of its two possible

states, that is, either heads or tails. In its quantum counterpart, however, a two-state quantum system can be found in any superposition of the two possible basis states, such as  $|\Psi\rangle = (1/\sqrt{2})(|0\rangle + |1\rangle)$ , where the two orthogonal basis states are denoted by  $|0\rangle$  and  $|1\rangle$ . In the classical world, two coins can be found in one of the states heads:heads, heads:tails, tails:heads, or tails:tails, and we can identify these four possibilities with the four quantum states  $|0\rangle_1|0\rangle_2$ ,  $|0\rangle_1|1\rangle_2$ ,  $|1\rangle_1|0\rangle_2$ , and  $|1\rangle_1|1\rangle_2$ , which describe the two-state quantum systems.

The superposition principle also applies to more than one quantum system; the two quantum particles are no longer restricted to the four previously mentioned “classical” basis states, but they can be found in any superposition, for instance, in the following four entangled states:

$$|\Psi^\pm\rangle = \frac{1}{\sqrt{2}}(|0\rangle_1|1\rangle_2 \pm |1\rangle_1|0\rangle_2), \quad (1)$$

$$|\Phi^\pm\rangle = \frac{1}{\sqrt{2}}(|0\rangle_1|0\rangle_2 \pm |1\rangle_1|1\rangle_2). \quad (2)$$

These entangled states are referred to as Bell states since they maximally violate a Bell inequality (Bell, 1964; Clauser *et al.*, 1969), showing a stark contradiction between classical local hidden variable theory and quantum mechanics (Brunner *et al.*, 2014). Quantum entanglement describes a physical phenomenon whereby the quantum states of a many-particle system cannot be factorized into a product of single-particle wave functions; this applies even when these particles are separated by a large distance. It was first recognized by Einstein, Podolsky, and Rosen (1935) and Schrödinger (1935) and experimentally generated by Wu and Shakhov (1950) in the annihilation radiation; it was then applied to the Bell test (Freedman and Clauser, 1972; Aspect, Grangier, and Roger, 1982).

Note that both single-particle and entangled-two-particle states can be applied to QKD. Single-particle states represent the prepare-and-measure scheme, such as BB84 (Bennett and Brassard, 1984), in which Alice sends each quantum bit (qubit) in one of four states of two complementary bases: B92 (Bennett, 1992), where Alice sends each qubit to one of two nonorthogonal states; the six-state protocol (Bruß, 1998), in which Alice sends each qubit to one of six states of three complementary bases. A description of the BB84 protocol is given in Fig. 2(a). The security of QKD is ensured by the no-cloning theorem (Wootters and Zurek, 1982), which prohibits the precise copying of an unknown quantum state. The no-cloning theorem prevents the eavesdropper from copying Alice’s qubits; information gain is possible only at the expense of introducing disturbance to the signal in any attempt to distinguish between the two nonorthogonal quantum states. Entanglement-based QKD, including schemes such as Ekert91 (Ekert, 1991), in which entangled pairs of qubits are distributed to Alice and Bob, who then extract key bits by measuring their qubits, as shown in Fig. 2(b); BBM92 (Bennett, Brassard, and Mermin, 1992), where each party measures half of the Einstein-Podolsky-Rosen (EPR) pair in one of two complementary bases. Note

that in Ekert91 Alice and Bob estimate Eve’s information based on Bell’s inequality test, whereas in BBM92, as in the case of BB84, Alice and Bob make use of the privacy amplification to eliminate Eve’s information regarding the final key (Lo and Chau, 1999).

After proposing the BB84 protocol, Charles Bennett and his colleagues performed the first proof-of-concept test in 1989 (Bennett *et al.*, 1992). A light emitting diode (LED) and photomultipliers fixed at two ends of the table represent the sender Alice and receiver Bob, i.e., the photon source and detectors, respectively; see Fig. 3. Pumped by current pulses, the LED emitted green light pulses, which were subsequently filtered using a  $550 \pm 20$  nm bandpass filter and initialized in a horizontal polarization state. For the encoding, the polarization of each light pulse was rotated to a horizontal, vertical, left-circular, or right-circular polarized state, randomly and independently, via the use of two Pockels cells to which modulated voltages were applied. A circular basis was exploited instead of a diagonal basis, so a lower voltage (quarter-wave voltage) was required to operate the Pockels cells. After transmission through a 32-cm-long free-space quantum channel from Alice to Bob, each encoded pulse was then projected in either a rectilinear or circular basis randomly and independently, using another Pockels cell and a calcite Wollaston prism, depending on whether the applied quarter-wave voltage was turned on or off. The calcite Wollaston prism was made of birefringent crystals, through which horizontally and vertically polarized light diverged onto two distinct paths and could then be detected by one of two photomultipliers, one placed in each path.

In principle, a bit of the key was successfully distributed when Alice encoded the bit and Bob measured it in the same basis. Nevertheless, owing to experimental imperfections such as dark counts and differences in the basis alignment between Alice and Bob, errors could still exist after the basis announcement. Therefore, reconciliation, such as a permutation and parity check, was performed on Alice’s and Bob’s bit sequence in order to discover and discard errors. According to the error rate, in the conservative sense in that all errors were induced by Eve, who might intercept and resend, or beam split, photons in the quantum channel, the number of bits of information leaked to Eve can be estimated. Using privacy amplification, shared consistent bits were compression encoded. Although fewer bits of the shared secret key were left, the amount of information potentially leaked to Eve decreased by several orders of magnitude. As an example of data from their experiment, Alice sent Bob 715 000 pulses with the mean photon number of each pulse set to 0.12. Finally, 754 bits of the secret key was shared between Alice and Bob. The experiment was preliminary as noted by Brassard (2012), who recalled that they “could literally hear the photons as they flew, and zeroes and ones made different noises.”

While the QKD is for the secure transmission of a classical message, another important aspect of quantum communications is quantum teleportation (Bennett *et al.*, 1993), which is a way to faithfully transfer quantum states. Quantum teleportation relies on both a classical channel and a quantum channel (entanglement) that are shared between the two

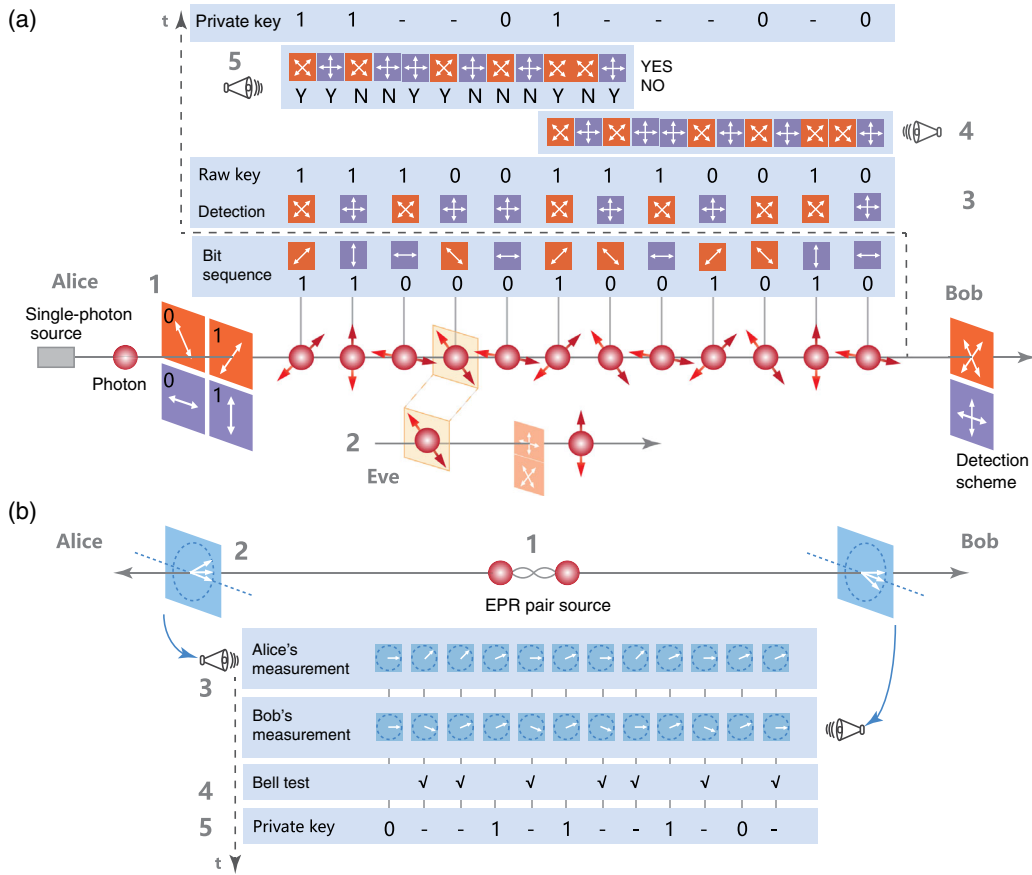


FIG. 2. Quantum cryptographic protocols. (a) BB84 protocol. The aim of this protocol is for the sender (Alice) to send a secret key to the receiver (Bob) by transferring single photons, encoding the information in the quantum states. This protocol exploits four polarization states of photons that span two bases (such as the horizontal polarization  $|H\rangle$ , the vertical polarization  $|V\rangle$ , the diagonal polarization  $|45^\circ\rangle$ , and the antidiagonal polarization  $|-45^\circ\rangle$ ). In information encoding, they use  $|H\rangle$  and  $|-45^\circ\rangle$  to represent bit 0, and  $|V\rangle$  and  $|45^\circ\rangle$  to represent bit 1. The operation steps are as follows. (1) Alice chooses a group of bits sequence and encodes these bits in the polarization of photons with a random choice of encoding basis. (2) Alice sends the photons to Bob. (3) Bob randomly chooses the detection scheme to measure the state and obtains the raw key. (4) Bob broadcasts his choice of measurement basis for each photon through a classical information channel. (5) Alice responds yes or no for the same or a different basis that they use for encoding and measurement for each photon. (6) They discard the events in which different bases were used and keep the remaining data for private key [any eavesdropping in step (2) could be detected in this final check]. (b) Ekert91 protocol. This protocol operates by sharing secret keys between Alice and Bob by distributing EPR pairs. (1) Alice and Bob first share an entangled photon pair in the singlet state  $|\Psi^-\rangle$ . (2) Alice and Bob receive the photon then randomly and independently choose their measurement bases, obtained by rotating the  $\{|H\rangle, |V\rangle\}$  basis with the angle from the set  $\{0, \pi/4, \pi/8\}$  for Alice and  $\{0, -\pi/8, \pi/8\}$  for Bob. (3) They measure and register a series of photon pairs. After that, they broadcast the measurement bases they have used while keeping the outcomes secret. (4) They use the measurement outcomes with the same angles as raw keys and use the others for the Bell inequality test. (5) If the Bell inequality is violated, the eavesdropping is excluded; therefore, the keys are safe (their keys are antialigned). Otherwise, they discard all the keys.

communication parties; see Fig. 4(a). The quantum state to be teleported can be the polarization of a single photon, which can be written as  $|\chi\rangle_1 = \alpha|H\rangle_1 + \beta|V\rangle_1$ , where  $\alpha$  and  $\beta$  are two unknown complex numbers satisfying  $|\alpha|^2 + |\beta|^2 = 1$  and  $|H\rangle$  and  $|V\rangle$  denote the horizontal and vertical polarization states, respectively, which can be used to encode the basic logic 0 and 1 for a qubit. The entangled state of a pair of photons can be written as  $|\phi^-\rangle_{23} = (|H\rangle_2|H\rangle_3 - |V\rangle_2|V\rangle_3)/\sqrt{2}$ , one of the four maximally entangled two-qubit Bell states. Alice performs a joint measurement on the to be teleported photons 1 and 2 from the entangled pair, projecting them into one of the four Bell states. The joint three-photon system is then in the following product state:

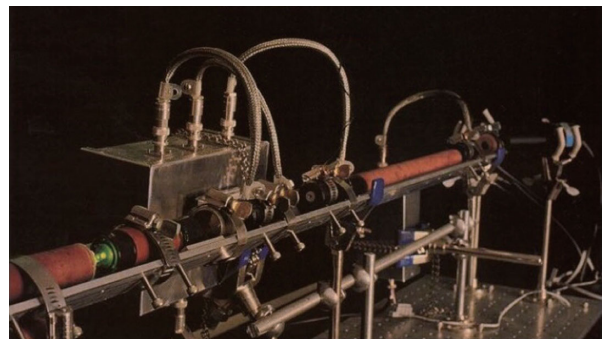


FIG. 3. Photograph of the apparatus used by Bennett *et al.* (1992).

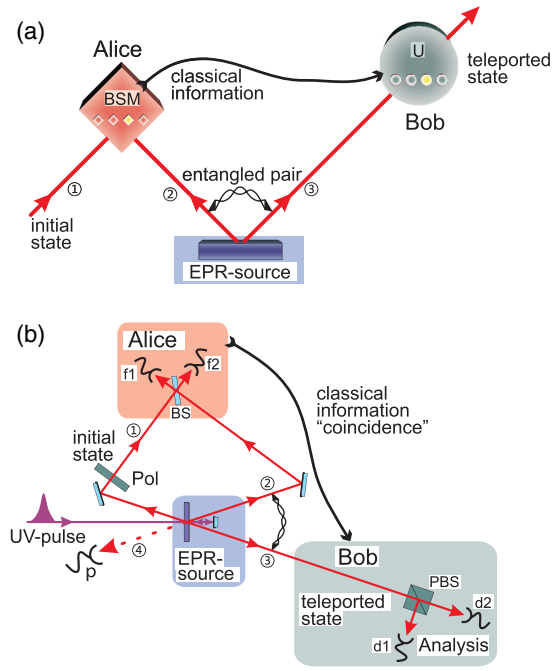


FIG. 4. (a) Principle of quantum teleportation. (b) Setup of the Innsbruck teleportation experiment (Bouwmeester *et al.*, 1997). A pulse of ultraviolet light passing through a nonlinear crystal creates an ancillary pair of entangled photons 2 and 3 in a polarization state  $|\psi^-\rangle_{12}$ . The pulse is reflected, and during its second passage through the crystal another pair of photons can be created.

$$|\psi\rangle_{123} = |\chi\rangle_1 \otimes |\phi^-\rangle_{23}, \quad (3)$$

which can be decomposed into

$$\begin{aligned} |\psi\rangle_{123} = & \frac{1}{2}[-|\psi^-\rangle_{12}(\alpha|H\rangle_3 + \beta|V\rangle_3) - |\psi^+\rangle_{12}(\alpha|H\rangle_3 \\ & - \beta|V\rangle_3) + |\phi^-\rangle_{12}(\alpha|V\rangle_3 + \beta|H\rangle_3) \\ & + |\phi^+\rangle_{12}(\alpha|V\rangle_3 - \beta|H\rangle_3)]. \end{aligned} \quad (4)$$

Bob is then informed about the outcome of the Bell-state measurement (BSM) via classical communication, and accordingly applies a Pauli correction to photon 3. Note that quantum teleportation does not violate the no-cloning theorem. After successful teleportation, photon 1 is no longer available in its original state, and therefore photon 3 is not a clone but instead the result of teleportation. Furthermore, the quantum state can only be recovered after Bob receives the classical information sent by Alice. According to relativity, the speed of the transmission of the classical information cannot exceed the speed of light. Thus, superluminal communication cannot occur as a result of quantum teleportation.

The first demonstration of quantum teleportation was reported by Bouwmeester *et al.* (1997) using the setup shown in Fig. 4(b). They developed a method for coherently controlling two independent pairs of down-converted entangled photons. Double passing the  $\beta$ -barium borate (BBO) crystal, the pulsed pump created two pairs of entangled photons. One pair (2, 3) was used as the entanglement channel, whereas photon 1 is prepared in the to be teleported state. The BSM of

photons 1 and 2 was achieved using a beam splitter, which, upon a coincidence detection of a single photon in each output of the beam splitter, unambiguously projected the two independent photons into the spatially asymmetric Bell state  $|\psi^-\rangle_{12} = (|H\rangle_1|V\rangle_2 - |V\rangle_1|H\rangle_2)/\sqrt{2}$ . An essential prerequisite to this method is to make the independently generated single photons 1 and 2 indistinguishable in their temporal, spatial, and spectral degrees of freedom. To do so, the two pairs of entangled photons, pumped by a femtosecond laser, were time synchronized, spectrally narrow band filtered, and coupled into single-mode fibers to ensure a sufficient wave-function overlap. The verification of the success of teleportation was then done using a four-photon coincidence detection. Owing to its capacity to faithfully transfer quantum states from one particle to another at a distance, quantum teleportation has been recognized as an important and elegant tool for long-distance quantum communication and distributed quantum networks.

## B. Early efforts toward longer distances

After the first proof-of-principle demonstrations, early efforts were made to extend the implementations to longer distances, with the aim of transforming the schemes into practical applications.

### 1. Quantum key distribution

Optical fibers are convenient, commercially available, and widely used in telecommunications, which is a straightforward way to extend the experimental range beyond that achieved in the initial tabletop free-space 32-cm-distance experiment. Experimental groups from the British Telecom laboratories in the United Kingdom (Townsend, Rarity, and Tapster, 1993a, 1993b; Townsend, 1994) used phase encoding to demonstrate quantum cryptography over a 10-km-long optical fiber, which was later extended to 30 km with raw-key rate of 260 bits/s and an error rate of 4% (Marand and Townsend, 1995); see Fig. 5. Later a Swiss group exploited polarization encoding to test quantum cryptography over 1.1 km optical fiber (Muller, Breguet, and Gisin, 1993). Methods were developed to overcome the time-dependent polarization changes during the transmission of photons in optical fibers (Franson and Ives, 1994).

The research efforts continued toward field tests using installed optical fibers in real-world environments. The first step in this direction was taken by researchers at Los Alamos National Laboratory, who used the minimal Bennett protocol (Bennett, 1992) to perform quantum key distribution over 14-km-long underground optical fiber (Hughes *et al.*, 1996) with an error rate of 1.2%; the same group later increased this distances to 48 km (Hughes, Morgan, and Glen Peterson, 2000) with an error rate of 9%. The Swiss group (Muller, Zbinden, and Gisin, 1996) exploited a 23-km-long standard telecommunication (telecom) optical fiber installed under a lake and demonstrated a quantum cryptography with an error rate of 3.4%. Note that there were serious practical security loopholes associated with these early QKD experiments, as discussed in Sec. III. For example, the photon-number-splitting (PNS) attack (Brassard *et al.*, 2000;

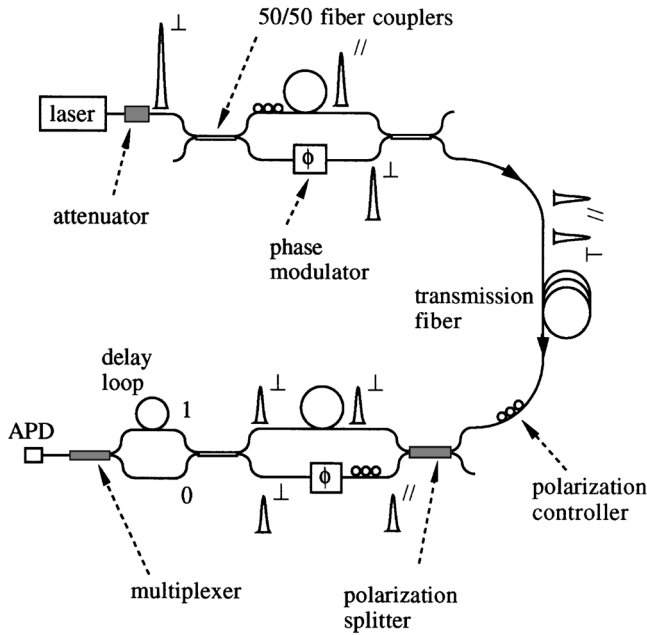


FIG. 5. Phase-encoding quantum cryptography scheme over 30 km fiber. The experimental system is based on a Mach-Zehnder interferometer. The source is a 1.3- $\mu\text{m}$ -wavelength semiconductor laser with a pulse duration of 80 ps and repetition rate of 1 MHz. The laser output is strongly attenuated such that the average photon number of the pulse pairs entering the transmission fiber is  $\sim 0.1$ . The received photons are detected by a liquid-nitrogen-cooled germanium avalanche photodiode. From Marand and Townsend, 1995.

Lütkenhaus, 2000) was proposed to target imperfect single-photon sources. Thus, these early implementations of QKD could not be used for real-life applications with realistic devices.

Jacobs and Franson (1996) considered another propagation medium, free space, which has the advantage of negligible birefringence, thus permitting the faithful transmission of the photon polarization states. The first attempt was over a 150 m hallway illuminated with fluorescent light, and over 75 m outdoors in bright daylight conditions (Jacobs and Franson, 1996). In addition, under fluorescent lighting conditions, Buttler, Hughes, Kwiat, Lamoreaux *et al.* (1998) performed the experiment over a 205 m indoor optical path, which was achieved by sending the emitted beam up and down a 17.1-m-long laboratory hallway six times via the use of ten mirrors and a corner cube. These preliminary tests suggested that the signal-to-noise ratio in free-space transmissions could be improved using a combination of detection timing, narrow band filters, and spatial filtering. Further experiments extended the work to outdoor environments with point-to-point free-space transmission of attenuated laser pulses over distances of 0.5 km (Hughes *et al.*, 2000), 1.6 km (Buttler *et al.*, 2000), 10 km (Hughes *et al.*, 2002) (see Fig. 6), and 23.4 km (Kurtsiefer *et al.*, 2002).

The straightforward method of directly sending signals (photons) through optical fibers or terrestrial free space suffers from two fundamental problems. First, channel losses cause a decrease in the transmitted photons that scales exponentially

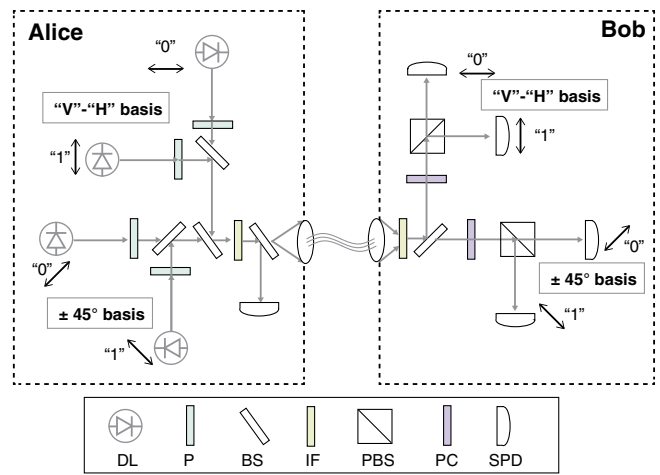


FIG. 6. Polarization optics of the QKD transmitter and receiver. The lasers in the transmitter are attenuated to have an average photon number less than 1. Multidetection events due to the multiphoton component of the weak coherent pulse are recorded but not used for key generation. From Hughes *et al.*, 2002.

down with the length; see Sec. III.B. Second, there are additional problems associated with the security of these practical implementations due to the imperfect single-photon source and detectors; see Sec. III.A.

## 2. Entanglement distribution

The previously described experiments used attenuated laser pulses to approximate the single photons. Such laser pulses have a nonvanishing probability of containing two or more photons per pulse, leaving the system susceptible to a PNS attack; see Xu *et al.* (2020) for details. Ekert (1991) proposed entanglement-based quantum cryptography using Bell's inequality to establish security, which results in an inherent source-independent security. In addition to its use in quantum cryptography, distributed entanglement is an essential resource in fundamental studies, such as tests of Bell's inequality (Bell, 1964) as well as in many quantum information tasks, such as quantum teleportation (Bennett *et al.*, 1993), distributed quantum networks for computing (Gottesman and Chuang, 1999), and metrology (Togan *et al.*, 2011).

Producing and distributing entangled photons over long distances is of great importance both for fundamental understanding and for possible applications; see Fig. 7. In 2000, three independent groups simultaneously reported implementation of the Ekert91 protocol, with two using polarization encoding (Jennewein *et al.*, 2000; Naik *et al.*, 2000) and one using time encoding (Tittel *et al.*, 2000).

The arrangement of the experiment (Jennewein *et al.*, 2000) is shown in Fig. 7. The entangled photons were produced by type-II spontaneous parametric down-conversion (Kwiat *et al.*, 1995). As shown in Fig. 7(a), pumped by a 351 nm laser, a BBO crystal produced entangled photons at a wavelength of 702 nm with a two-photon coincidence rate of  $\sim 1700$  Hz. The photons were coupled into 500-m-long optical fiber and transmitted to Alice and Bob, respectively, who were physically separated by 360 m [Fig. 7(b)]. Jennewein *et al.* (2000) utilized Wigner's inequality to establish the security of the

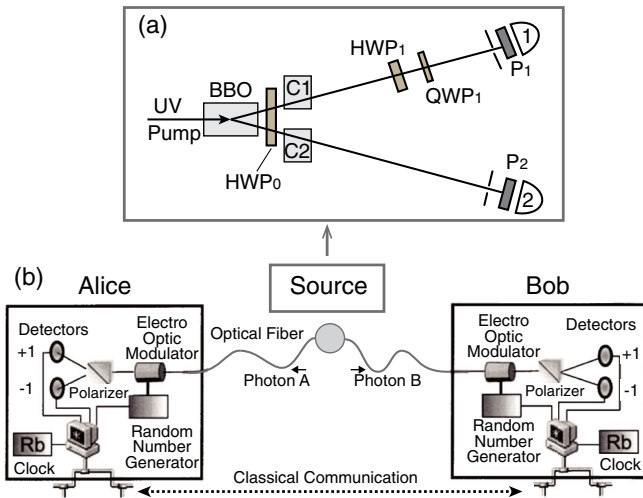


FIG. 7. (a) Experimental configuration to produce entangled photon pairs using spontaneous parametric down-conversion (Kwiat *et al.*, 1995). Type-II noncollinear phase matching in  $\beta$ -barium borate (BBO) produces high-fidelity polarization entanglement. The extra birefringent crystals C1 and C2 along with the half-wave plate (HWP) are used to compensate the birefringent walk-off effect in the crystal. (b) First full implementation of entanglement-based quantum cryptography over a distance of 360 m. The polarization-entangled photon pairs are transmitted via optical fibers that are then analyzed and detected.

quantum channel, which has a higher efficiency than the original Ekert protocol. The two communication parties varied their analyzers randomly between two settings: Alice used  $-30^\circ$ ,  $0^\circ$  and Bob used  $0^\circ$ ,  $30^\circ$ . The two-photon coincidence counts of the combinations of the settings of  $(-30^\circ, 30^\circ)$ ,  $(-30^\circ, 0^\circ)$ , and  $(0^\circ, 30^\circ)$  were used to derive a violation of Wigner's inequality, thus ensuring the security of the key distribution. The coincidence detection obtained at the parallel settings  $(-30^\circ, 0^\circ)$ , which occurred in a quarter of all events, were used to generate keys. Over a fiber distance of 500 m, the raw-key rate was 420 bits/s and the quantum bit error rate was 3.4%.

The entanglement-based quantum cryptography was later extended to a distance of 8.5 km using an optical fiber inside a laboratory by Ribordy *et al.* (2000). They utilized a time-bin encoding and, at a wavelength of 1550 nm, the experiment generated a raw-key rate of 134 Hz with an error rate of 8.6%. Poppe *et al.* (2004) demonstrated a successful run of the entanglement-based quantum cryptography system where the produced key was directly handed over to an application that was used to send a quantum secured on-line wire transfer from the city hall to the headquarters of Bank-Austria Creditanstalt over a physical distance of 650 m, showing a real-world application scenario outside of ideal laboratory conditions.

In 2003, entanglement distribution outside the laboratory over free space was performed in Vienna over a physical separation of 600 m (Aspelmeyer *et al.*, 2003). One of the entangled photons was distributed over 150 m and the other one over 500 m, to different sides of the Danube River. The 600 m free-space link attenuation was estimated to be 12 dB. The two-photon count rate was measured to be 10 kHz locally

and 15 Hz after the free-space distribution. Nevertheless, the two surviving photons showed a state fidelity of  $0.87 \pm 0.03$  and a violation of Bell's inequality.

### 3. Quantum teleportation

The first demonstration of quantum teleportation of quantum states (Bouwmeester *et al.*, 1997) inspired many subsequent experiments, such as an extension to continuous-variable systems (Furusawa *et al.*, 1998) and teleportation of more complete photonic states (Pan, Gasparoni, Aspelmeyer *et al.*, 2003; Takeda *et al.*, 2013; Wang *et al.*, 2015), as also covered in a review by Pirandola *et al.* (2015). The restriction of postselection, where teleported photons have to be detected (i.e., destroyed) to verify the success of the procedure of Bouwmeester *et al.* (1997), was removed six years later using a new method (Pan, Gasparoni, Aspelmeyer *et al.*, 2003) reporting free propagating teleported single photons. The success probability (1/2) of the Bell-state measurement using beam splitters was improved to near unity using a hybrid technique combining both a discrete variable and a continuous variable that resulted in a deterministic quantum teleportation of photonic quantum bits (Takeda *et al.*, 2013). Quantum teleportation has also been extended to the composite state of two photons (Zhang *et al.*, 2006), multiple degrees of freedom (Wang *et al.*, 2015), and higher dimensions of a single photon (Luo *et al.*, 2019).

In addition to photons, quantum teleportation has been demonstrated in other physical systems, such as nuclear magnetic resonance (Nielsen, Knill, and Laflamme, 1998), atomic ensembles (Sherson *et al.*, 2006; Chen *et al.*, 2008), trapped atoms (Barrett *et al.*, 2004; Riebe *et al.*, 2004), and various solid-state systems (Steffen *et al.*, 2013; Pfaff *et al.*, 2014). In pure matter-based systems such as trapped atoms (Barrett *et al.*, 2004; Riebe *et al.*, 2004), teleportation is typically performed only over short distances for atoms near each other. One method to extend the distance of matter qubit teleportation involves developing light-matter quantum interfaces. Using light-to-matter teleportation (Olmschenk *et al.*, 2009), the flying photonic qubits can be stored in stationary media, which is essential for the construction of a scalable quantum network based on the quantum repeater scheme; see Sec. IV for additional details. However, the achievable range of quantum teleportation is determined by the distance across which the entanglement can be distributed. Thus, early experiments suffered limitations similar to the QKD experiments. The early experiments were limited to, for example, a 2-km-long optical fiber linking two laboratories physically separated by 55 m (Marcikic *et al.*, 2003) and over 600 m across the Danube River (Ursin *et al.*, 2004).

The capability of multiphoton manipulation (Pan *et al.*, 2012) opens the way not only to quantum teleportation (Bouwmeester *et al.*, 1997) but also to entanglement swapping (Pan *et al.*, 1998) and entanglement purification (Pan, Gasparoni, Ursin *et al.*, 2003), which combined with quantum memory are important tools for quantum repeaters; see Sec. IV. Quantum teleportation can be considered a method for probabilistic quantum nondemolition measurement that can be exploited as a quantum relay (a simpler version of a quantum repeater without quantum memory) to moderately

extend the distance of quantum communications (Jacobs, Pittman, and Franson, 2002; Waks, Zeevi, and Yamamoto, 2002). For example, using teleportation, one can increase the distance by approximately 3 times that of the direction transmission of a single photon at the same signal-to-noise ratio (de Riedmatten *et al.*, 2004).

### III. CHALLENGES IN PRACTICAL AND LARGE-SCALE APPLICATIONS

#### A. Security loopholes

There are practical security limitations associated with the early implementations using realistic QKD devices in Sec. II. Ideally, only when perfect single-photon sources and detectors are utilized will quantum cryptography be secure. Ideal devices do not exist in practice. In reality, the imperfections of realistic QKD implementations might introduce deviations (or side channels) from the idealized models used for security analysis. Eve might exploit these imperfections and launch quantum attacks. For this reason, an arms race has been ongoing for more than 20 years in quantum cryptography among quantum code makers and quantum code breakers. The race participants aim to assess the deviations of the real system from the ideal system, thus establishing the *practical security* for QKD with realistic devices (Xu *et al.*, 2020).

Right after the security proofs were established in the early 2000s (Lo and Chau, 1999; Shor and Preskill, 2000; Mayers, 2001), a well-known quantum hacking strategy was proposed, the PNS attack (Brassard *et al.*, 2000; Lütkenhaus, 2000), which targets the practical laser source. Since there would occasionally be two identical photon events in pulses from a quasi-single-photon source, the so-called PNS attack allows Eve to selectively suppress single-photon signals and split two-photon signals by keeping one copy for herself without being noticed by Alice and Bob. Because of this loophole, the secure distance of QKD in optical fiber was limited to 10 km.

To resolve this problem, decoy-state QKD was theoretically proposed (Hwang, 2003; Lo, Ma, and Chen, 2005; Wang, 2005) and has been experimentally demonstrated (Peng *et al.*, 2007; Rosenberg *et al.*, 2007; Schmitt-Manderbach *et al.*, 2007) to increase the practicality of QKD with standard weak coherent pulses (WCPs) generated by attenuated laser pulses. Decoy-state QKD has become a standard technique in current QKD experiments. After the decoy-state method, quantum code breakers turned to attack other components, particularly imperfect single-photon detectors (Makarov, 2009). For instance, one can use a specially tailored strong light to “blind” a single-photon detector. Thus, the detector can respond only when the light intensity is greater than its threshold. If the eavesdropper sends a light pulse with an intensity higher than the threshold, the detector will click only when Bob’s measurement basis is the same as that of the input light. Therefore, the eavesdropper can fully control the detectors. Measure-device-independent QKD was proposed theoretically (Lo, Curty, and Qi, 2012) and experimentally (Liu *et al.*, 2013; Rubenok *et al.*, 2013; Tang *et al.*, 2014; Yin *et al.*, 2016; Cao *et al.*, 2020) to increase the security of QKD against any detector imperfections. Measure-device-independent QKD completely eliminates all security loopholes in detection

systems and allows QKD networks to be secure with *untrusted* relays. See the reviews given by Horodecki *et al.* (2009), Sangouard *et al.* (2011), Pan *et al.* (2012), Brunner *et al.* (2014), Reiserer and Rempe (2015), and Xu *et al.* (2020) for further details. Thus far, the security of the quantum cryptographic system, which combines measurement-device-independent QKD with a self-calibrated homemade source, is believed to be sufficient for practical QKD at the level of theoretical unconditional security.

#### B. Long distances

Having covered the typical early small-scale experiments on quantum communications, here we raise the following question: what limits the distance of quantum communications? There are inevitable photon losses in both the fiber optics and terrestrial free-space channels that scale up exponentially with the transmission length in optical fibers. Gisin and Thew (2010) highlighted that at 1000 km, even with a perfect single-photon source of 10 GHz, ideal photon detectors, and 0.2 dB/km fiber losses, one would detect only 0.3 photon on average per century. In classical communications, it is possible to amplify the signals 0 and 1. In contrast, an unknown quantum superposition state cannot be noiselessly amplified. This is known as the quantum no-cloning theorem, a fundamental no-go theorem in quantum mechanics. While it underpins the security of QKD, it excludes the possibility of simply amplifying quantum signals over long-distance quantum communications.

### IV. QUANTUM REPEATER AND ITS PROGRESS

One strategy for extending the distance of quantum communications is using the divide-and-conquer strategy. Unlike classical repeaters that work only for classical bits, quantum repeaters (see Fig. 8) combine entanglement swapping, entanglement purification, and light storage and, in principle, can enable quantum communication at arbitrarily large scales. This section covers the principle and progress made with quantum repeaters.

The key mechanism behind an extension of quantum communication distance by quantum repeaters is to change the exponential scaling of the photon loss to a polynomial relation as a function of the channel length. To do so, the entire channel must be divided into  $N$  segments [see Fig. 8(a)] such that, within each segment, direct transmission can yield a reasonably good signal-to-noise ratio. The problem now hinges on how to efficiently connect these segments in a quantum compatible way. It turns out that entanglement swapping (Żukowski *et al.*, 1993) (a variant of quantum teleportation in which the particle to be teleported is itself part of an entangled pair) provides an ideal method for entangling the remote particle without a direct interaction; see Fig. 8(b). The key step in entanglement swapping involves performing a Bell-state measurement for two single photons, each from an entangled pair. The two photons should arrive simultaneously through a beam splitter and must be quantum mechanically indistinguishable.

The first experimental demonstration of entanglement swapping was reported by Pan *et al.* (1998), who showed

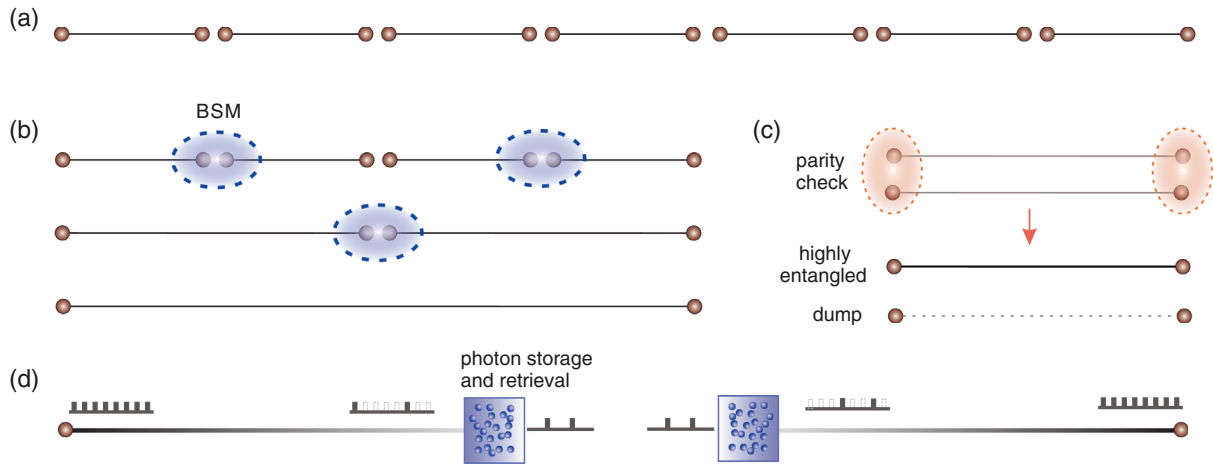


FIG. 8. Principle of quantum repeaters. (a) Dividing the communication channel into  $N$  segments. (b) Using entanglement swapping to establish entanglement between remote nodes. (c) Using entanglement purification to distill highly entangled pairs between remote nodes. (d) Using quantum memory to store single photons for a sufficiently long time and retrieve the single photon for time-synchronized two-photon interference. From Briegel *et al.*, 1998, and Duan *et al.*, 2001.

the possibility of entangling two independent photons without direct interaction; see Fig. 9. The precision of entanglement swapping was improved to 0.98 in later experiments (Pan, Gasparoni, Ursin *et al.*, 2003), meeting the stringent requirement of fault-tolerant quantum repeaters (Briegel *et al.*, 1998). Entanglement swapping has been used as a ubiquitous tool to entangle distant qubits such as those in trapped ions (Maunz *et al.*, 2007), cold atomic ensembles (Yuan *et al.*, 2008), and nitrogen-vacancy centers in diamond (Hensen *et al.*, 2015) by the joint projection of two flying photons. Furthermore, it has been extended to field tests over tens of kilometers of optical fibers using the fine synchronization of two arriving photons (Sun *et al.*, 2017; Yu *et al.*, 2019).

The quantum repeater protocol also considers the presence of noise and decoherence as the entangled photons propagate through the channel (such as optical fibers that can induce undesired polarization rotation), which can induce the degradation of the entanglement fidelity compared to those of locally prepared ones. To overcome the decoherence, entanglement purification (Bennett *et al.*, 1996) was proposed to distill highly entangled pairs remotely separated from an ensemble of less entangled pairs. The protocol of entanglement purification uses only local operation and classical communication.

In the proposed protocol, the local operations involved controlled-NOT (CNOT) logic gates between the qubits. Owing to the weak interaction between independent photons, however, the CNOT gates were difficult to implement. Although there eventually were some experimental demonstrations (O'Brien *et al.*, 2003; Gasparoni *et al.*, 2004; Zhao *et al.*, 2005), the photonic CNOT gates required ancillary photons and exhibited only moderate gate fidelity, as well as low efficiency.

Using only linear optics, Pan *et al.* (2001) put forward a feasible scheme for entanglement purification with high precision and efficiency. It was observed that the CNOT gates were not necessary. In fact, the polarizing beam splitter (PBS), an off-the-shell high-precision linear optical element that transmits horizontal polarization and reflects vertical polarization, was exploited by Pan *et al.* to function as a parity checker that was sufficient to perform entanglement purification. The parity

checking function of the PBS was found to apply to resource-efficient linear optical quantum computation (Browne and Rudolph, 2005). Two years thereafter, Pan, Gasparoni, Ursin *et al.* (2003) experimentally demonstrated entanglement purification, achieving an enhanced entanglement fidelity after the purification. Walther *et al.* (2005) further achieved the violation of Bell's inequality after the purification of two copies of less entangled pairs that were insufficient to violate Bell's inequality. Reichle *et al.* (2006) later used trapped ions to demonstrate entanglement purification.

Notably, the development of multiphoton interferometry and entanglement (Bouwmeester *et al.*, 1997; Pan *et al.*, 2000) also laid the technological foundation for entanglement swapping (Pan *et al.*, 1998), entanglement purification (Pan, Gasparoni, Ursin *et al.*, 2003), and measurement-device-independent QKD (Liu *et al.*, 2013; Rubenok *et al.*, 2013), which are key ingredients for long-distance quantum communications. In fact, quantum teleportation and entanglement swapping can be considered methods for probabilistic quantum nondemolition measurements, which can be exploited to extend the distance of quantum communications by up to 4 times. This can be viewed as a simplified version of a quantum repeater without quantum memory, which has also been referred to as quantum relay (de Riedmatten *et al.*, 2004).

The last element of the quantum repeater (Briegel *et al.*, 1998) is the quantum memory (Lvovsky, Sanders, and Tittel, 2009; Afzelius, Gisin, and de Riedmatten, 2015), which can convert the quantum information carried in fast-flying photons into stationary matter qubits, store it for a certain time, and convert it back into photons on demand. Several physical systems (Simon *et al.*, 2010) have been considered as candidates for quantum memory, such as cold atomic ensembles (Sangouard *et al.*, 2011), rare-earth elements (Tittel *et al.*, 2010), single trapped atoms (Reiserer and Rempe, 2015) and ions (Duan and Monroe, 2010), and color centers in diamond (Gao *et al.*, 2015; Atatüre *et al.*, 2018). These systems can be categorized into single-particle approaches and ensemble approaches. With single particles, it is advantageous to scale up to multiple qubits and perform gate operations.

Nevertheless, challenges still exist in improving the coupling with single photons by employing either a high finesse cavity or a high-numerical-aperture lens. Conversely, with atomic ensembles, it is much easier to achieve efficient coupling with single photons because of the collectively enhanced interaction among a large number of atoms. Nevertheless, one must tackle inhomogeneous decoherence. After many years of extensive experimental investigations, the performance of each system was significantly improved. To be employed in quantum repeaters, a quantum memory must possess many crucial properties, such as a long lifetime and a good storage efficiency. A system must simultaneously exhibit high values for these parameters to be suitable for use in quantum repeaters. As a milestone, the approach of utilizing cold atomic ensembles afforded an efficient quantum memory with a subsecond lifetime in 2016, with the two parameters fulfilling the requirement of long-distance quantum repeaters for the first time (Zhao *et al.*, 2009; Bao *et al.*, 2012; Yang *et al.*, 2016). Further development needs to incorporate efficient entanglement creation, telecom interfaces, multiqubit storage, gate operation, etc.

Based on numerical analysis (Rozpedek *et al.*, 2019; Wu, Liu, and Simon, 2020; Singh *et al.*, 2021), achieving a 1000 km quantum repeater requires demanding parameters that are still significantly beyond the capabilities of the state of the art, such as trapped ions and cold atomic ensembles. Therefore, it is unlikely that quantum repeaters will become practical within ten years, so alternative and more efficient routes for global-scale quantum communications are necessary. Note that new quantum repeater concepts were recently developed, such as all-optical repeaters (Azuma, Tamaki, and Lo, 2015) and repeaters that do not require two-way classical communications (Muralidharan *et al.*, 2014).

## V. SATELLITE-BASED FREE-SPACE CHANNELS

Generally, the attenuation in free space is lower than that in fiber for optical signals. For instance, values of 0.07 dB/km can be achieved at 2400 m above sea level (Schmitt-Manderbach *et al.*, 2007) with higher absorption attenuations at lower altitudes. In the vacuum above Earth's atmosphere, the absorption attenuations are reduced to almost zero. Furthermore, the almost nonbirefringent character of the atmosphere guarantees the preservation of a polarization state to a high degree. However, terrestrial free-space channels alone are not enough. They suffer from obstruction by objects in the line of sight, from possible strong attenuations due to weather conditions and aerosols, and from the effects of Earth's curvature (Aspelmeyer, Jennewein *et al.*, 2003). Therefore, to fully exploit the advantages of free-space links, it is necessary to exploit space and satellite technologies. Furthermore, the effective thickness of the atmosphere is approximately 5–10 km, and most of the photon's propagation path is in empty space with negligible absorption and turbulence, which is crucial for transmitting single photons that cannot be amplified. Therefore, in the application of QKD networking with global-scale coverage, satellite-based free-space channels hold promise as a potential route and a new platform for quantum optics experiments at an astronomical scale. The attenuation of the fiber and free-space channel with

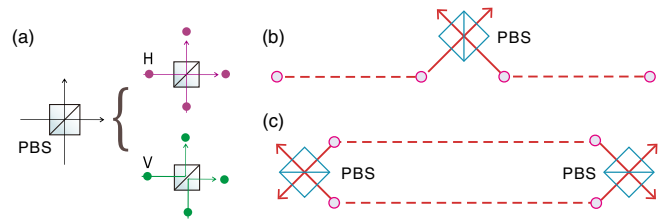


FIG. 9. Experimental scheme for entanglement swapping and purification with high-precision polarization beam splitters (PBSs). (a) The PBS transmits horizontally ( $H$ ) polarized photons and reflects vertically ( $V$ ) polarized photons. Suppose that two single photons are superposed on a PBS. If we postselect the output case where there is one photon in each side, there are two quantum-mechanically indistinguishable possibilities: either both photons are transmitted or both photons are reflected. (b) Entanglement swapping by interfering two photons on a PBS. The two distant photons become entangled upon the Bell-state measurement on the PBS. (c) Entanglement purification by locally two-photon interferences on the two PBSs. See Pan *et al.* (2001) for details.

distance is simulated according to the parameters of the commercial fiber and the Micius satellite, as shown in Fig. 10. We can see that for a distance of over 70 km the satellite-based free-space channel is superior to the fiber-based channel in terms of total losses.

To build the QKD network, trusted-node topologies are being built for fiber networks. However, ground-based nodes are at fixed locations, which lack flexibility and are vulnerable to constant surveillance and probes. By placing a satellite above Earth's atmosphere, one can establish direct links between ground stations and the satellite, thus enabling communication between any distant points on the planet. Furthermore, many more network topologies can be easily implemented with satellites by employing the downlink, uplink, and intersatellite channels. Moreover, more ambitious projects aimed at extending the network scale to deeper space,

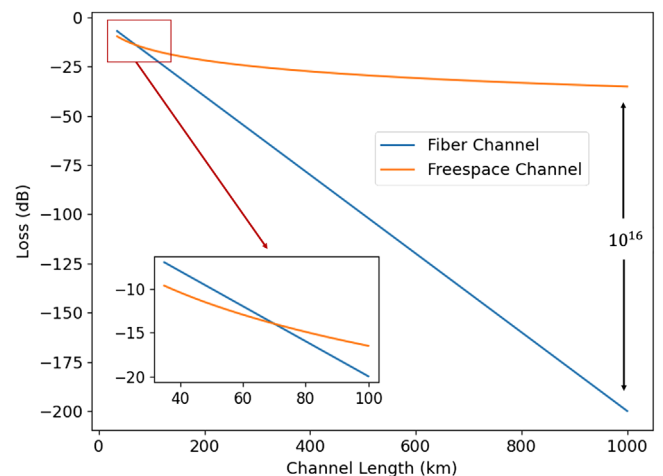


FIG. 10. Typical losses in fiber and free-space channels. The attenuation parameter of fiber is  $\sim 0.2$  dB/km. The parameters of the free-space channel are based on the design of the Micius satellite. The free-space channel shows an advantage for a distance over  $\sim 70$  km.

such as to the Moon or to planets in the Solar System, can be also realized with satellites.

Global-scale classical communications have already employed satellites to conveniently cover the entire world. In principle, quantum communications have a bright future, considering that the advantages of using satellites and free-space channels are even more physically significant. There are enormous challenges to actually move the quantum optics setup inside well-shielded laboratories to space. To realize satellite-based quantum experiment platforms in space, intensive engineering efforts should be devoted to its design and to strict step-by-step verifications. Considering a feasible low-Earth-orbit satellite within a realistic budget, one should carefully analyze the link efficiency and transmission fidelity of the free-space channels as well as every relevant parameter, such as the designed quantum light sources, which is reviewed in this section. The quantum science satellite Micius is within the framework of the Chinese Academy of Science (CAS) Strategic Priority Research Program on Space Science. Major scientific goals include (1) satellite-to-ground QKD, (2) a quantum entanglement distribution from the satellite to two ground stations, and (3) ground-to-satellite quantum teleportation. Strictly following such engineering requirements for each of the three goals, ground-based experimental tests of the feasibility of satellite-based quantum communications were then carried out, as reviewed in Sec. VI.

### A. Analysis of space-ground links

Several factors influence the attenuation of quantum communication channels when photons propagate between a ground station and a satellite. The fixed attenuations are affected mainly by the efficiencies of the optical transmitting system  $\eta_t$  and receiving system  $\eta_r$ , including the optical and detection efficiencies. During transmission, the optical beam will be broadened or deflected by diffraction, air turbulence, and mispointing, which will induce the losses  $\eta_d$ ,  $\eta_{at}$ , and  $\eta_p$ , respectively. Atmospheric absorption brings the attenuation  $\eta_{as}$  relay to photon wavelength and air composition. Considering all these factors, one-way channel attenuation between a satellite and a ground station can be simulated as follows:

$$\eta = \eta_t \eta_r \eta_d \eta_{at} \eta_p \eta_{as}. \quad (5)$$

*Beam diffraction.*—In free-space quantum communication, the diffraction of an optical beam depends mainly on its spatial mode, its wavelength, and the telescope aperture. We generally assume that the beam from the transmitting antenna is Gaussian with a waist radius of  $\omega_0$ . At a distance of  $z$ , the spot radius  $\omega_d(z)$  will be

$$\omega_d(z) = \omega_0 \sqrt{1 + (z/z_R)^2}, \quad (6)$$

where the Rayleigh range  $z_R = \pi\omega_0^2/\lambda$  relays to the wavelength  $\lambda$ . For a telescope with the aperture radius  $r$ , the receiving efficiency  $\eta_d$  can be as high as

$$\eta_d(r) = 1 - \exp\left(-\frac{2r^2}{\omega_d^2}\right). \quad (7)$$

Note that the spot radius  $\omega_d(z)$  increases linearly with  $z$  when the distance  $z \gg z_R$ . The divergence half angle of the beam far from the waist is given by  $\theta \approx \lambda/\pi\omega_0$ . Therefore, the diffraction loss in long-distance quantum communications can be mitigated by choosing relatively shorter photon wavelengths or a large waist radius. But the transmitting antenna truncates the beam sent to the ground, causing significant losses if the beam waist is larger than the telescope radius. For a downlink, it is recommended to set the FWHM beam waist to be half of the transmitting telescope diameter (Stutzman and Thiele, 2012).

*Air turbulence.*—This is one of the main factors limiting the channel efficiency in free-space quantum communication. It induces the atmospheric refractive index inhomogeneity, which changes the direction of the propagating beam. In terms of the beam size, large-scale turbulence causes beam deflection, while small-scale turbulence induces beam broadening (Vasylyev, Semenov, and Vogel, 2016). For the receiver, by accumulating the randomly moving spots, the average long-term spot theoretically tends to follow a Gaussian intensity distribution (Dios *et al.*, 2004). The equivalent radius of this spot is given by

$$\omega_{at}(z) = \omega_d(z) \sqrt{1 + \omega_a} = \omega_d(z) \sqrt{1 + 1.33\sigma_R^2 \Lambda^{5/6}}, \quad (8)$$

where  $\omega_a$  represents the effect of air turbulence on the optical beam,  $\sigma_R^2$  represents the Rytov variance for a plane wave, and  $\Lambda$  represents the Fresnel ratio of the beam at the receiver. More details were provided by Andrews and Phillips (2005).

*Pointing error.*—To establish the link between the ground and the high-speed moving satellite, a high-precision and high-bandwidth APT system, which generally consists of coarse and fine tracking systems, should be developed. Closed-loop coarse tracking usually works at a frequency of several hertz, and the field of view (FOV) is relatively large, which induces a large pointing error. A fine tracking system with a frequency of up to kilohertz can point precisely, and the FOV is small. The combination of coarse and fine tracking can provide a large FOV, a high closed-loop bandwidth, and pointing precision. The pointing error will induce spot jitter, where the instantaneous spot can be described using the Rice intensity distribution. We can define  $\eta_p$  as the expected value of the mispointing loss, which is given by

$$\eta_p = \frac{\omega_{at}^2}{\omega_{at}^2 + 4\sigma_p^2}, \quad (9)$$

where we assume that the pointing probability density follows a Gaussian distribution with variance  $\sigma_p$  (Toyoshima and Araki, 1998).

*Atmosphere transmittance.*—Atmospheric transmittance is reduced by the air absorption and the scattering of the propagating beam. The atmospheric components include mainly gas molecules and small particles (such as water droplets, dust, and aerosols). The gas molecules have certain

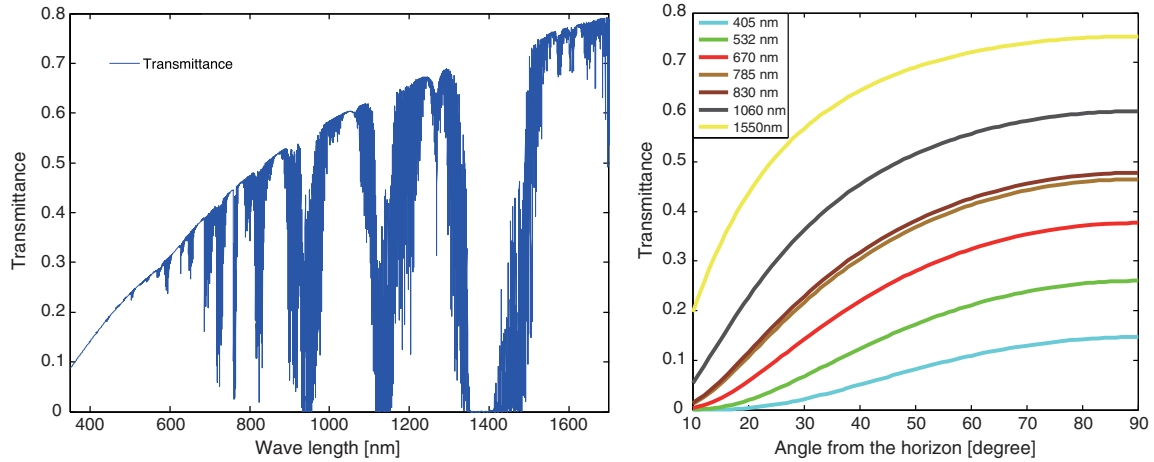


FIG. 11. Simulated atmospheric transmittance for a zenith with different wavelengths (left panel) and different altitude angles (right panel).

specific absorption lines, and the scattering can be described as Rayleigh scattering  $I(\lambda) \propto I_0(\lambda)/\lambda^4$  for the incident light intensity  $I_0(\lambda)$ . The particles in the atmosphere are distributed mainly on the ground surface, with a decreasing concentration as the altitude increases. The transmittance is related to the visibility. When the particle size is equivalent to or larger than the wavelength, Mie scattering theory can be employed to describe the scattering phenomenon. The scattering intensity is proportional to  $\lambda^2/r_p^2$ , where  $r_p$  is the particle radius.

MODTRAN software, which was developed by Spectral Sciences and the Air Force Research Laboratory, can be used to simulate and analyze the atmospheric transmittance. Figure 11 shows the simulated atmospheric transmittance in a rural sea-level location with 5 km visibility (Bourgoin *et al.*, 2013). The transmittance is good at a high altitude angle because of the relatively short propagation time in the atmosphere.

*Downlink and uplink channels.*—Satellite-based quantum science experiments can be performed using two different channels, namely, downlink (from the satellite to the ground) and uplink (from the ground to the satellite). For downlink transmissions, the beam reaches air turbulence with a large size and is received immediately after the atmosphere is crossed; thus, the impacts are marginal on the beam broadening and deflection induced by turbulence. On the contrary, for the uplink, photons encounter air turbulence at the beginning of propagation and subsequently transmit to the satellite. Therefore, turbulence-induced distortion will significantly increase the beam divergence angle and result in a larger channel attenuation than that in the case of the downlink transmission. Although the downlink channel has more advantages in terms of efficiency, the uplink channel is still competitive in some cases, such as when one wants to simplify the payloads. Note that the effects of turbulence can be partly compensated for in theory using an adaptive optics system with feedback devices.

## B. Feasible channel parameters for the low-Earth-orbit satellite

Typically, owing to the low channel attenuation of a downlink, the satellite-based QKD and entanglement

distributions are suitable for one-downlink and two-downlink channels, respectively. Conversely, considering the limitation of satellite resources and the flexibility of the ground system, some experiments may be more suitable for uplink transmission, such as quantum teleportation based on a multi-photon entanglement source. Therefore, one-downlink, two-downlink, and one-uplink channels are the basic elements for constructing a global-scale quantum network.

According to Eqs. (5)–(9) and using typical parameters, one finds that the expected total loss of above three types of channels can be evaluated as shown in Table I. When the satellite-based channel loss is estimated, the relevant constraints, including technology, resources, and cost, must be considered. Considering the technology’s maturity and affordability, the 1-m-diameter ground-based telescope and the satellite-borne transmitter with a divergence angle of  $15 \mu\text{rad}$  and a central wavelength of 850 nm is reasonable. For a QKD based on a one-downlink channel, the distance ( $Z$ ) is 500–1200 km, the optical diameter of the receiving telescope ( $D$ ) on the ground is 1.2 m, and the efficiency of the optical transmitting system can be set to 100% only for QKD based on the weak coherent state source (approximately 25% for the two-downlink entanglement distribution). The efficiency of the optical receiving system (including optical, filter and detection efficiencies) is approximately 0.2, the effective divergence angle of the transmitter ( $\theta$ ) after considering the effect of diffraction and atmospheric turbulence is  $\sim 15 \mu\text{rad}$  (approximately 20–30  $\mu\text{rad}$  for uplink channels), the atmospheric transmittance is typically 0.5, and the mispointing loss is 0.5. The geometry attenuation can be evaluated to about 19 dB when  $Z = 1000$  km through the approximation formula  $2[D/(\theta Z)]^2$ . Thus, the total channel loss is estimated to be  $-35$  dB. Similarly, for an entanglement distribution based on two-downlink channels and a quantum teleportation based on the one-uplink channel, the total channel losses are expected to be approximately  $-75$  and  $-53$  dB, respectively, as shown in Table I.

Using the estimated total channel loss and the requirements of the satellite mission as the input condition, one can output the specifications of key technologies. For example, when

TABLE I. Estimated total loss for one-downlink, two-downlink and one-uplink channels. In this estimation, the distance is set to 1000 km for the three types of channels. The divergence angles of the transmitter for the downlink channels are set to about 15  $\mu$ rad, and for uplink channels the divergence angles are extended to 20  $\mu$ rad due to the stronger effect of turbulence. The diameter of the receiving telescope is set to 1.2 and 0.3 m for ground-based and satellite-based tests, respectively. The geometry attenuation is evaluated using the distance, the divergence angle, and the diameter of the receiving telescope.

	One-downlink channels for QKD	Two-downlink channels for entanglement distribution	One-uplink channels for quantum teleportation
Geometry attenuation ( $\eta_G$ )	0.0128	0.000 164	0.000 45
Atmosphere attenuation ( $\eta_A$ )	0.5	0.25	0.5
Transmitter efficiency ( $\eta_T$ )	1	0.25	0.5
Receiver efficiency ( $\eta_R$ )	0.4	0.16	0.4
Coupling efficiency ( $\eta_C$ )	0.5	0.25	0.5
Detector efficiency ( $\eta_D$ )	0.5	0.25	0.5
Mispointing ( $\eta_M$ )	0.5	0.25	0.5
Total loss ( $\eta_G\eta_A\eta_T\eta_R\eta_C\eta_D\eta_M$ )	-35 dB	-75 dB	-53 dB

considering the mission of a satellite-based entanglement distribution with the two-downlink channels, the total experimental time will be limited by the conditions of the satellite altitude angle and the weather of the two ground stations. If the total experimental time is set to 10 000 s, according to the total loss of -75 dB the output brightness of a satellite-borne entangled-photon source must be over  $2 \times 10^6$  pair/s to obtain more than 1000 coincidence events. Furthermore, to achieve the raw-key rate of 1 kbit/s, the repetition frequency of the satellite-borne decoy-state source must be at least 100 MHz when the channel loss is approximately -35 dB. The mispointing value of 0.5 indicates that the tracking accuracy of the APT system should be achieved to 4  $\mu$ rad.

Furthermore, Fig. 12 shows the complete evaluation of the total required experimental time and the effective fidelity of the received entangled photon pairs on the ground with different total channel losses when we consider the specific parameters of the background noise, the target detected coincident events on the ground, the fidelity of the satellite-borne entangled-photon source, and the time synchronization

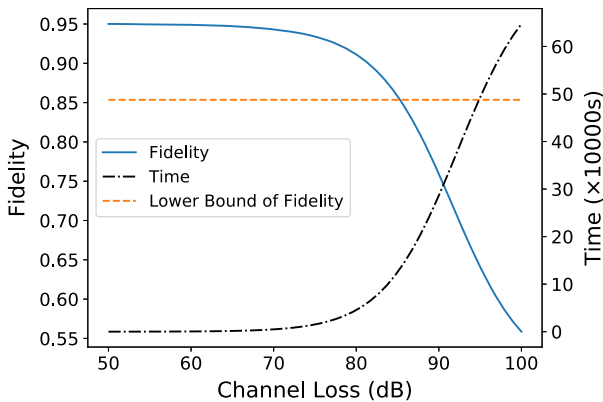


FIG. 12. The effective fidelity and total experimental time with different two-downlink channel losses. The original state fidelity of the entangled-photon source is 95%, which degrades with the increase of channel loss due to the inevitable noise. The lower bound of the fidelity is defined as the minimum value for a violation of the Bell inequality. The time coordinate represents the total required experimental time to accumulate 1000 coincident events on the ground.

accuracy. According to this estimation, we can further conclude that the fidelity of the satellite-borne entangled-photon source should be larger than 95%, and the total channel loss should be less than 80 dB (it will be 40 dB for the one-downlink channel) when the total experimental time is limited to < 10 000 s.

Regarding ground-to-satellite quantum teleportation, a similar simulation study is shown in Fig. 13. To realize the mission target of 400 coincident counts, the total channel loss should be less than 55 dB and the fidelity should be more than 75% when the total experimental time is limited to < 40 000 s.

Finally, based on the previous analysis and a simulation of the feasible channel parameters, we can summarize the main requirements of satellite-based quantum science experiments, as shown in Table II. These specific technical indicators can be used as direct verification targets for the ground-based feasibility studies (see Sec. VI), and the design input can be employed to develop payloads (see Sec. VII). Furthermore, we emphasize that only once we have performed this comprehensive analysis can we conduct the ground-based feasibility study and develop key technologies following a systematic approach.

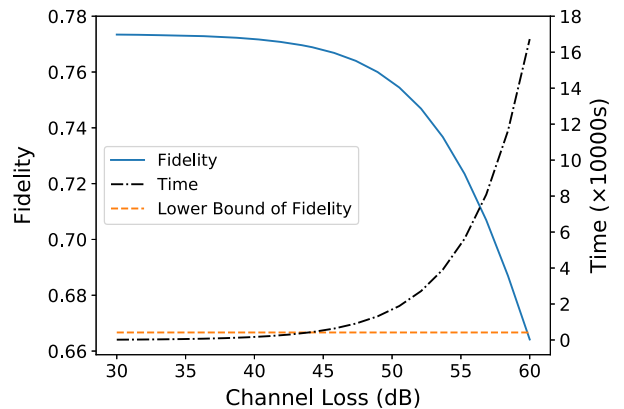


FIG. 13. The effective fidelity and total experimental time with different one-uplink channel losses. The lower bound of the fidelity is the classical limit of the fidelity on a single copy of the qubit. The time coordinate represents the total required experimental time to accumulate 400 coincident events.

TABLE II. Main practical requirements of satellite-based quantum science experiments.

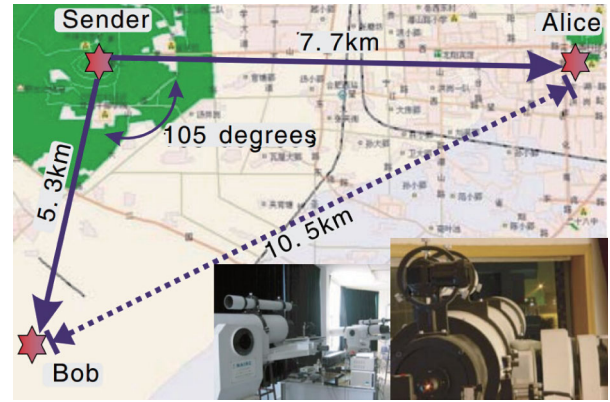
List of feasible design baselines	
Satellite operating lifetime	$\geq 2$ yr
Time synchronization accuracy	$\leq 1$ ns ( $1\sigma$ )
Satellite-to-ground QKD	
Raw-key rate	$\geq 1$ kbit/s
QBER	$\leq 3.5\%$
Total experimental time	$\geq 20000$ s
Total channel loss	$\leq 40$ dB
Satellite-based entanglement distribution	
Received coincident count	$\geq 1000$
Effective fidelity	$\geq 85\%$
Total experimental time	$\geq 10000$ s
Total channel loss	$\leq 80$ dB
Ground-to-satellite quantum teleportation	
Received coincident count	$\geq 400$
Effective fidelity	$\geq 75\%$
Total experimental time	$\geq 40000$ s
Total channel loss	$\leq 55$ dB

## VI. GROUND-BASED FEASIBILITY STUDIES AND KEY TECHNOLOGIES

This section reviews the systematic ground-based feasibility studies and key technologies based on the requirements for the three Micius satellite missions specified in Sec. V. Before constructing and launching a costly satellite, thorough preliminary studies and simulations on the ground must be systematically performed to verify the scientific possibilities, evaluate the risks, and develop the technologies. Questions of interest include the following: Can the single and entangled photons pass through the effective thickness of the atmosphere (which is about 10 km)? Can the quantum optics experiments be performed (with a sufficient count rate and signal-to-noise ratio) under the conditions of large attenuations and various turbulence on moving platforms? The ground-based feasibility demonstration and the development of key technologies cover the following five aspects: overcoming the effective atmospheric thickness, testing the feasibility of satellite-ground channels, testing moving objects, time synchronization, and polarization maintenance and compensation. Emphatically, only after developing all these technologies and combining them compatibly was the Micius program officially approved and the construction of the satellite started.

### A. Overcoming the effective atmospheric thickness

The first step involves verifying whether the effective atmospheric thickness is favorable for the passage of single and entangled photons. In 2005, entangled photon pairs were bidirectionally distributed over Hefei, China, one arm across 5.3 km and the other across 7.7 km, thereby conclusively exceeding the effective atmospheric thickness, as shown in Fig. 14 (Peng *et al.*, 2005). Narrow band (2.8 nm) filtering and time synchronization (with a precision of 20 ns) were employed to reduce the background counts from the noisy city environment. The two-photon count rates were 10 kHz and 150–300 Hz for the sender and receivers, respectively.

FIG. 14. Overview of the Hefei 13 km entanglement distribution experiment. From Peng *et al.*, 2005.

This corresponded to channel attenuation values in the range of 15.2–18.2 dB, depending on the weather conditions. The physical separation between the two receivers was 10.5 km, which enabled the performance of a spacelike Bell test with a measured  $S$  value of  $2.45 \pm 0.09$ . Three years later, single photons were transmitted over the Great Wall of China at an optical free-space distance of 16 km (Jin *et al.*, 2010). These studies demonstrated that entanglement can still survive after both entangled photons have passed through the noisy ground atmosphere, with a distance beyond the effective thickness of the atmosphere. This is a step toward low-Earth-orbit satellite-to-ground downlink quantum experiments.

### B. Feasibility of satellite-to-ground one- and two-downlink channels and ground-to-satellite uplink channel

To experimentally verify the feasibility of satellite-based QKD through a one-downlink channel, Wang *et al.* (2013) conducted a full verification study of the decoy-state QKD over a 97 km free-space link and demonstrated the possibility of achieving a high signal-to-noise ratio and overcoming the obstacle of a high-loss environment. The total loss achieved in the experiment was over 50 dB, which is more than the expected value of  $\sim 35$  dB with the one-downlink channel mentioned in Sec. V.

Two-downlink channels are needed for the satellite-to-ground entanglement distribution, which requires two independent channels among the three different locations. From 2008 to 2010, a ground-based feasibility study was performed in Qinghai Lake (Yin *et al.*, 2012). In the study, entangled photon pairs were distributed over a two-link free-space channel with distances of 51.2 and 52.2 km to two receivers separated by 101.8 km (Fig. 15). For the study, a crucial enabling technology was developed, i.e., closed-loop tracking, which was operated with a bandwidth and precision of 150 Hz and  $3.5 \mu\text{rad}$ , respectively. This tracking bandwidth was sufficient to overcome most of the atmospheric turbulence. Yin *et al.* (2012) obtained a two-photon rate of 6.5 MHz and measured two-photon correlation functions violating Bell's inequality by 2.4 standard deviations. The average overall two-link attenuation was measured to be 79.5 dB, which is higher than the estimated two-downlink loss (approximately

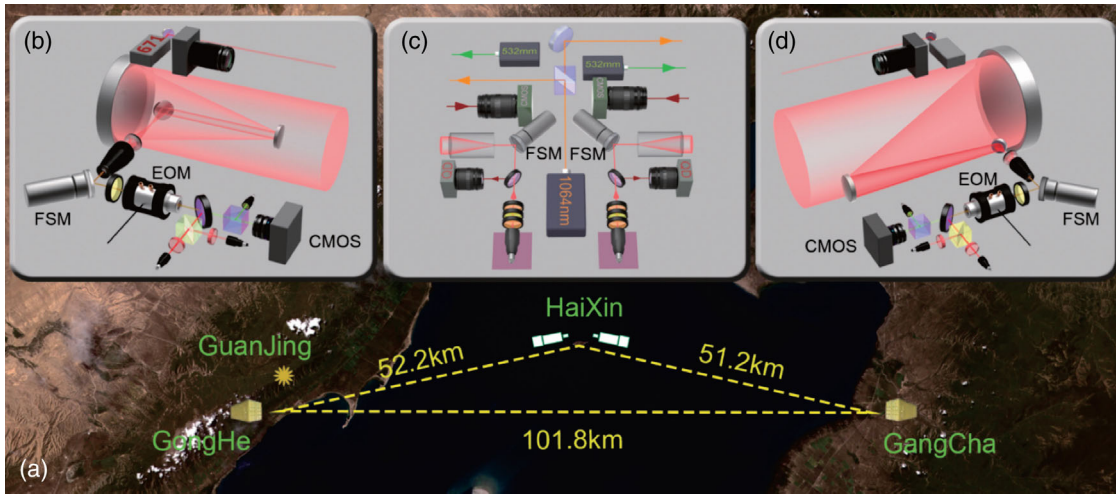


FIG. 15. Bidirectional two-link entanglement distribution over Qinghai Lake at a distance of 101.8 km. From Yin *et al.*, 2012.

75 dB, as mentioned in Sec. V) based on the low-Earth-orbit (LEO) satellite.

If one goes beyond the previously mentioned up to two-photon experiments, a multiphoton platform can be employed to test more sophisticated experiments on the quantum teleportation of independent single photons. In terms of satellite-based teleportation over the one-uplink channel, more tolerance for the channel attenuation is required. Yin *et al.* (2012) investigated quantum teleportation through a free-space channel over 97 km in Qinghai Lake. When a high-brightness multiphoton interferometry was employed (Yao *et al.*, 2012) with a four-photon count rate of 2 kHz after the teleported photon over 97 km with a channel loss of 35–53 dB was teleported, a final count rate of 0.08 Hz was obtained. For the three missions, the total channel attenuation in these works was higher than the estimated values in Sec. V, which provided sufficient verification for the three types of quantum channels.

### C. Testing with moving and vibrating objects

Real implementations of satellite-based quantum communications require high-bandwidth and high-accuracy APT. All the ground-based feasibility studies mentioned thus far are based on stationary systems. For eventual satellite-based quantum communications, one should consider the notion that the satellite performs rapid, relative angular motions with respect to the ground stations, which may include unwanted random motion. For a typical LEO satellite at an altitude of 400–800 km, the angular velocity can reach 20 mrad/s and the angular acceleration can reach 0.23 mrad/s<sup>2</sup>. A verification environment that incorporates all possible motion modes and simulations of extreme events, including vibration, random motion, and attitude change, is highly desirable.

To this end, Wang *et al.* (2013) carried out two other experiments, in addition to the 97 km high-loss one mentioned in Sec. VI.B for the direct and full-scale experimental verifications of satellite-ground QKD. Simulation experiments with a turntable and a hot-air balloon were implemented to simulate the platform in a rapidly moving orbit as well as the vibration, random motion, and attitude change related to

the LEO satellite. The turntable [see Fig. 16(a)] provides motion with a maximum angular velocity of 21 mrad/s and a maximum angular acceleration of 8.7 mrad/s<sup>2</sup>. With a distance of 40 km between the transmitter and receiver, such a motion regime completely covers the possible range of motion parameters for a 400–800 km LEO satellite. The floating hot-air balloon [see Fig. 16(b)], which was 20 km from the ground receiver, was employed as a randomly vibrating and floating platform that afforded an average angular velocity of 10.5 mrad/s and an average angular acceleration of 1.7 mrad/s<sup>2</sup> owing to its random motion. The balloon could perform random and dramatic motions, which positioned it out of view of the field. This motivated the researchers to recapture the target rapidly, typically within 3 to 5 s; see Fig. 16(c). The performance of the acquiring, tracking, and positioning system, including both coarse control and fine control, is summarized in Table III. These verification environments incorporate more extreme events, including vibration, random movement, and attitude change, than would result from an actual LEO satellite.

On the other hand, by utilizing the cube-corner retroreflector on satellites to simulate the quasi-single-photon source, one can verify the feasibility of establishing a quantum signal link between the satellite and the ground station (Villoresi *et al.*, 2008). Yin *et al.* (2013) performed an experimental simulation of a quasi-single-photon transmitter on the satellite with an average photon number of 0.85 per pulse and a full divergence angle of 38  $\mu$ rad sent to the ground.

### D. Time synchronization

Since the transmitter and receiver are separated by a large distance and have independent reference clocks, time synchronization is conducted to determine the absolute photon number and distinguish the signal photons from the noise. As the distance between the transmitter and receiver changes all the time when the satellite passes over the ground station, both the Global Positioning System (GPS) pulse-per-second (PPS) signal and an assistant pulse laser are employed in the typical synchronization scheme. Between the works of Peng *et al.*

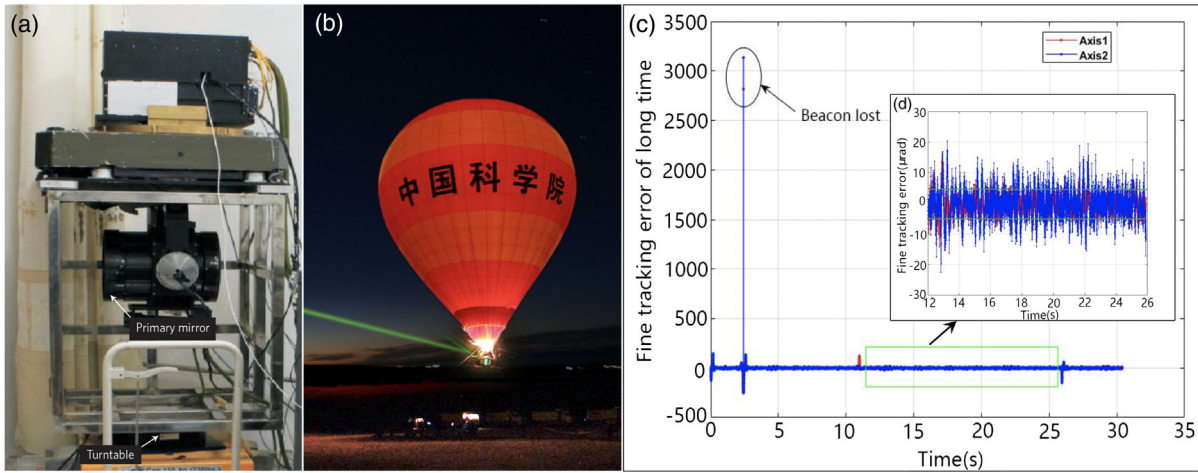


FIG. 16. (a) QKD transmitter mounted on a turntable with the approximate dimensions of  $500 \times 450 \times 600 \text{ mm}^3$  [but  $500 \times 500 \times 1000 \text{ mm}^3$  including the supporting metal frame]. This is used for a simulation of satellite orbiting. When the turntable undergoes a complex motion, the transmitter terminal will move accordingly. The simulation was done with an angular velocity and angular acceleration larger than that of a typical LEO. (b) Photo of the rising and erupting hot-air balloon in the floating platform experiment. (c) Tracking error in the hot-air balloon simulation. Long-time fine tracking error with the beacon light sometimes out of the field of view. Inset: fine tracking error in the stabilized time area. When the beacon light is in the tracking field, the tracking accuracy is about  $5 \mu\text{rad}$ . From Wang *et al.*, 2013.

(2005) and Yin *et al.* (2012), this synchronization method was continuously developed and improved.

In the experiment of Yin *et al.* (2012), a pulsed laser (1064 nm, 10 kHz, 50 mW,  $200 \mu\text{rad}$ ) is employed for time synchronization. A pulse length of this laser was 2.65 ns (full width at half maximum), with a rising edge of 2 ns. The GPS PPS is added to synchronize the starting time. They addressed the forefront of the detected signals with the constant fraction discriminator technique and utilized a high-accuracy time-to-digital converter (TDC) with a time resolution of 100 ps to record the arrival time of the synchronization signals at both Alice's and Bob's stations. Through the previously mentioned methods, in most cases the jitter caused by the laser pulse itself and energy shaking is reduced. Finally, a time synchronization of better than 1 ns for the quantum channel is achieved, as shown in Fig. 17. The technique of time synchronization

developed in these works can be applied directly in satellite-based quantum science experiments.

### E. Polarization maintenance and compensation

Polarization encoding is employed in the long-distance free-space quantum communication experiments. The relative motion of the satellite and the ground station can induce a time-dependent rotation of the photon polarization observed by the receiver. Thus, polarization maintenance and compensation are necessary. Wang *et al.* (2013) developed the following methods to improve a system's polarization visibility: (1) all the reflection mirrors are coated with tailored films to maintain high polarization ( $\geq 1000:1$ ), (2) two mirrors are used for phase matching in polarization deflection, and (3) other optical elements (PBSs, etc.) are custom-made with a

TABLE III. Parameters of the APT system. From Wang *et al.*, 2013.

Components	Transmitter terminal	Receiver terminal
Telescope diameter	200 mm	300 mm
Coarse pointing system		
Actuator	Two-axis gimbal mount	Two-axis gimbal mirror
Tracking range	Azimuth: $\pm 45^\circ$ Elevation: $\pm 70^\circ$	Azimuth: $\pm 5^\circ$ Elevation: $\pm 5^\circ$
Field of view	$2^\circ$	$1^\circ$
Camera size	$1000 \times 1000$ pixels	$640 \times 480$ pixels
Course tracking errors	$\pm 200 \mu\text{rad}$	$\pm 200 \mu\text{rad}$
Fine point system		
Actuator	Fast steering mirror	Fast steering mirror
Tracking range	$\pm 0.7 \text{ mrad}$	$\pm 0.7 \text{ mrad}$
Field of view	$512 \mu\text{rad}$	$512 \mu\text{rad}$
Camera size and frame	$128 \times 128$ pixels; 2300 Hz	$128 \times 128$ pixels; 2300 Hz
Fine tracking errors	$\pm 5 \mu\text{rad}$	$\pm 5 \mu\text{rad}$

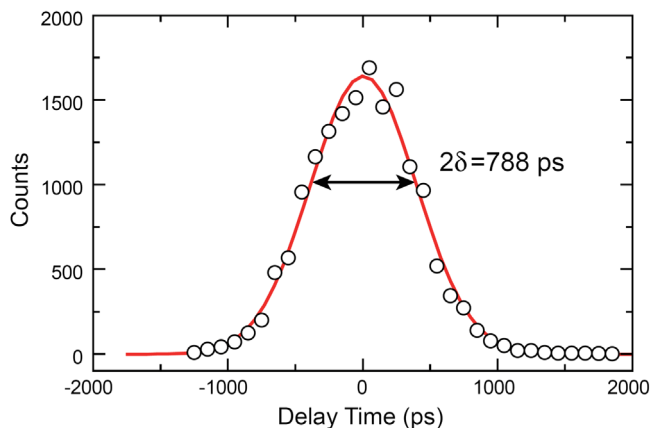


FIG. 17. A typical recorded arrival time of the 1064 nm laser signals at both stations. A synchronization accuracy of 788 ps was observed. From Yin *et al.*, 2012.

high extinction ratio. When all of these features were considered while the optical system was set up, a polarization extinction ratio of 200:1 was obtained for both the transmitter and receiver systems. Further, when the transmitter and receiver were connected during an experiment, the total polarization extinction ratio was as high as 100:1, which meets the requirements of the satellite-based QKD.

Another crucial challenge associated with satellite-ground quantum communication, attributed to the kinematical reference system, is the polarization compensation in real time. While the satellite reference frame keeps changing during the satellite motion, the satellite and ground are relatively static when the two sides face each other at any specific time in this frame. In most cases, the polarization state changes over time because of the two-dimensional rotation of the telescope. Following the telescope azimuth or elevation rotation, a pair of mirrors changes its position, which leads to changes in polarization. This problem can be solved by inputting the real-time data of the orbit prediction into an autorotatable half-wave-plate (HWP) for polarization tracking, which was verified by Yin *et al.* (2013) and later employed by ground stations for the Micius satellite. The extinction rate of the polarization under tracking was tested to be more than 100:1 with this method.

#### F. Other parallel ground-based free-space experiments

In parallel to the previously reviewed comprehensive and systematic ground-based verification works dedicated to the Micius satellite, many other experiments were implemented around the world. The scientific conclusions have been consolidated. In an experiment that was performed in Vienna (Resch *et al.*, 2005), one of the entangled photons was detected locally, while the other was sent through free space across 7.8 km. A new test bed for free-space quantum communications (the link between the Canary Islands of La Palma and Tenerife) was employed by Schmitt-Manderbach *et al.* (2007) for testing decoy-state QKD over a distance of 144 km. Later Ursin *et al.* (2007) adopted the same experimental configuration as Resch *et al.* (2005) to send triggered single photons across a distance of 144 km (one link) using a

free-space link between the Canary Islands of La Palma and Tenerife. Because of the various atmospheric influences on such a long-distance scale, the apparent bearing of the receiver station varied from tens of seconds to minutes. To maximize and stabilize the link efficiency, an active stabilization of the optical link was implemented via a closed-loop tracking system to correct the beam drifts induced by atmospheric changes, thereby reducing the beam drift from 70  $\mu\text{rad}$  (10 m) to 7  $\mu\text{rad}$  (1 m). Using this one-link free-space channel, quantum teleportation was also demonstrated (Ma *et al.*, 2012) with a channel attenuation of approximately 30 dB. A further experiment from the same group upgraded the BBO crystal into a more efficient down-conversion crystal, i.e., periodically poled KTiOPO<sub>4</sub>, which generated entangled photons at  $\sim 1$  MHz and sent the two photons through the free-space channel across 144 km (Fedrizzi *et al.*, 2007, 2009).

To test the APT with moving objects, Nauerth *et al.* (2013) conducted a QKD experiment from an airplane to the ground. The airplane was moving at a speed of 290 km/h at a distance of 20 km, which corresponds to an angular velocity of 4 mrad/s. The transmitting beam was narrowed by a divergence of 180  $\mu\text{rad}$ . To establish a stable link with this divergence, fine-pointing assemblies were implemented and optimized on both sides, with a precision upper bound of 150  $\mu\text{rad}$ . With these efforts, the experiment yielded an asymptotically secure key at a rate of 7.9 bits/s.

In addition to employing moving platforms to demonstrate the feasibility of downlink channels, Bourgoïn *et al.* (2015) verified uplink channels with a truck and airplane. In 2015, they reported the first demonstration of QKD from a stationary transmitter to a receiver platform located on a moving truck. In this experiment, QKD was implemented with a moving receiver at an angular speed similar to that of a satellite at an altitude of 600 km. Furthermore, they equipped a receiver prototype on an airplane to demonstrate QKD via an uplink channel (Pugh *et al.*, 2017). They specifically designed the receiver prototype to consist of many components that were compatible with the environment and resource constraints of a satellite. Their previously mentioned ground-based feasibility experiments on uplink channels with moving platforms provided solid technical support for the follow-up satellite project QEYSSat.

Takenaka *et al.* (2017) used a classical laser source on the LEO satellite *SOCRATES* to test the feasibility of the satellite-to-ground quantum-limited link. Günthner *et al.* (2017) completed a similar experiment using the classical laser source from a geostationary satellite.

## VII. DEVELOPMENT AND TESTING OF THE SATELLITE PAYLOADS

The Micius program was officially approved in 2011. Construction of the first prototype satellite started in 2012 and was completed in 2014. Thereafter, the project turned to the building of the flight model of the satellite, which was completed in November 2015. After a series of environmental tests, including thermal-vacuum, thermal cycling, shock, vibration, and electromagnetic compatibility tests, etc., the Micius satellite, weighing 635 kg, was well prepared and ready to be launched. On August 16, 2016, the Micius satellite

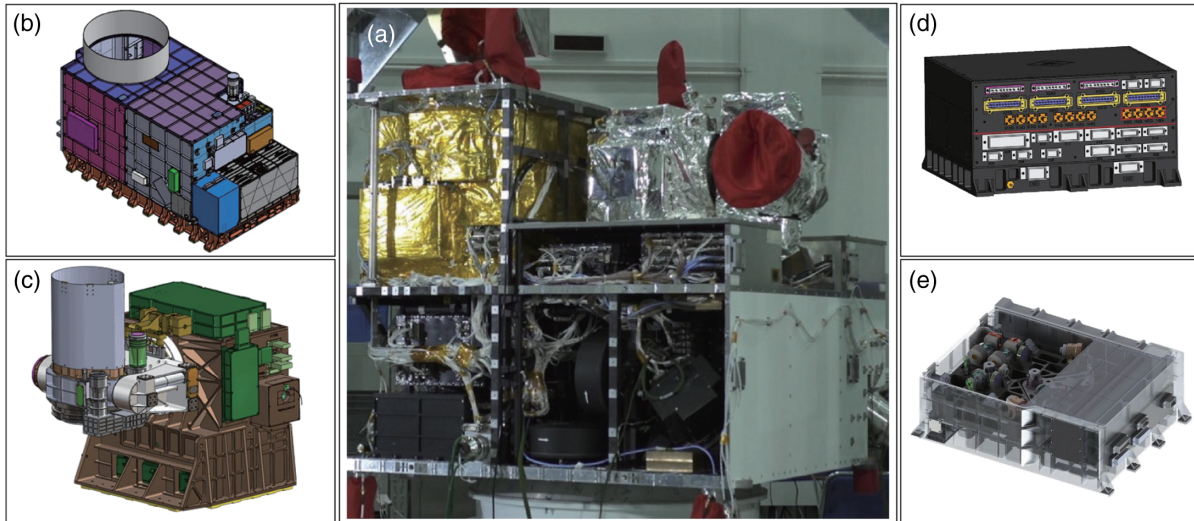


FIG. 18. Full view of the Micius satellite and the main payloads. (a) Photograph of the Micius satellite prior to launch. (b) Transmitter 1 for QKD, entanglement distribution, and teleportation. (c) Transmitter 2, especially designed for entanglement distribution. (d) Experimental control box. (e) Entangled-photon source.

was successfully launched by the Long March 2D rocket, from the Jiuquan Satellite Launch Centre in China. The orbit was circular and sun synchronous, with an altitude of 500 km.

#### A. Payload design

The Micius satellite has a double-decker design; see Fig. 18. The payloads for the science experiments are composed of two optical transmitters (transmitters 1 and 2), a spaceborne entangled-photon source (the upper layer of the satellite), an experimental control processor, and two APT control boxes (the lower layer of the satellite), as shown in Fig. 18(a).

The dimension of the experimental control box, as shown in Fig. 18(d), is  $280 \times 264 \times 150 \text{ mm}^3$ , and the weight is 7.5 kg. The experimental control box has six main functions: experimental process management, random-number generation and storage, modulation of the decoy-state photon source, synchronization-pulse recording, QKD postprocessing (including raw-key sifting, error correction, and privacy amplification to obtain the secure final keys), and encryption management.

Transmitter 1, with a diameter of 300 mm and a total weight of 115 kg, as shown in Fig. 18(b), is involved in all three main scientific goals. It comprises eight laser diodes with drivers, a BB84 polarization encoding module, a telescope, a receiving module [including a quarter-wave plate (QWP), a HWP, a PBS, and two single-photon detectors], and the APT system [including a beacon laser, a coarse camera, two-axis mirror, a fine camera, a fast steering mirror (FSM), etc.], as shown in Fig. 19(a). Transmitter 2, with a diameter of 180 mm and a total weight of 83 kg, as shown in Fig. 18(c), is specially designed for the quantum entanglement distribution from the satellite to two separate ground stations. Further, it can serve as transmitter 1's backup for the satellite-based QKD. Both transmitters contain a telescope and an optical box. To reduce the emission loss, an off-axis telescope design is employed in transmitter 2. The optical box consists mainly of a fine

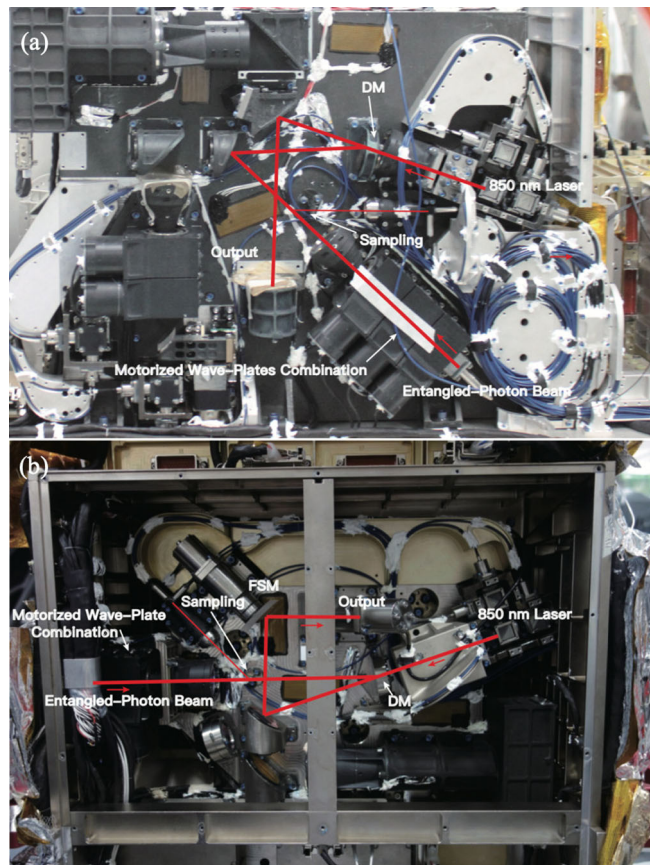


FIG. 19. Top view of a transmitter's optics head. The collimated beam from the entangled-photon source passes through a motorized wave-plate combination and a beam expander and then is combined with the 850 nm synchronization laser using a dichroic mirror. (a) Transmitter 1's optics head. (b) Transmitter 2's optics head. From Liao *et al.*, 2017a.

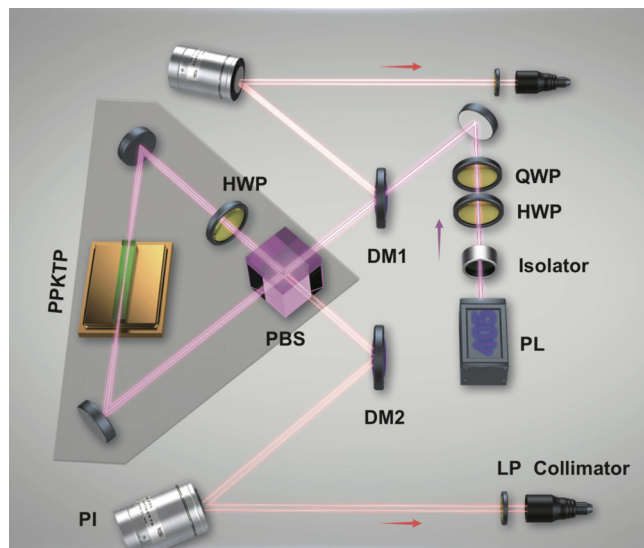


FIG. 20. Schematic of the satellite-borne entangled-photon source. The entangled-photon source in the Micius satellite is based on type-II periodically poled  $\text{KTiOPO}_4$  (PPKTP) crystal and the Sagnac interferometer. PL, pump laser; DM, dichromatic mirror; PI, piezoelectric steering mirror; QWP, quarter-wave plate; HWP, half-wave plate; PBS, polarizing beam splitter. From Yin *et al.*, 2017a.

tracking system, an integrated receiving module for sampling measurement, and a motorized wave-plate combination for polarization correction, as shown in Fig. 19(b).

Additionally, both transmitters contain a multistage APT system. The first stage involves satellite altitude control, where the system keeps the photons pointing to the ground station with an error of less than  $0.5^\circ$ . The second stage is the coarse control loop involving the two-axis gimbal mirror for transmitter 1 and the two-dimensional rotatable telescope for transmitter 2. The third stage is the fine control loop, which involves a FSM driven by piezoceramics and a camera.

The spaceborne entangled-photon source (SEPS) is an optomechanics integration payload with a dimension of  $430 \times 355 \times 150 \text{ mm}^3$  and a total weight of 23.8 kg, as shown in Fig. 18(e). The schematic of SEPS is shown in Fig. 20. A continuous-wave laser diode with a central wavelength of 405 nm and a linewidth of 160 MHz was employed to pump a periodically poled  $\text{KTiOPO}_4$  (PPKTP) crystal inside a Sagnac interferometer. The pump laser, which is split by a PBS, passes through the nonlinear crystal in the clockwise and counterclockwise directions simultaneously, producing down-converted photon pairs at a wavelength of 810 nm, as polarization-entangled states close to the form  $(|H\rangle_1|V\rangle_2 + |V\rangle_1|H\rangle_2)/\sqrt{2}$ , where  $H$  and  $V$  denote the horizontal and vertical polarization states, respectively, and the subscripts 1 and 2 denote the two output spatial modes. This source is robust against various vibrations, temperatures, and electromagnetic conditions. With a pump power of 30 mW, the source emits  $5.9 \times 10^6$  entangled-photon pairs per second, with a state fidelity of  $0.907 \pm 0.007$ .

The optical elements are mounted and glued on both sides of a 40-mm-thick optical bench. The optical bench is composed of titanium alloy, which has a good balance of

rigidity, thermal expansion, and density. The most sensitive structure of the SEPS, the Sagnac interferometer, is integrated into a palm-sized Invar material plate with a thickness of 15 mm and then embedded in a thermoinsulated fashion in the titanium plate to achieve an optimal stability once the satellite is launched and in orbit. The input and output beams of the Sagnac interferometer are collimated because of the confocal design, which relaxes the requirement of a high mounting accuracy for the couplers. In addition, two piezoelectric steering mirrors (PIs) are employed to correct the pointing offset of the beam. The Sagnac interferometer module in the SEPS has passed a series of space environment adaptability tests, such as thermal-vacuum and vibration tests, that help to release thermodynamic stress in advance and enhance system stability. The SEPS is guided to two optical transmitters through two single-mode fibers with lengths of 280 and 410 mm, respectively. After a 5 times beam expander is utilized, a mirror is placed at the edge of the beam to sample the entangled photons by 1%. An integrated BB84 receiving module consisting of two Wollaston prisms and one beam splitter realized a random measurement of four polarizations ( $0^\circ$ ,  $90^\circ$ ,  $45^\circ$ , and  $135^\circ$ ). Through the 1% sampling in both entangled-photon transmitters, the source brightness can be estimated in orbit.

The APT control box dimensions are  $326 \times 244 \times 242 \text{ mm}^3$ , with a weight of 10 kg, and the control box contains mainly the control electronics for the coarse tracking loop and the fine tracking loop. It functions specifically as a motor driver, FSM driver, coarse feedback loop controller and fine feedback loop controller.

## B. Testing the payload under various conditions

For the design of the payloads, besides the functional requirements, it is also important to ensure adaptability in the space environment. In general, there are three main types of space environment tests: vibration, thermal, and vacuum tests. The vibration test can be subdivided into sinusoidal, random vibration, and impact tests. The thermal and vacuum tests include thermal-vacuum, thermal cycling, and thermal-vacuum-optical measurements. When one considers all the payloads described in Sec. VII.A, each payload must be subjected to these three space environmental simulation tests. After every payload has passed the test separately, all the payloads are combined for the final test in the thermal-vacuum environment. During the development of the Micius satellite, two integral space environment tests for the payload combination, the thermal-vacuum-optical measurement and the thermal-balance testing for the entire satellite, are implemented; see Fig. 21.

For the thermal-vacuum-optical measurement shown in Fig. 21(a), the integration of all the scientific payloads are integrated into a thermal-vacuum chamber. The special design of this type of thermal-vacuum chamber is the optical window connected to a large aperture collimator, which can provide measurements on the optical parameters in real time in various thermal-vacuum environments. The divergence angle is one of the key typical optical parameters for the two satellite-based transmitters, and it directly affects the channel loss. The test results of the divergence angles are shown in Fig. 22, which

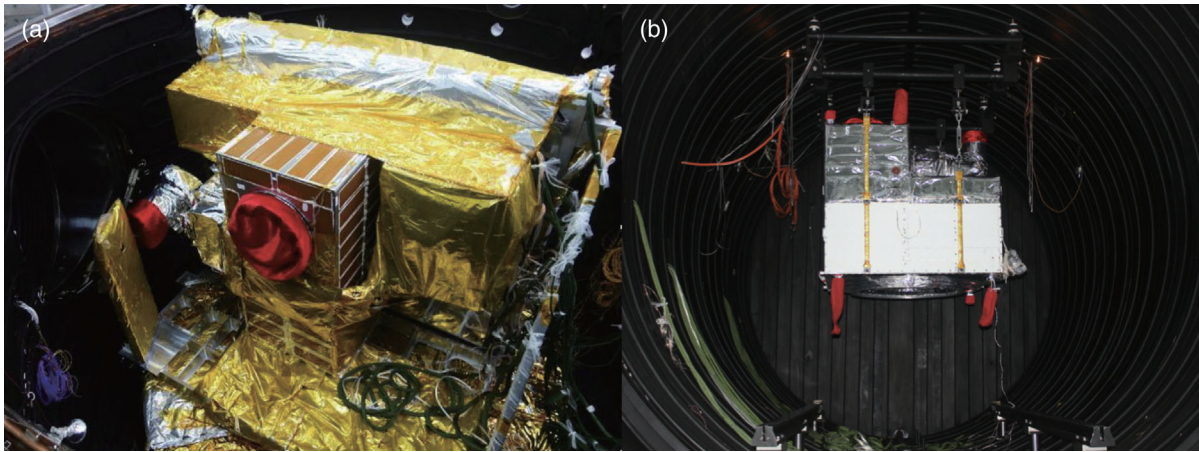


FIG. 21. (a) Thermal-vacuum-optical measurement and (b) thermal balancing testing for a payload combination.

displays the optimum operating temperatures of the two transmitters at 810 and 850 nm, respectively. Furthermore, for transmitters 1 and 2, the divergence angle meets the requirement of  $< 15 \mu\text{rad}$  when the temperature ranges from  $18^\circ\text{C}$  to  $22^\circ\text{C}$ .

Figure 21(b) displays a photo of the entire system of the Micius satellite when thermal-balance testing is carried out, which is typically a part of the systemwide thermal-vacuum testing. It has two main objectives: obtaining thermal data for analytic thermal model correlation and verifying the function of the thermal control of the entire system or the subsystems. The test for the entire system of the Micius satellite lasted for 18 days, and six thermal-balance operating conditions and four thermal cyclings were completed in total.

In addition to the previous three types of space environmental tests, the radiation test is also important. The Micius satellite contains the silicon avalanche photodiodes (Si APDs) in both transmitters for implementing the experiment of the ground-to-satellite quantum teleportation, and for sampling the entangled photons to test the in-orbit performance of the satellite-borne entangled-photon source. The Si APD is a radiation-sensitive device; thus, radiation degrades its performance by increasing dark currents, as well as decreasing responsivity and gain. The radiation test was performed on the spaceborne Si APDs of the Micius satellite using a 50 MeV proton source that effectively penetrated the APD package front glass window. According to the results of the

radiation test, the in-orbit radiation-induced dark count rate (DCR) increment of the silicon APD increased by  $\sim 219$  counts/s each day. Several solutions were developed to mitigate the APD radiation-induced DCR increment rate and guarantee the detector reliability, including multistage cooling technologies and specialized driver electronics for spaceborne low-noise detectors. Through these solutions, the expected detector in-orbit DCR increment rate can be reduced to less than 1 count/s each day, thereby satisfying the requirement of satellite-based quantum science experiments (Ren *et al.*, 2017; Yang *et al.*, 2019).

## VIII. CONSTRUCTION OF COOPERATIVE GROUND STATIONS

To coordinate with the quantum science satellite in implementing experiments, new ground stations need to be built or existing ones upgraded. There is a total of five ground stations in China: four of them receive via downlink channels, while a single station transmits via uplink channels. Every receiving ground station has a large-diameter telescope, i.e., the 1-m-diameter telescope at the Xinglong, China, station of the National Astronomical Observatories (upgraded and rebuilt) for the satellite-to-ground QKD, the 1.8-m-diameter telescope at Lijiang station of the Yunnan Astronomical Observatory (upgraded and rebuilt) for the entanglement distribution experiment, the 1.2-m-diameter telescope at the Nanshan Observatory of the Xinjiang Astronomical Observatory (newly built) for the entanglement distribution and QKD experiments, and the 1.2-m-diameter telescope at the Qinghai station of the Purple Mountain Observatory (newly built) for the entanglement distribution and QKD experiments; see Fig. 23.

The transmitting station with three small transmitter telescopes located in Ngari (Ali), Tibet, was specially constructed for the quantum teleportation experiment from the ground to the satellite, as shown in Fig. 25.

The ground station in Xinglong was upgraded and rebuilt in 2014 for satellite-to-ground QKD experiments. As shown in Fig. 23(b), it consists of a Ritchey-Chrétien telescope, a red beacon laser (671 nm, 2.7 W, 0.9 mrad), a coarse camera (FOV is  $0.33^\circ \times 0.33^\circ$ ,  $512 \times 512$  pixels, frames/s of 56 Hz),

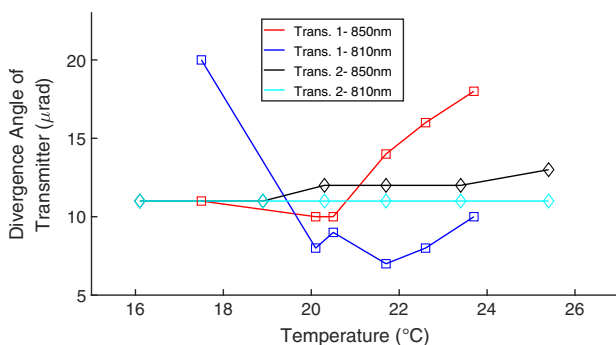


FIG. 22. Test results of divergence angles in thermal-vacuum conditions.

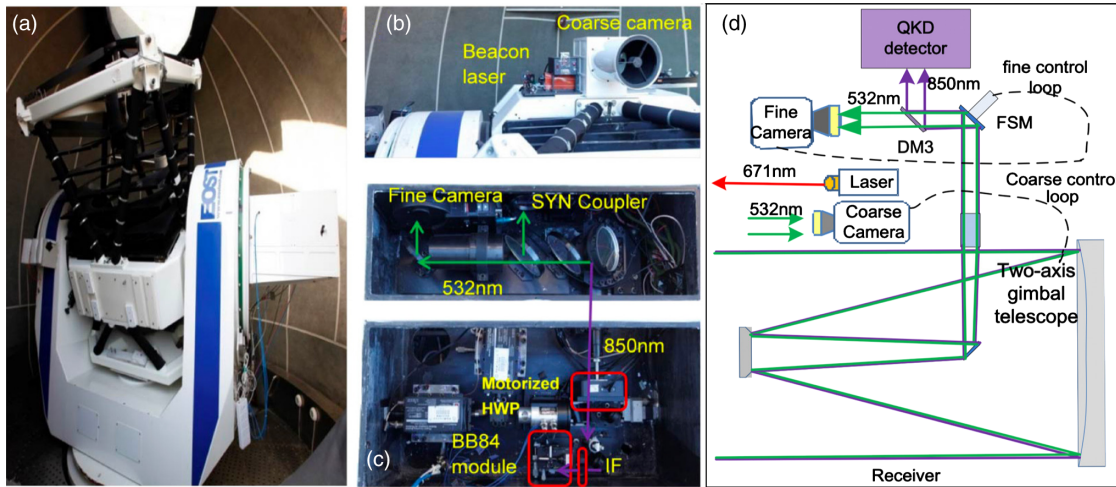


FIG. 23. Typical receiving ground station for the Micius satellite. (a) Two-axis gimbal telescope. (b) Beacon laser and coarse camera. (c) One of the two layers of the optical receiver box. (d) Typical optical design of the receiver including the receiving telescope, the ATP system, and the QKD-detection module. From Liao *et al.*, 2017a.

and an optical receiver box that is installed on the arm of the gimbal. A two-axis gimbal in a control loop with a coarse camera is employed to realize the coarse tracking function. The 532 nm beacon laser coming from the satellite is detected by the coarse camera. Guided by the 532 nm beacon laser, the 671 nm beacon laser transmitted from the ground telescope can point to the satellite precisely. The fine tracking system and the BB84 measurement module are mounted in the receiver box. The fine tracking system includes mainly a FSM based on voice coil and a fine camera (FOV is  $1.3 \times 1.3$  mrad,  $128 \times 128$  pixels, frames/s of 212 Hz). A dichroic mirror was used to separate the 850 nm photons from the 532 nm beam. A beam splitter (BS) was used to divide the 532 nm beam into two parts: one was detected by the fine camera for tracking, while the other was coupled to the fiber linked to a single-photon detector for the time synchronization. The 850 nm photons are measured using a customized BB84 polarization analysis module after passing them through a beam expander, a motorized HWP, and an interference filter. The detectors' electrical output pulses and the GPS-PPS signal are fed into a TDC that records the detection time and the channel number of the detectors.

For the mission of the satellite-based entanglement distribution, three ground stations located, respectively, in Delingha, Urumqi, and Lijiang, China, are involved. The distance between Delingha and Lijiang (Nanshan, China, in Urumqi) is approximately 1203 km (1120 km). Two new telescopes (with a diameter of 1.2 m) with the same design were built in Nanshan and Delingha in 2015, mainly for entanglement distribution experiments, as well as satellite-to-ground QKD experiments. All the optical elements in the two telescopes have a polarization-maintaining property. The measurement boxes are installed on one of the rotating arms, and they rotate along with the telescopes, as shown in Fig. 23(a). The Lijiang ground station was upgraded in 2016 specifically for the satellite-based quantum entanglement distribution experiments. At the Lijiang station, the original telescope with a large diameter of 1.8 m was modified for the quantum satellite-based experiments. The designs of

the measurement boxes in these three stations are similar; see Fig. 24.

Typically, the FSM and the camera are combined to construct a closed-loop fine tracking system. The 850 and 532 nm photons are coupled into multimode fibers with a  $320 \mu\text{m}$  core for the synchronization. Together with a Pockels cell, an integrated 810 nm module with a PBS inside achieved a random polarization analysis of the signal photons. For the Bell test, quantum random-number generators were employed to afford the random measurement basis choice.

The Ali ground station was completed in 2016, and it has the highest altitude (5100 m) of the five stations. Three optical telescopes with a diameter of 130 mm were employed as the transmitting antennas for the ground-to-satellite teleportation, as shown in Fig. 25(a). To improve the transmitting efficiency, a double off-axis parabolic structure is employed in these telescopes; see Fig. 25(b). All the optical components in the transmitting antenna have polarization-maintaining capabilities. The wave-plate combinations are employed to correct the unknown transformations applied by the single-mode fibers and to automatically compensate for the deviation of the polarized base vector caused by the movement of the satellite. The polarization fidelity of the entire system exceeded 99.5%. The FSM and a high-speed CCD constitute the ground fine tracking system, which realizes the pointing and tracking for the satellite at high accuracy. The tracking accuracy of the entire system is less than  $3 \mu\text{rad}$  ( $1\sigma$ ). Two 671 nm beacon lasers (power, 2 W; divergence angle, 1.2 mrad) are installed atop the two transmitting telescopes for satellite tracking on the ground.

For time synchronization, the 532 nm beacon laser in the satellite-based transmitter is designed as a pulse laser to perform synchronization; it is a passive  $Q$ -switching-type laser with a repetition frequency of  $\sim 10$  kHz and an optical pulse width of 0.88 ns. A part of the laser is guided into a fast photodiode to convert it into an electrical pulse signal. Both the pulse signal and the GPS-PPS signal from the satellite are fed into the TDC module of the transmitter.

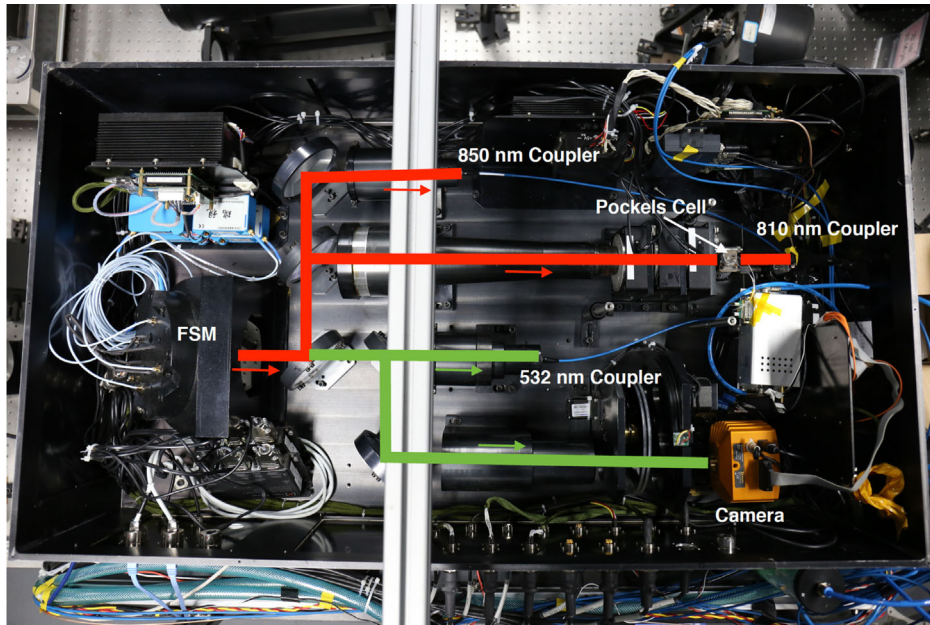


FIG. 24. Photograph of the measurement box at Lijiang station, which represents the typical design of the satellite-based entanglement distribution. From Yin *et al.*, 2017a.

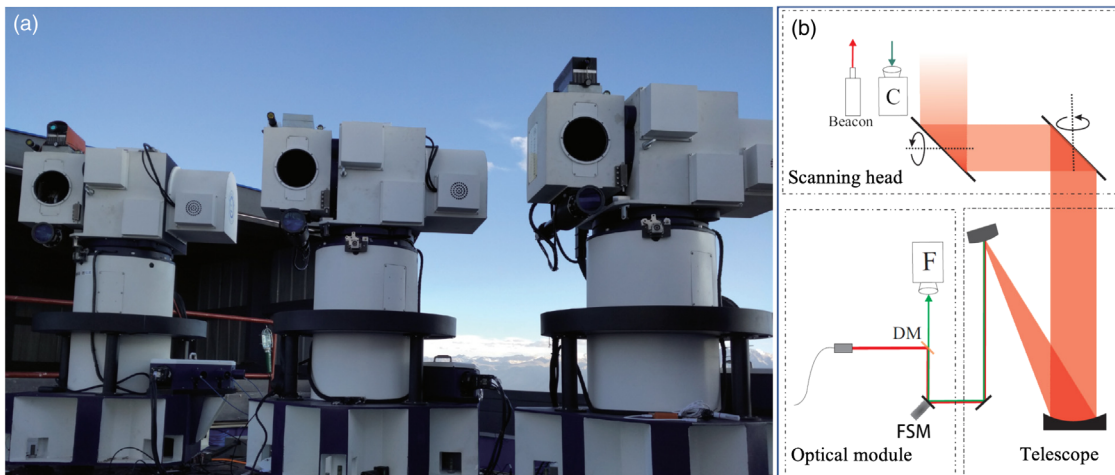


FIG. 25. Transmitting telescope and optical design. (a) Photograph of three transmitting optical antennas, which are placed side by side on a platform and which back up each other. Quantum signals generated from the lab at floor 1 are transmitted to three telescopes. The beacon lasers and sync laser are equipped on top of the transmitting antennas. (b) Optical design of the transmitting telescope, which comprises a scanning head, a transmitting telescope, and an optical module. From Ren *et al.*, 2017.

The acquired data are stored in memory for further processing. In the ground station, a part of the 532 nm laser beam is sent to a single-photon detector. The output signal of the single-photon detector, together with the four single-photon detectors' electrical output pulses and the GPS-PPS signal, is fed into a TDC. The time synchronization process between the satellite and the ground can be divided into two steps. First, according to the predicted light-flight time and the GPS-PPS signal, the received synchronization laser pulse sequence on the ground can be matched with the satellite. Second, based on the results of step 1, the time between the satellite and the ground will be synchronized. Finally, a typical temporal distribution of QKD photons with

a standard deviation is obtained at around 529 ps, with a signal time window of 2 ns (Liao *et al.*, 2017a).

## IX. SATELLITE-BASED QUANTUM EXPERIMENTS WITH MICIUS

After our full verification of the feasibility of satellite-based quantum communication, we review in this section the development of a sophisticated satellite named after the ancient Chinese scientist Micius. It was successfully launched in August 16, 2016, in Jiuquan, China, orbiting at an altitude of  $\sim 500$  km. Coordinated ground observatory stations have been built worldwide to conduct the designed

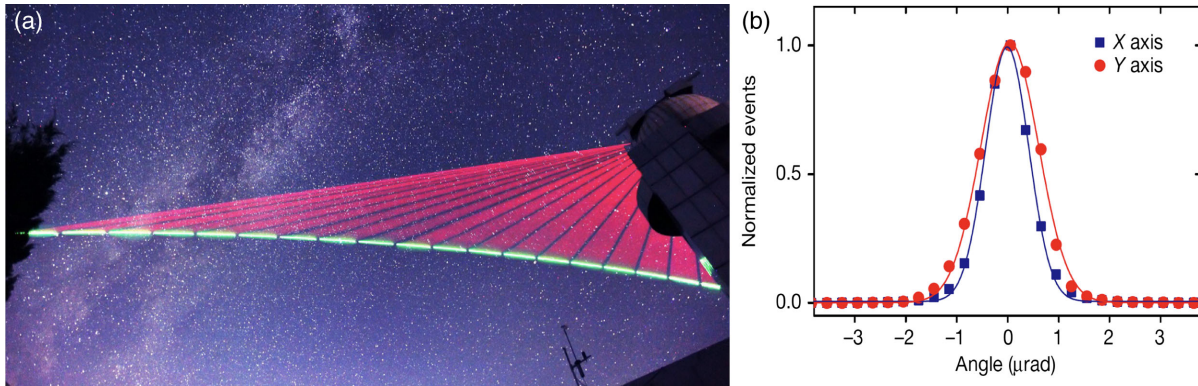


FIG. 26. Establishing a reliable space-to-ground link for the quantum state transfer. (a) Overlaid and time-lapse photographs of the beacon lasers for tracking when the satellite flies over the Xinglong ground station. Red and green lasers are sent from the ground and the satellite, respectively, with divergence angles of 0.9–1.25 mrad. (b) Distribution of longtime tracking errors (shown as the number of detected events normalized by the maximum count in each bin) of the  $x$  and  $y$  axes extracted from the real-time images read out from the fast camera. From [Liao \*et al.\*, 2017a](#).

experiments for QKD, entanglement distribution, quantum teleportation, and foundational tests in quantum physics.

#### A. Satellite-to-ground quantum key distribution

After the satellite Micius was launched, the first goal was to establish a space-ground quantum link and perform QKD from satellite to ground ([Liao \*et al.\*, 2017a](#)). The Chinese team observed the first “handshake” between the satellite and Xinglong ground station near Beijing, China, ten days after the launch; see Fig. 26(a) for overlaid and time-lapse photographs of a tracking laser as the satellite flies over a ground station. As discussed in Sec. V.A, the downlink has reduced beam spreading compared to the uplink because the beam wandering occurs at the end of the transmission path, which is typically smaller than the effect from the beam diffraction. The 300-mm-aperture telescope equipped in the satellite produced a near-diffraction-limited far-field divergence of about  $10 \mu\text{rad}$ . Such a narrow divergence beam from the fast-traveling satellite (with a speed of about 7.6 km/s)

requires a fast and precise APT. A tracking accuracy of approximately  $1.2 \mu\text{rad}$  [see Fig. 26(b)] was achieved, which is much smaller than the beam divergence. Note that, due to the quiet environment in outer space, the tracking accuracy is better than it was in previous ground tests, which deliberately set a more stringent condition. A diffraction loss of approximately 22 dB was obtained at 1200 km, whereas the loss due to a pointing error was below 3 dB. Additionally, the loss due to atmospheric absorption was 3–8 dB.

The satellite passes each ground station with a Sun-synchronous orbit at midnight local time daily for a duration of about 5 min. Figure 27 shows an experimental procedure for the satellite-to-ground QKD. The Scientific Experiment Plan Center arranged the experiment for days in which the calculated maximum elevation angle of the satellite to the ground station is greater than  $30^\circ$  (based on predicted satellite orbits) and clear nighttime skies are forecast. If these conditions are met, instruction sequence files for the satellite are made and sent to the ground support center. The instruction file, which is translated into a coding file, is then executed.

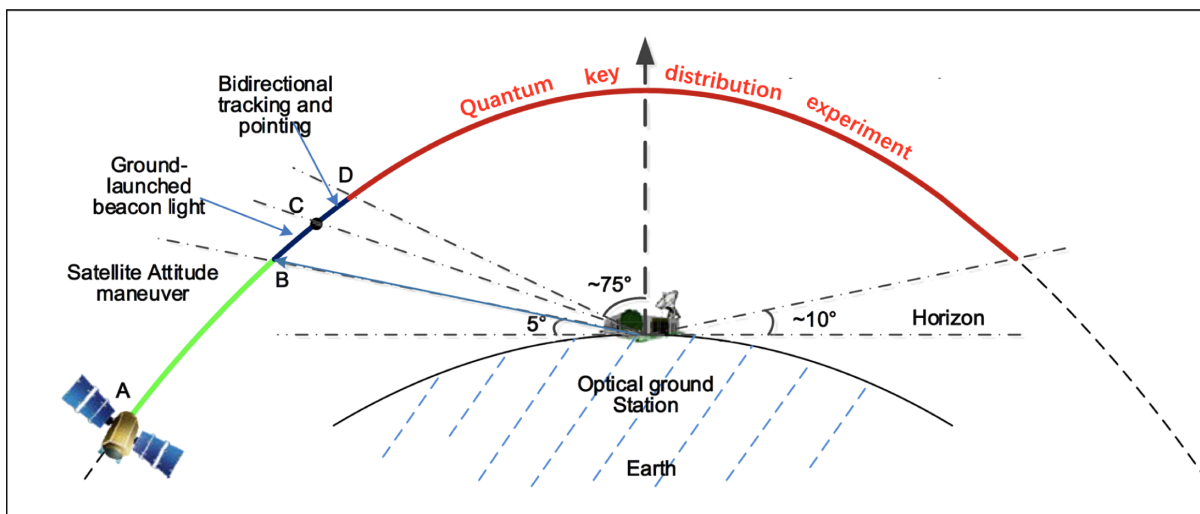


FIG. 27. Tracking and QKD processes during an orbit. From [Liao \*et al.\*, 2017a](#).

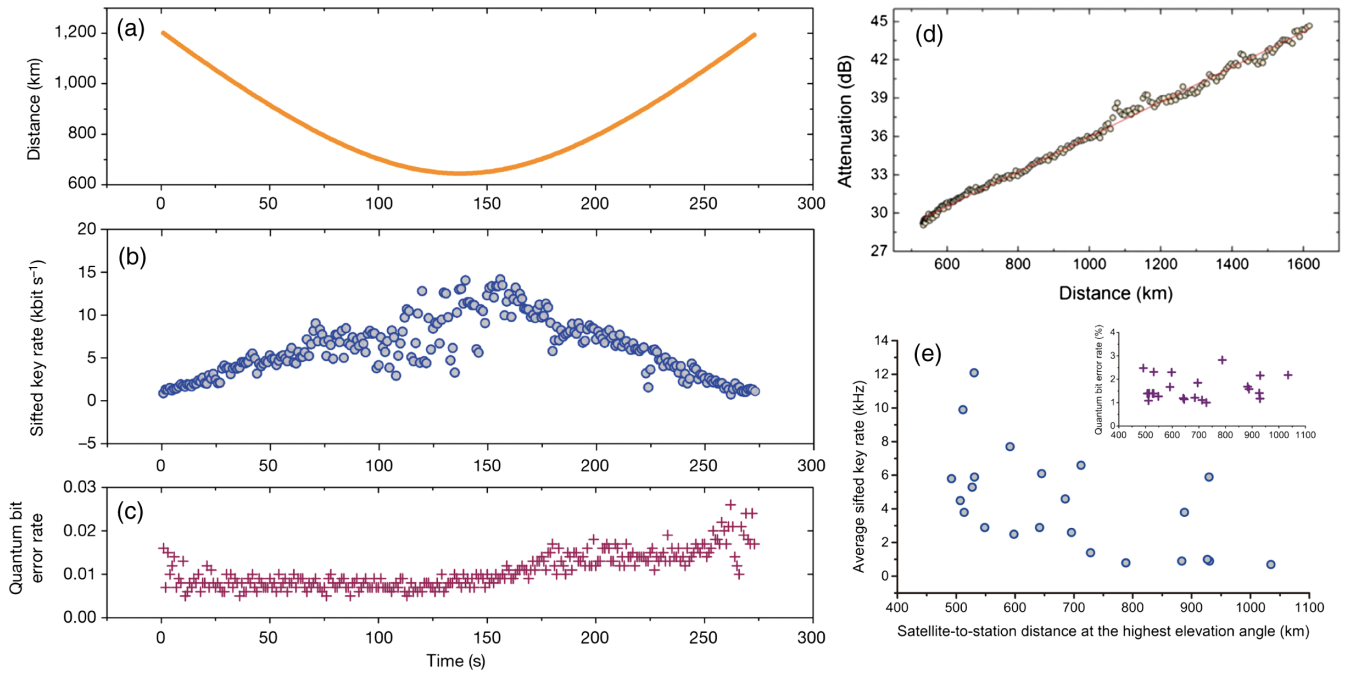


FIG. 28. Performance of satellite-to-ground QKD during one orbit. (a) Trajectory of the Micius satellite measured at the Xinglong ground station. (b) Sifted key rate as a function of time and physical distance from the satellite to the station. (c) Observed quantum bit error rate. (d) Attenuation of the downlink channel with different distances between the satellite and the ground. (e) Summary of the QKD data obtained on 23 different days. The  $x$  axis is the shortest satellite-to-station distance, which occurs at the highest elevation angle and varies on different days. The  $y$  axis is the average sifted key rate. From [Liao \*et al.\*, 2017a](#).

The attitude of the satellite is adjusted to point at the ground station 10 min before the satellite enters the shadow zone. When the satellite's angle of elevation exceeds  $5^\circ$ , its attitude control system ensures that the transmitter is pointing to the ground station with a coarse orientation accuracy of better than  $0.5^\circ$ . The closed-loop APT systems then start bidirectional tracking and pointing, ensuring that the transmitter and receiver are robustly locked with a tracking accuracy of  $\sim 1.2 \mu\text{rad}$  through the entire orbit; see Fig. 26(b). From a  $15^\circ$  elevation angle, the decoy-state QKD transmitter sends signal and decoy photons together, which are received and decoded by the ground station, until the satellite reaches an angle of elevation of  $10^\circ$  in the other end when a single-orbit experiment ends.

Apart from being used in the APT, the beacon laser also serves for obtaining the arrival time of the single photons in order to compensate for the space-ground clock drift. The obtained time synchronization jitter, which is useful for filtering the background noise, is 0.5 ns. Additionally, a spectral bandpass filter is used in the receiver to reduce the background scattering. Finally, a motorized half-wave plate is used to dynamically compensate for the time-dependent photon polarization rotation during the satellite passage.

In the experiment, we employed the decoy-state BB84 protocol, a form of QKD that uses weak coherent pulses at high channel loss and is immune to photon-number-splitting eavesdropping. Since September 2016, QKD has been performed routinely under good atmospheric conditions. An example of relevant QKD data obtained on December 19, 2016 is shown in Fig. 28. The satellite-observatory separation ranged from 645 to 1200 km. The experiment collected

3 551 136 detection events in the ground station after 273 s and 1 671 072 bits of sifted keys. In Fig. 28(b), the sifted key rate was about 12 kbits/s at 645 km and 1 kbits/s at 1200 km. This was due mainly to an increase in both the physically separated distance and the effective thickness of the atmosphere near Earth at smaller elevation angles. The observed bit error rate had an average of 1.1%. By performing error correction and privacy amplification, the secure final key was 300 939 bits when the statistical failure probability was set to  $10^{-9}$ , corresponding to a key rate of 1.1 kbits/s.

Meanwhile, similar QKD experiments were routinely performed at other ground stations, such as Delingha. The typical LEO satellite-to-ground channel attenuation was calibrated during one orbit and varied from 29 dB at 530 km to 44 dB at 1600 km, as plotted in Fig. 28(d). Figure 28(e) shows a summary of QKD experiments performed over 23 days, with the physical distance between the satellite and the ground station varying each day.

The performance of the satellite-based QKD can then be compared to the conventional method of direct transmission through telecommunication fibers. Figure 29 shows the extracted link efficiency at the distance of 645–1200 km from the observed count rate, with the theoretically calculated link efficiency using fibers with a 0.2 dB/km loss. At 1200 km, the satellite-based QKD within the 273 s coverage time demonstrated a channel efficiency approximately 20 orders of magnitudes higher than that using the optical fiber. Comparing the data in Fig. 29, using a 1200 km fiber, even with a perfect 10 GHz single-photon source and ideal single-photon detectors with no dark count, we can obtain only one bit sifted key over  $6 \times 10^6$  yr.

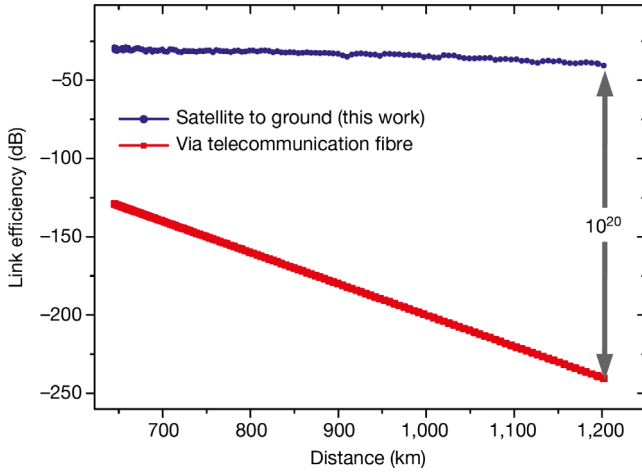


FIG. 29. Link efficiencies for direct transmission through telecommunication optical fibers (red line) and following the satellite-to-ground approach (blue line). The link efficiencies for the latter were calculated by dividing the photon intensity that arrived in front of the detectors at the ground station by that from the output of the satellite's transmitter. From [Liao \*et al.\*, 2017a](#).

Improving the final key rate is always one of the main goals of the practical QKD. Recently the average secret-key rate has been improved to 47.8 kbits/s for a typical satellite pass, which is more than 40 times higher than previous results ([Liao \*et al.\*, 2017a](#)), as shown in Fig. 30. Such an improvement of the final key rate is due to the following: (1) The signal state ratio increased from 0.5 to 0.72, the Z-base ratio increased

from 0.5 to 0.889 at the satellite and 0.5 to 0.9 on the ground station, thereby enhancing the key rate by 2.34 times. (2) The repetition frequency increased from 100 to 200 MHz. (3) The ground telescope aperture increased from 1 to 1.2 m, corresponding to an increment of about 1.5 times. (4) The quantum bit error rate (QBER) is reduced and the raw-key size increased to about 2 times. (5) The ground coupling efficiency increased from 14% to 40%, corresponding to an increment of about 3 times ([Chen \*et al.\*, 2021](#)).

## B. Satellite-based entanglement distribution

The second planned mission of the Micius satellite was a bidirectional distribution of its spaceborne entangled photons to two distant locations on Earth ([Yin \*et al.\*, 2017a](#)). Long-distance entanglement distribution is essential for both foundational tests of quantum physics and scalable quantum networks. Owing to channel loss, however, the previously achieved distance was limited to  $\sim 300$  km ([Inagaki \*et al.\*, 2013](#)). This is due mainly to the photon loss in the channel (optical fibers or terrestrial free space), which normally scales exponentially with the channel length. For example, using a bidirectional distribution of an entangled source of photon pairs with a 10 MHz count rate directly through two 600 km telecommunication fibers with a loss of 0.2 dB/km, we can obtain only  $10^{-17}$ /s two-photon coincidence events.

For the mission of entanglement distribution, three ground stations, located at Delingha in Qinghai, China, Nanshan in Urumqi, Xinjiang, China, and Gaomeigu Observatory in Lijiang, Yunnan, China, are cooperating with the satellite.

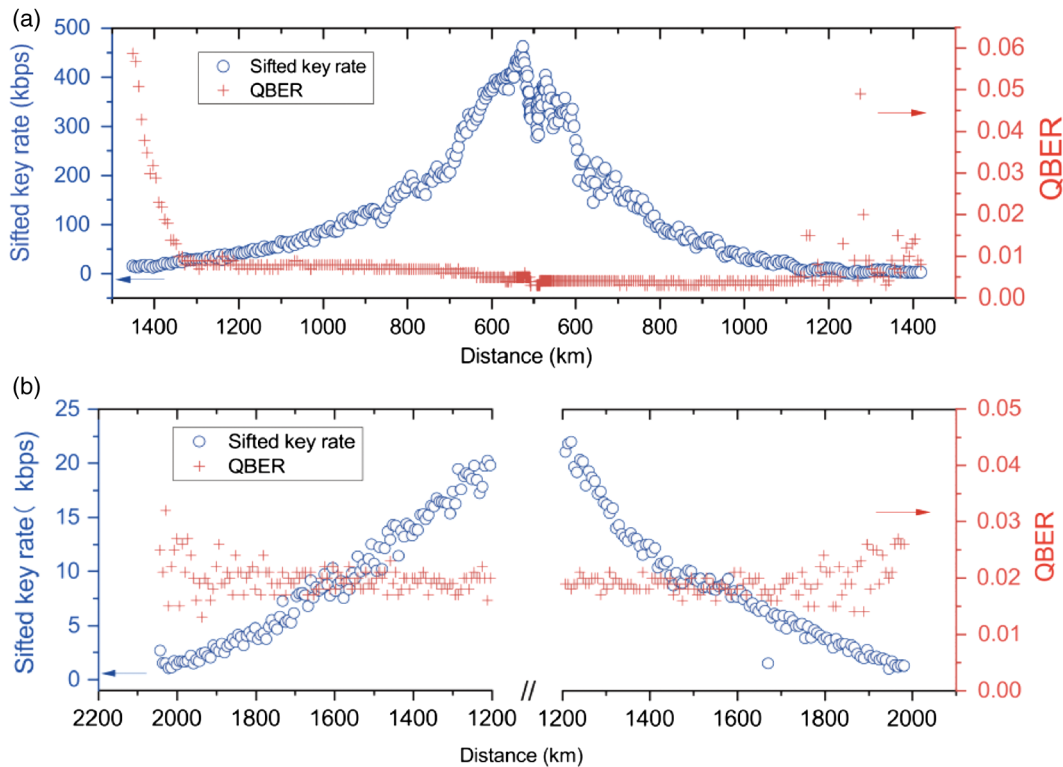


FIG. 30. Performance of high-speed satellite-to-ground QKD. (a) Sifted key rate and observed QBER as a function of physical distance from the satellite to the Nanshan station. (b) Test for long-distance satellite-to-ground QKD. The sifted key rate and observed QBER are at a distance beyond 1200 km. From [Chen \*et al.\*, 2021](#).

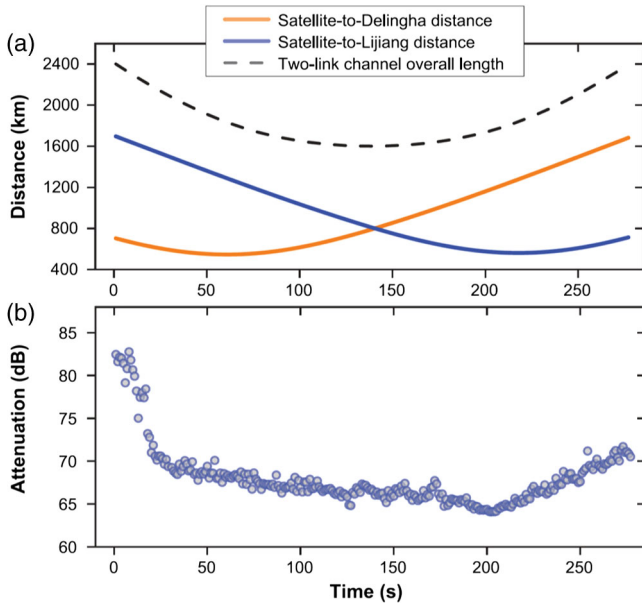


FIG. 31. (a) Typical two-downlink transmission from the satellite to Delingha and Lijiang that lasted for about 275 s in one orbit. The distance from the satellite to Delingha varies from 545 to 1680 km. The distance from the satellite to Lijiang varies from 560 to 1700 km. The overall length of the two-downlink channel varies from 1600 to 2400 km. (b) Measured two-downlink channel attenuation in one orbit using the high-intensity reference laser coaligned with the entangled photons. The highest loss is 82 dB at a total distance of 2400 km, when the satellite has just reached a  $10^\circ$  elevation angle observed from Lijiang station. Since its telescope (the largest) has a diameter of 1.8 m and thus has a higher receiving efficiency than other stations, when the satellite flies over Lijiang at an elevation angle of more than  $15^\circ$ , the channel loss remains relatively stable (from 64 to 68.5 dB). From [Yin \*et al.\*, 2017a](#).

The physical distance between Delingha and Lijiang (Nanshan) is 1203 km (1120 km). The separation between the orbiting satellite and these ground stations varies from 500 to 2000 km. At Delingha, Lijiang, and Nanshan stations, the receiving telescopes have diameters of 1200, 1800, and 1200 mm, respectively. The entanglement distribution was achieved both between Delingha and Lijiang and between Delingha and Nanshan. The experiment involving Delingha and Lijiang is described later. Figure 31(a) plots the physical distances from the satellite to Delingha and Lijiang during one orbit and the sum channel length of the two downlinks.

The satellite (Fig. 20) emits  $5.9 \times 10^6$  entangled photon pairs per second, which are then sent out using two telescopes. Cascaded multistage closed-loop APT systems are designed in both transmitters and receivers, establishing two independent satellite-to-ground quantum links simultaneously. Using a reference laser on the satellite, the overall two-downlink channel attenuation can be measured in real time, which varies from 64 to 82 dB [Fig. 31(b)]. A slight asymmetry is observed in the attenuation curve, when the satellite moves closer to Lijiang. Furthermore, the link efficiency is higher because Lijiang station has a larger-aperture telescope.

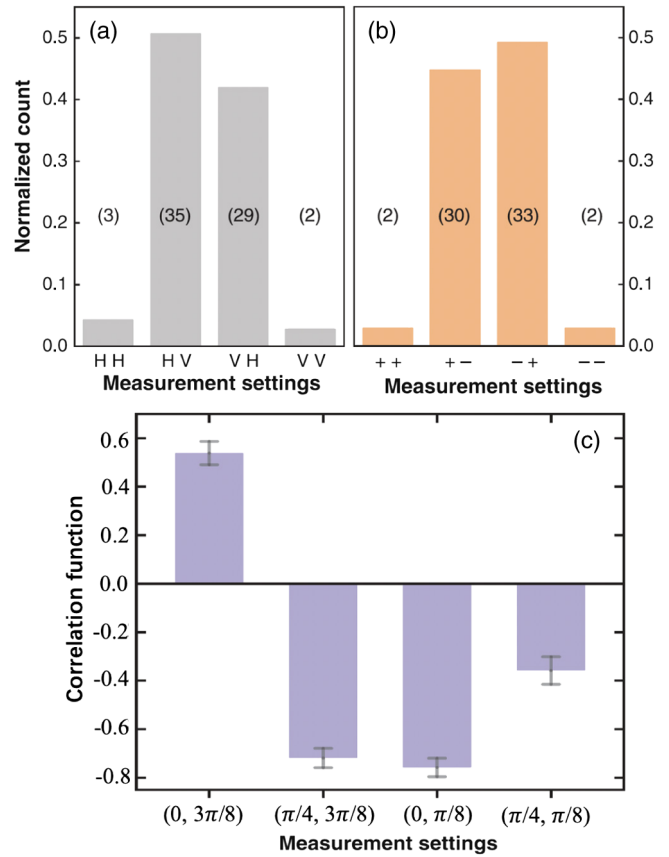


FIG. 32. (a) Normalized two-photon coincidence counts in the measurement setting of the  $H/V$  basis. (b) Normalized counts in the diagonal basis. (c) Correlation functions of a Clauser-Horne-Shimony-Holt-type Bell inequality for the entanglement distribution. Error bars are 1 standard deviation and are calculated from propagated Poissonian counting statistics of the raw photon. From [Yin \*et al.\*, 2017a](#).

The experiment observed an average two-photon count rate of 1.1 Hz, with a signal-to-noise ratio of 8:1. Compared to the previous entanglement distribution method by direct transmission of the same two-photon source using the common commercial telecommunication fibers with a loss of 0.2 dB/km (the best performance fiber with a loss of 0.16 dB/km), the effective link efficiency of the satellite-based approach within a 275 s coverage time is 17 (12) orders of magnitude higher than the one with the same transmission distance in fibers.

The received photons were analyzed using a half-wave plate, a polarizing beam splitter, and a Pockels cell controlled by 4 Mbits/s random numbers. To verify whether both photons are still entangled after passing an overall distance ranging from 1600 to 2400 km, we obtained 134 coincidence counts during an effective time of 250 s in satellite-orbit shadow time. From the  $H/V$  and diagonal basis measurements, the state fidelity of the two photons distributed over 1203 km was estimated to be  $0.869 \pm 0.085$ .

The distributed entangled two photons were then employed for a Bell test. The experimental configuration and Pockels cells used were fast enough to close the locality and freedom-of-choice loopholes. The Bell test ran 1167 trials during an

effective time of 1059 s, with the observed data summarized in Fig. 32. A violation of the Bell inequality of  $2.374 \pm 0.093$  by 4 standard deviations was obtained. The result again confirms the nonlocal feature of entanglement and excludes the models of reality, which sit on the notions of locality and realism, in a new space scale with thousands of kilometers.

### C. Entanglement-based quantum key distribution

In the experiment involving the entanglement distribution between Lijiang and Delingha over 1200 km, the observed two-photon count rate of 1.1 Hz and signal-to-noise ratio of 8:1 was sufficient for violating Bell's inequality. However, the key rate and the quantum bit error rate there (8.1%) were insufficient for performing entanglement-based quantum cryptography (Ekert, 1991). Entanglement-based QKD is particularly attractive because of its inherent source-independent security (Koashi and Preskill, 2003; Ma, Fung, and Lo, 2007), which allows security to be established without any assumption of trusted relay.

Inside laboratories, the record length of QKD was about 500 km in coiled fiber (Yin *et al.*, 2016; Boaron *et al.*, 2018; Chen *et al.*, 2020). The satellite-to-ground decoy-state QKD reviewed in Sec. IX.A achieved a point-to-point distance of 1200 km (Liao *et al.*, 2017a), which, however, was not for two ground users. Without using trusted relays, the QKD distance

for two ground users was about 100 km over terrestrial free space (Ursin *et al.*, 2007; Yin *et al.*, 2012).

After the first satellite-based entanglement distribution (Yin *et al.*, 2017a, 2017b), an experiment (Yin *et al.*, 2020) was performed between the ground stations of Delingha and Nanshan, which are separated by 1120 km. The receiving efficiencies were considerably improved using a higher efficiency telescope and follow-up optics. Both ground stations used newly built telescopes with diameters of 1.2 m. In the telescopes, the main lens was recoated and the beam expander was redesigned. In the follow-up optics, the collection efficiency was enhanced by optical pattern matching, particularly by shortening the optical path by reducing spectral splitting to avoid the beam spread. With these technical improvements, Yin *et al.* observed an average two-photon count rate of 2 Hz (corresponding to an increase of the two-photon link efficiency by a factor of 4), which significantly increased the obtained key rate and decreased the quantum bit error rate from 8.1% to 4.5%.

Yin *et al.* (2020) made a special effort to ensure that its implementation was practically secure against all known side channels. Because of the source-independent nature of the entanglement-based QKD, the system was immune to any loopholes in the source, and all that remained was to ensure the security on the detection sides at both ground stations. In general, the side channels (known and to be known) on the detection sides primarily violate the assumption of fair

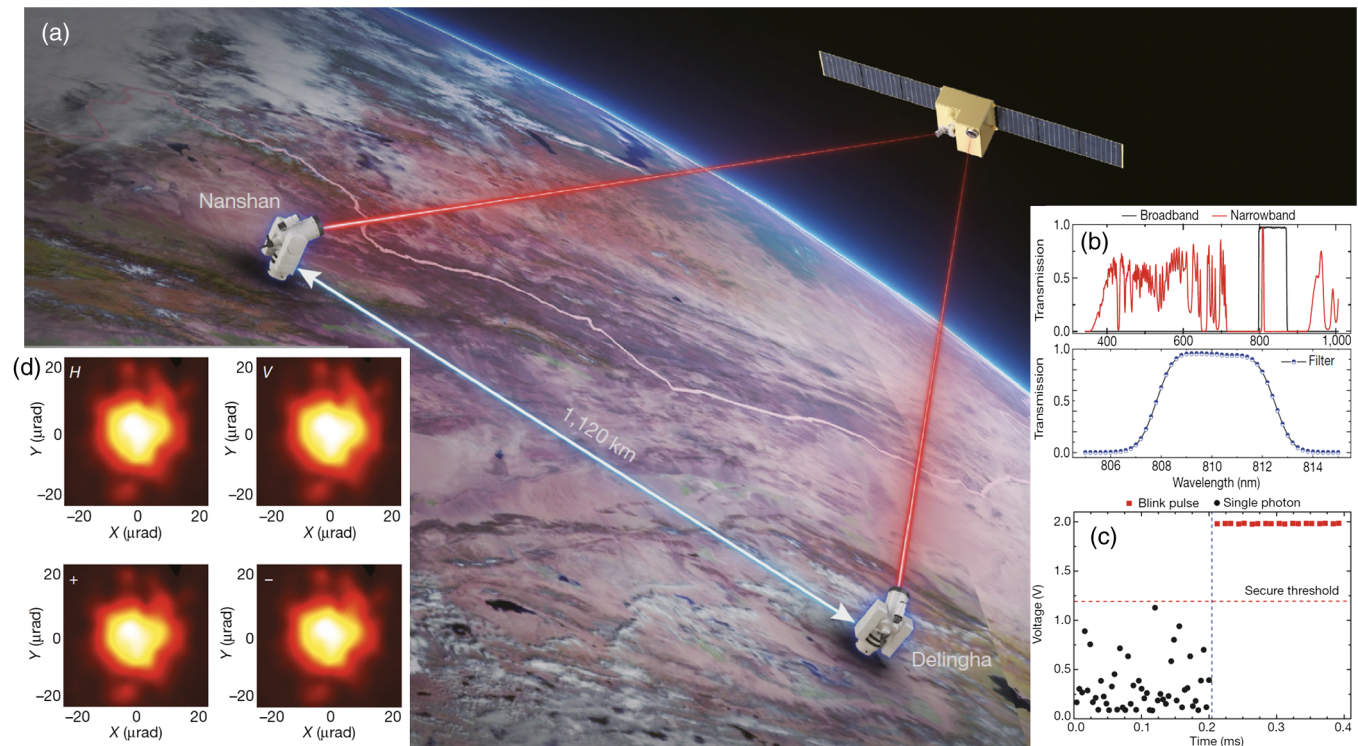


FIG. 33. Overview of the experimental setup of quantum key distribution based on the entanglement distribution. (a) Illustration of the Micius satellite and the two ground stations. From the Fengyun-3C/Visible and Infrared Radiometer. (b)–(d) Monitoring and filtering against the side channels. (b) Transmission of broad-bandwidth and narrow-bandwidth filters. (c) Output of monitoring circuit with or without a blinding attack. Without a blinding attack, the outputs are random avalanching single-photon-detection signals (black dots). With a blinding attack (starting at 0.2 ms), the output signals are at around 2 V, which is above the security threshold, thus triggering the security alarm. (d) System detection efficiency of the four polarizations in the spatial domain. With the spatial filter, the four efficiencies are identical. From Yin *et al.*, 2020.

sampling. Note that the concept of “fair sampling” refers here to the consistency of different receiving detectors on spatial and spectral freedom of the arrival beams, which differs from the experimental requirement of addressing the “fair-sampling loophole” of the Bell test. Experimentally, Yin *et al.* ensured the validity of the fair sampling by filtering in different degrees of freedom, including frequency, spatial, and temporal modes. In addition, countermeasures were taken for the correct operation of the single-photon detectors, as shown in Fig. 33. They considered all known detection attacks, including detector-related attacks (Zhao *et al.*, 2008; Lydersen *et al.*, 2010; Weier *et al.*, 2011), wavelength-dependent attacks (Li *et al.*, 2011), spatial-mode attacks (Sajeed *et al.*, 2015), and other possible side channels. For example, for the side channels targeting the operation of detectors, such as blinding attacks (Lydersen *et al.*, 2010), additional monitoring circuits were used to monitor the anode of the load resistance in the detection circuit to counter the blinding attack. For time-shift attacks (Zhao *et al.*, 2008) and dead-time attacks (Weier *et al.*, 2011), the countermeasure was to operate the detector in free-running mode, in which the detector records all the detection events and postselects the detection windows such that the detection efficiency is guaranteed to be at a nominal level. Consequently, the secret key generated by this QKD system is secure under realistic devices.

By running 1021 trials of the Bell test during an effective collection time of 226 s, Yin *et al.* observed that the parameter  $S$  was  $2.56 \pm 0.07$ , with a violation of local realism by 8 standard deviations. Having violated the Bell’s inequality, they demonstrated the entanglement-based QKD using the protocol presented by Bennett, Brassard, and Mermin in 1992 (BBM92), where both Alice and Bob took measurements randomly along the  $H/V$  and  $+/-$  bases (Bennett, Brassard, and Mermin, 1992). Owing to their efforts to ensure the fair-sampling assumption, the practical security of the BBM92 protocol is compatible with the Ekert91 one.

Within 3100 s of data collection time, 6208 initial coincidences were obtained, which gave 3100 bits of sifted keys with 140 erroneous bits. The quantum bit error rate was  $4.5\% \pm 0.4\%$ . After error correction and privacy amplification, the secure key rate of 0.43 bits/s in the asymptotic limit of an infinite long key and a finite secret-key rate of 0.12 bits/s were obtained. More details on the final key rate were discussed by Lim *et al.* (2021). The secure key rate was 11 orders of magnitude higher than would be obtained by direct transmission of entangled photons over 1120 km through the best commercial fibers. The results increase the secure distance of practical QKD for ground users by 10 times of the order of a thousand kilometers, representing a key step toward the holy grail of cryptography. Note that using the newly developed entangled-photon source with a 1 GHz generation rate (Cao *et al.*, 2018) can increase the secure key rate by about 2 orders of magnitude.

#### D. Ground-to-satellite quantum teleportation

The third mission of the Micius satellite was to perform quantum teleportation of a single photon from an observatory ground station in Ngari to the satellite, which is an uplink; for an overview, see Fig. 34(a) (Ren *et al.*, 2017). The uplink

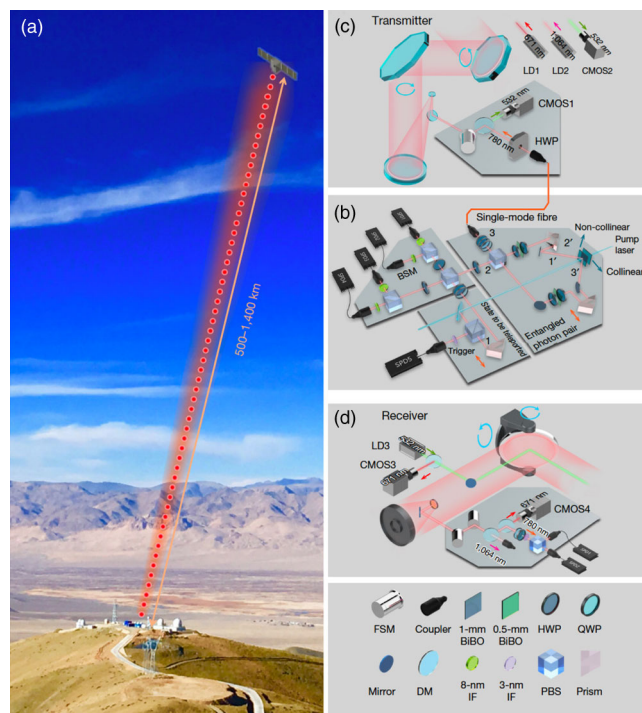


FIG. 34. Overview of the setup for ground-to-satellite quantum teleportation of a single photon over distances of up to 1400 km. (a) Schematic of the satellite overlaid on a photograph of the Ngari ground station in Tibet. The separation between the satellite and the ground station varies from about 500 to 1400 km during quantum teleportation. (b) Compact multiphoton setup for teleportation at the ground station. (c) Transmitter at the ground station. (d) Receiver on the satellite. From Ren *et al.*, 2017.

teleportation experiment has two additional challenges compared to the previous downlink work. First, the teleportation of an independent single photon requires a multiphoton interferometry with a coincidence count rate several orders of magnitude lower than typical single- or two-photon experiments. Second, the atmospheric turbulence in the uplink channel occurs at the beginning of the transmission path, which causes beam wandering and broadening that increases the amount of spreading of the traveling beams.

A compact design of ultrabright four-photon sources that used both collinear and noncollinear spontaneous parametric down-conversion (SPDC) [see Fig. 34(b)] was employed to meet the extreme conditions of the field experiment in Ngari. The four-photon interferometry system was integrated into a compact platform with dimensions of  $460 \times 510 \times 100 \text{ mm}^3$  and weighing less than 20 kg. The pump laser was used for two identical multiphoton modules built sequentially, where the multiplexed four-photon count rate was 8200/s. Note that using the newly developed SPDC source (Zhong *et al.*, 2018) improved the four-photon count rate by a factor of  $\sim 10$ .

The teleported single photons from a single-mode fiber were transmitted through a 130-mm-diameter off-axis reflecting telescope [Fig. 34(c)] and were received by a 300-mm-diameter telescope in the satellite [Fig. 34(d)]. Both the transmitter and the receiver were equipped with APT systems to optimize the uplink efficiency. Figure 35 shows the time

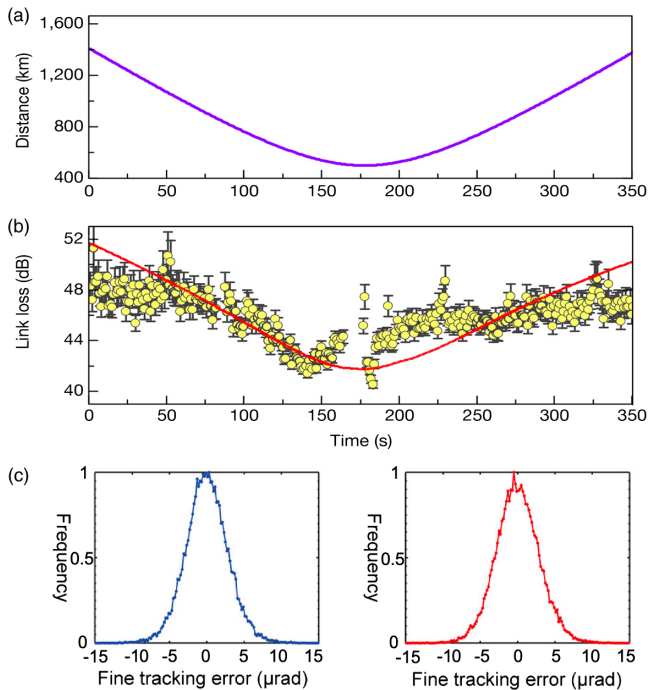


FIG. 35. Distance from the ground station to the orbiting satellite and the measured attenuation during one orbit. (a) Trajectory of the Micius satellite measured from the Ngari ground station over one orbit with a duration of 350 s. (b) The measured ground-to-satellite channel loss using a strong reference laser as a function of time. The highest loss is about 52 dB at a distance of 1400 km (when the satellite is at an angle of  $14.5^\circ$ ). The lowest loss is about 41 dB at a distance of around 500 km (when the satellite is at an angle of  $76.0^\circ$ ). The red curve is a model that considers the effect of distance variation. Error bars show 1 standard deviation, calculated from Poissonian counting statistics. Owing to the structure of the altazimuth telescope at the ground station, the rotation speed of the optical transmitter has to be increased as a function of the increasing altitude angle of the satellite. When the satellite reaches the top altitude angle, the speed that is required can be large and beyond the ability of the APT system. The tracking accuracy is therefore reduced with increasing rotational speed, leading to larger measured channel attenuation when the satellite is closer to the ground station. As a result, the trend in the data appears more compressed than in the model. This model does not fully capture all of the features of the measured data of the channel loss. (c) Performance of the APT system on the  $x$  (horizontal; blue curve) and  $y$  (vertical; red curve) axes. From Ren *et al.*, 2017.

trace of channel attenuation measured during one orbit of the satellite passing through the Ngari station. The physical distance between the ground station and the satellite varies from a maximum of 1400 km (at an altitude angle of  $14.5^\circ$ , the starting point of our measurement) to a minimum of 500 km (at the highest altitude angle of  $76.0^\circ$ , when the satellite passes through the ground station above the top). Here the channel loss of the uplink falls from 52 to 41 dB when measured using a high-intensity reference laser.

An important technical note is that, when they are exposed to radiation in the space environment, the dark count of the single-photon detectors increases significantly. To mitigate

this problem, the detectors are carefully shielded and cooled down to  $-50^\circ\text{C}$ . This reduces the dark counts to less than 150 Hz over three months. The teleportation data, with an overall 911 four-photon counts, was collected in 32 orbits. For the set of the six input states on a mutually unbiased basis, the teleportation state fidelities produced an average of  $0.80 \pm 0.01$ .

### E. Satellite-relayed intercontinental quantum key distribution

The Micius satellite can be further exploited as a trustful relay to conveniently connect any multiple points on Earth to form a network for high-security key exchange. To further demonstrate the Micius satellite as a universal and robust platform for quantum experiments with different ground stations on Earth, the satellite downlink to the Nanshan ground station near Urumqi and the Graz, Austria, ground station near Vienna were successfully performed. Typical satellite-to-ground QKD performances between May and July 2017 are summarized in Fig. 36, with the final key length ranging from 400 to 833 kbits (Liao *et al.*, 2018).

Upon request from the ground command, the satellite acts as a trusted relay to establish secure keys among any two ground stations. Figure 37 shows an example of a key exchange between the Xinglong and Graz stations. We denote the random keys shared between Micius and Xinglong as MX, and those between Micius and Graz as MG. Micius can simply perform a bitwise exclusive OR operation ( $\oplus$ ) between MX and MG of the same string length, which then yields a new string  $\text{MX} \oplus \text{MG}$ . The new string can then be sent through a classical communications channel to Xinglong or Graz, which decodes other original keys using another exclusive OR operation [i.e.,  $\text{MG} = (\text{MX} \oplus \text{MG}) \oplus \text{MX}$ ]. This process can be easily understood since Micius uses MX to encrypt MG and Xinglong decrypts the cipher text to recover MG, which is shared with Graz. Such a key is known only to both communicating parties and the satellite and not to a fourth party.

For demonstration, a 100 kB secure key was established between Xinglong and Graz. Approximately 10 kB of the key was used to transmit a picture of Micius (with a size of 5.34 kB) from Beijing to Vienna, and a picture of Schrödinger (with a size of 4.9 kB) from Vienna to Beijing, using one-time-pad encoding. The other 70 kB of the secure key was combined with the advanced encryption standard-128 protocol and used in a video conference between Beijing and Vienna for 75 min with a total data transmission of about 2 GB.

### F. Probing gravity-induced decoherence

The Micius satellite also provides the feasibility for testing the entanglement decoherence induced by the gravitation of Earth (Joshi *et al.*, 2018). Quantum mechanics and relativity form the bedrock of modern physics. The general theory of relativity predicts a kind of exotic spacetime structure called the closed time curve (CTC) (Friedman *et al.*, 1990). The CTC is interesting because it violates causality and in principle can be formed from the quantum fluctuations of spacetime itself (Morris and Thorne, 1988; Deutsch, 1991; Politzer, 1992;

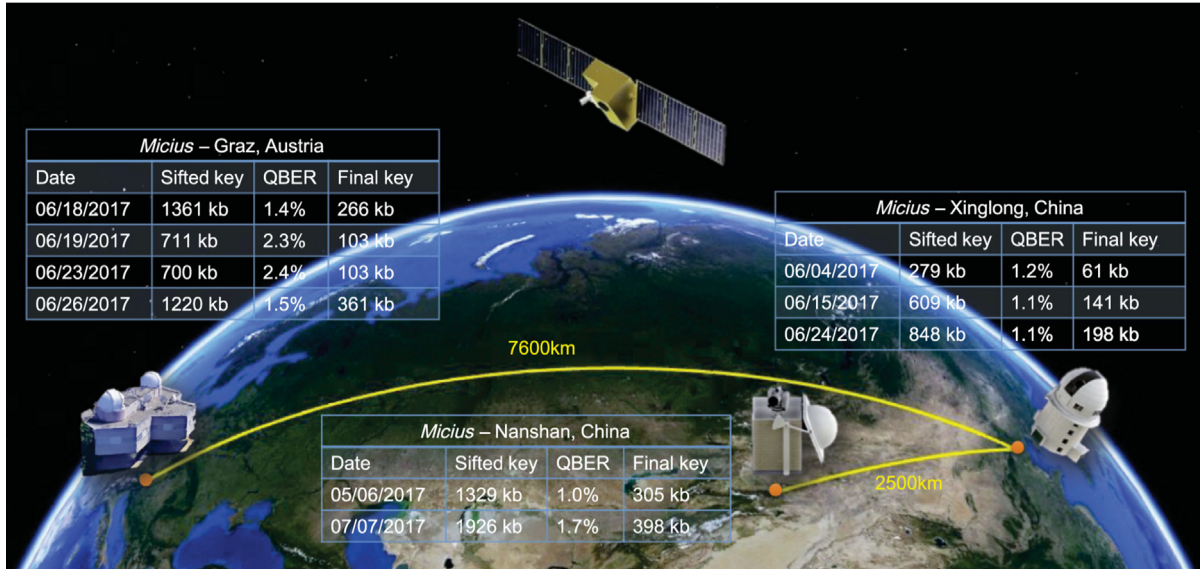


FIG. 36. Illustration of the three cooperating ground stations (Graz, Nanshan, and Xinglong). Listed are all paths used for key generation and the corresponding final key length. From Liao *et al.*, 2018.

Hartle, 1994; Hawking, 1995). To theoretically describe the quantum fields in both exotic spacetime containing CTCs and ordinary spacetime, Ralph, Milburn, and Downes (2009) reported the event formalism of quantum fields. This theory predicts that the different evolutions of quantum fields may probabilistically induce time decorrelation of two entangled photons passing through different regions of curved spacetimes, which are able to keep the entanglement in standard quantum theory.

Considering the curved spacetime caused by Earth's gravitation, one can test the decoherence effect by distributing the entanglement between the ground station and the satellite.

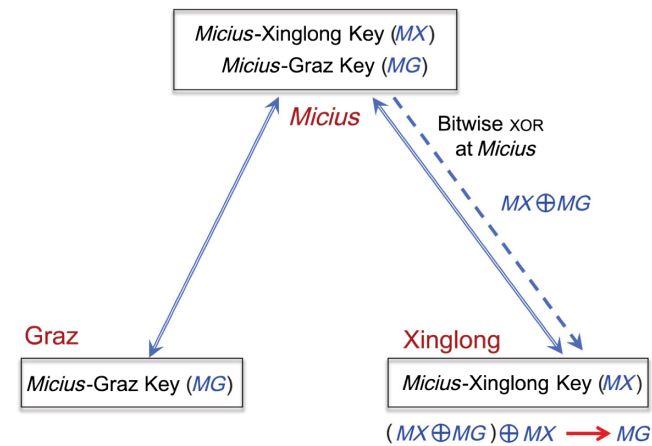


FIG. 37. Schematic of a key exchange procedure between Graz and Xinglong with the satellite as a trusted relay. After Micius distributes a key with Graz (MG) and Xinglong (MX), it performs a bitwise exclusive OR operation between those keys ( $MX \oplus MG$ ) and sends this combined key via a classical channel toward the Xinglong station. Combining the XORed key at Xinglong with MX leads to the same key (MG) on both sides. From Liao *et al.*, 2018.

The probability of entanglement losing is characterized by the decorrelation factor  $D$ , which is given by

$$D \approx \exp(-0.5\Delta_t^2/d_t^2), \quad (10)$$

where  $d_t$  denotes the photon coherence time and  $\Delta_t$  is derived as follows from the effect of the curved spacetime (Joshi *et al.*, 2018):

$$\Delta_t \approx \int_{r_e}^{r_e+h} \frac{M}{r} \left( 1 + \frac{2M}{r} + \frac{r_e^2 \tan^2(90^\circ - \theta)}{r^2} \right)^{1/2} dr. \quad (11)$$

In Eq. (11)  $r_e$  is Earth's radius,  $h$  is the satellite altitude,  $m$  is the mass of Earth expressed in a unit of length, and  $\theta$  is the altitude angle.

In the implementation, a polarization-entangled photon pair was prepared at the Ngari ground station, as shown in Fig. 38. The photon in path 2 is detected on the ground after passing through the ordinary spacetime, while its twin is received by the satellite Micius after propagating in the curved spacetime. Since gravity cannot induce the decoherence of classical correlation, it is possible to use the coherent laser as a reference. The entangled photons are combined with the faint coherent laser pulses in path 1 before transmission. The transmitted coherent photons are then classically correlated with the photons in path 3 on the ground. Two trains of entangled and coherent photons are shifted by half a pulse interval ( $\sim 6$  ns), thereby allowing the satellite to distinguish the photons by their arrival times.

The altitude of the satellite Micius is about 500 km. According to Eq. (10), it can be shown that the decorrelation factor  $D$  is a function of the altitude angle  $\theta$  only for a given photon source. To estimate the factors  $D(\theta)$  in the experiment, the observed coincident counts were compared with the expected counts in the standard quantum theory.  $C_{\text{exp,EPR}}(\theta)$  and  $C_{\text{exp,COH}}(\theta)$  denote the measured two-photon coincidence events of entangled and coherent states, respectively. From the

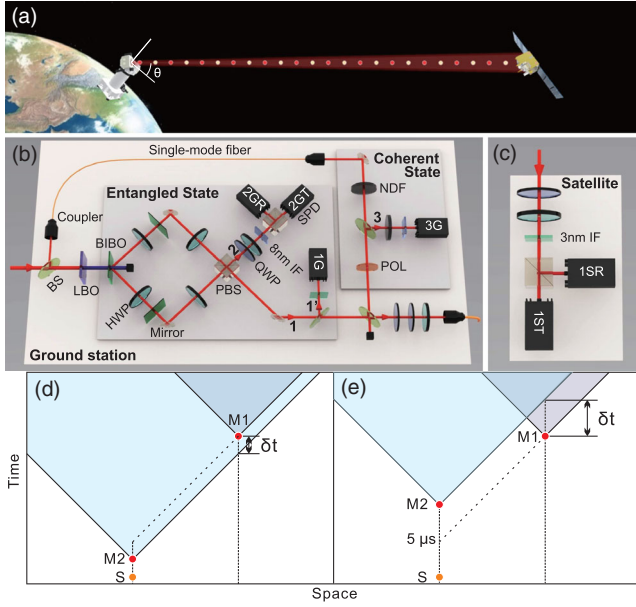


FIG. 38. Setup of an experimental test of gravity-induced entanglement decoherence. From Xu *et al.*, 2019.

standard quantum theory, the coincident counts of entangled photon pairs are  $C_{\text{SQT,EPR}}(\theta) = \eta_2 S_{\text{EPR}}(\theta)$ , where  $S_{\text{EPR}}(\theta)$  is the number of entangled photons detected on the satellite and  $\eta_2$  is the efficiency of detecting photons in path 2. For the faint coherent laser pulses, coincidence counts are estimated as  $C_{\text{SQT,COH}}(\theta) = S_{\text{COH}}(\theta) S_3 t_p / t_{\Delta\theta}$ , where  $S_{\text{COH}}(\theta)$  and  $S_3$  are the numbers of detected coherent photons at the satellite and in path 3, respectively,  $t_p$  is the repeat frequency of the pulse laser, and  $t_{\Delta\theta}$  is the data collection time. Thus, the decorrelation factors can then be given as

$$D_{\text{EPR}}(\theta) = C_{\text{exp,EPR}}(\theta) / C_{\text{SQT,EPR}}(\theta) \quad (12)$$

for entangled photon pairs and

$$D_{\text{COH}}(\theta) = C_{\text{exp,COH}}(\theta) / C_{\text{SQT,COH}}(\theta) \quad (13)$$

for faint coherent pulse lasers.

The experiment can be implemented with and without fulfilling the no-signaling condition to account for the quantum collapse models. Using 1 km fiber to delay the photons in the ground station, the detection events of entangled photons on the ground and satellite are separated in a spacelike manner; see Fig. 39. By collecting data when the altitude angle of the satellite varies from  $40^\circ$  to  $60^\circ$ , the estimated decoherence factors for both spacetime settings are shown in Fig. 39 (Xu *et al.*, 2019).

The experimental results are consistent with the standard quantum theory and hence do not support the event formalism. However, they may be explained by a weaker decoherence effect. When the clock local to the detector is used as the global reference, the expression of  $\Delta_t$  is given by

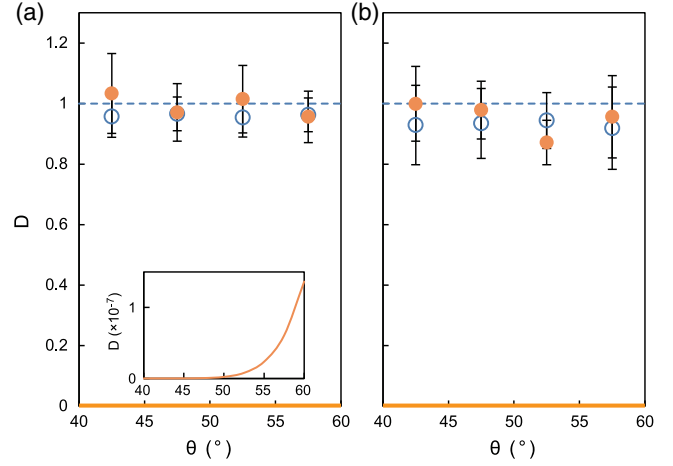


FIG. 39. Experimentally estimated decorrelation factors at different altitude angles ( $\theta$ ) of the satellite (a) when fulfilling and (b) when not fulfilling the nonsignaling condition. From Xu *et al.*, 2019.

$$\Delta_t = \int_{r_e}^{r_e+h} \left( \frac{M}{r} - \frac{M}{r_e+h} \right) \left( 1 + \frac{2M}{r} + \frac{r_e^2 \tan^2(90^\circ - \theta)}{r^2} \right)^{1/2} dr. \quad (14)$$

The corresponding  $D(\theta)$  value is between 0.96 and 0.98 for  $40^\circ < \theta < 60^\circ$ . The future testing of such a model may be performed using a satellite in higher orbit.

## X. OTHER QUANTUM SATELLITE PROJECTS

The positive results and encouraging prospects kick-started an international race on quantum experiments in space. Many satellite projects for quantum communications have been approved and supported, as shown in Fig. 40. For instance, the QEYSSat project in Canada has been studied by the Canadian Space Agency since 2010, and it has received \$1.5 million and \$30 million funding in 2017 and 2019, respectively. Its mission concept was developed in partnership with Honeywell Aerospace. In contrast to many other missions, it proposes a quantum uplink while equipping the receiver at the microsatellite and placing the quantum source on the ground (Jennewein *et al.*, 2014; Pugh *et al.*, 2017). Oberhaus (2020) recently reported that NASA plans to build a quantum satellite link that will be called Marconi 2.0. The main idea behind Marconi 2.0 is to establish a space-based quantum link between Europe and North America by the mid- to late-2020s.

In addition to the traditional “big-space” paradigm of satellites, many other teams worldwide have started a new paradigm based on nanosatellites, even the CubeSat standard (Oi *et al.*, 2017). The CubeSat Quantum Communications Mission (CQuCoM), which was jointly undertaken by the University of Strathclyde, the Austrian Academy of Sciences, Clyde Space Ltd., the Technical University of Delft, Ludwig-Maximilian University, the University of Padua (in collaboration with the Italian Space Agency), and the National University of Singapore, will perform satellite-to-ground entangled-photon transmission and QKD using a CubeSat platform deployed from the ISS. CubeSat employed in

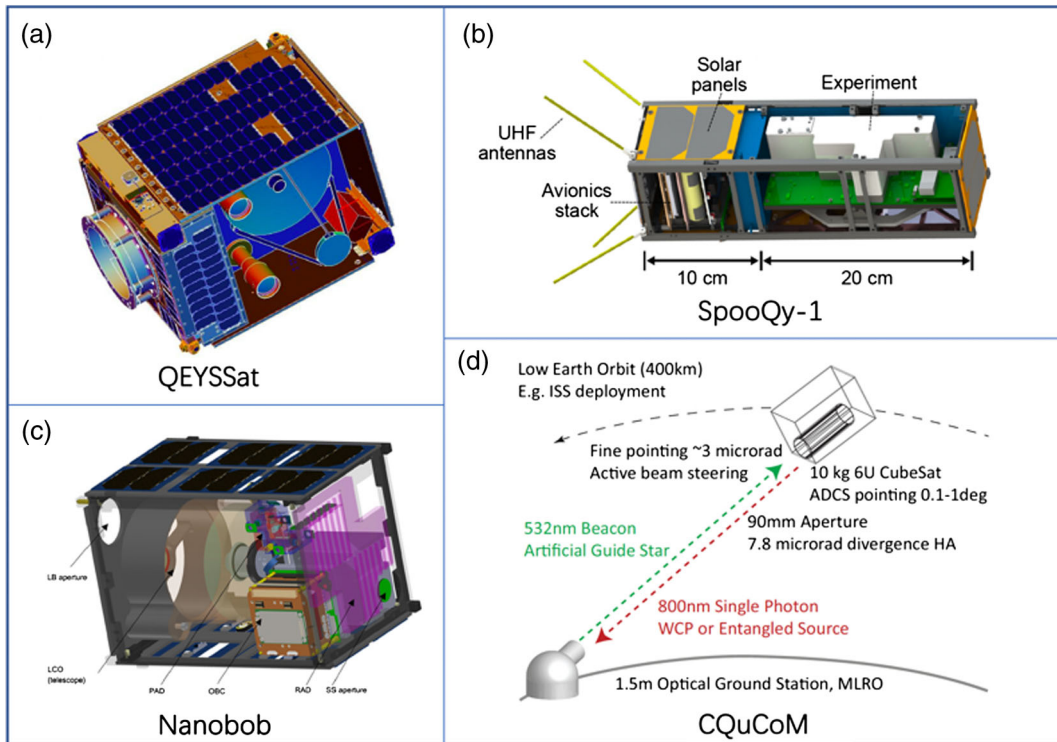


FIG. 40. Other quantum satellite plans besides Micius. (a) Quantum Encryption and Science Satellite (QEYSSat) project in Canada. From [Jennewein \*et al.\*, 2014](#), and [Pugh \*et al.\*, 2017](#). (b) 3U CubeSat involving an entangled-photon source developed by a group at the National University of Singapore. From [Villar \*et al.\*, 2020](#). (c) CubeSat-based mission concept Nanobob proposed by researchers in France and Austria. From [Kerstel \*et al.\*, 2018](#). (d) CubeSat Quantum Communications Mission (CQuCoM) jointly undertaken by a joint research team. From [Oi \*et al.\*, 2017](#).

CQuCoM will be a 10 kg and 6 l mass-volume envelope that will first be carried up to the ISS on a regular resupply mission (Dragon, Cygnus, H-II Transfer Vehicle, Automated Transfer Vehicle, Progress, and Soyuz) and then deployed into orbit using the NanoRacks CubeSat Deployer mounted upon the Japanese Experimental Module Remote Manipulator System. CQuCoM calls for two missions, the first to demonstrate the pointing mechanism with a high-brightness transmission source that can also be used for a WCP source-based QKD, and the second to distribute entanglement between space and the ground. CubeSat exploits advances in nanosatellite attitude determination and control systems such as coarse pointing by rotating the satellite body to align the transmitting telescope with the ground station. CQuCoM would be a pathfinder for the nanosatellite payloads and operations and would establish the basis for a quantum constellation of LEO trusted relays for the quantum-secure communication ([Oi \*et al.\*, 2017](#)).

Another CubeSat-based mission concept, Nanobob, was proposed by researchers of France and Austria in 2018. They studied the feasibility of implementing ground-to-space optical quantum communication by placing the quantum source on the ground and the 12U CubeSat with the “Bob” detection system only. In addition to its main scientific aim of demonstrating space-based QKD using a CubeSat and uplink configuration, the Nanobob mission has other technological aims, such as accurate clock synchronization and a fast classical optical communication with approximately 1 Gbits/s ([Kerstel \*et al.\*, 2018](#)).

A group at the National University of Singapore has been committed to designing and developing quantum sources based on nanosatellites and CubeSat platforms. They developed a correlated photon-pair source as the pathfinder for their future plan of space applications. Their first attempt was unsuccessful when the launched vehicle (CRS Orb-3) failed shortly after takeoff, although the payload was successfully recovered intact and found to be fully operational ([Tang, Chandrasekara, Yue \*et al.\*, 2016](#)). Their second attempt was successful. The source was launched onboard the Galassia CubeSat (PSLV C29) to an orbit of approximately 550 km at the end of 2015, which laid the foundation of their future space-based quantum experiment mission ([Tang, Chandrasekara, Tan \*et al.\*, 2016](#); [Grieve \*et al.\*, 2018](#)). Recently they developed an entangled photon-pair source onboard a 3U CubeSat, SpooQy-1, which was launched successfully to ISS in April 2019. The CubeSat was then deployed into orbit from ISS on June 17, 2019 ([Villar \*et al.\*, 2020](#)).

Furthermore, some feasibility tests for using smaller or high-orbit satellites have been reported ([Vallone \*et al.\*, 2015](#); [Dequal \*et al.\*, 2016](#); [Günthner \*et al.\*, 2017](#); [Takenaka \*et al.\*, 2017](#); [Vedovato \*et al.\*, 2017](#)). [Bedington, Arrazola, and Ling \(2017\)](#) provided a table of notable satellite QKD proposals.

In addition to university consortia and national agencies, the international space race also involves private companies such as QKDSat (ArQit) ([ESA, 2018b](#)) and QUARTZ ([ESA, 2018a](#)). A more ambitious quantum communication infrastructure project is taking shape in Europe. The European

Quantum Communication Infrastructure (EuroQCI) initiative aims to build a secure quantum communication infrastructure that will span the entire European Union (EU), including its overseas territories. Since June 2019, all 27 EU member states have signed the EuroQCI declaration, thereby indicating their commitment to the EuroQCI initiative. The EuroQCI will include a terrestrial segment relying on fiber communications networks linking strategic sites on the national and cross-border levels and a space segment based on satellites. It will link national quantum communication networks across the EU and provide global coverage (Scudo and Lewis, 2021).

## XI. OUTLOOK

Although Sec. IX showed that the Micius satellite greatly enhances the scale and capability of quantum experiments in space, Micius marks only the beginning. For the Chinese quantum satellite plans, there are two goals in the next five to ten years. The first is to develop three to five small LEO satellites dedicated to QKD missions, which will provide more practical and efficient QKD services. The second goal is to develop a medium-Earth-orbit-to-geosynchronous-orbit (GEO) quantum science satellite that involves several ambitious scientific objectives. Compared to LEO satellites, high-orbit satellites can provide much longer service and wider coverage. The combination of a high-orbit satellite and multiple LEO satellites can form a quantum constellation for global services. Furthermore, with such a new generation space platform, researchers plan to realize the high-precision satellite-ground time-frequency transfer and GEO satellite-based optical clocks to verify the technology of the wide-area optical frequency standard. Further research includes

fundamental tests of quantum physics and its interface of general relativity to deepen understanding of the basic laws of nature.

### A. Daytime quantum communications

There is much room for improvement. One of the main drawbacks of the current satellite-based quantum communication missions is that they work only at night, which greatly limits their practical applications. In satellite-based classic communication, the Iridium system (Pratt *et al.*, 1999) provides worldwide connectivity. Similarly, the quantum satellite constellation, which is composed of a few dozen satellites, can provide global real-time quantum communication. Such a satellite constellation is expected to operate with both LEO and high-Earth-orbit (HEO) satellites, such as GEO satellites. The probability of a satellite being in Earth's shadow zone decreases rapidly with an increasing orbit height (Fig. 41). A LEO satellite system has an  $\sim 70\%$  probability of being in the sunlight area; for GEO satellites, this probability increases to  $\sim 99\%$  (Gilmore, 2002). Therefore, a step toward the quantum satellite constellation is to demonstrate daylight free-space quantum communication.

The main challenge is the strong background noise from the scattered sunlight, which is typically 5 orders of magnitude greater than the background noise at nighttime. To this end, as reviewed in Sec. II, early indoor and outdoor tests (Jacobs and Franson, 1996; Buttler, Hughes, Kwiat, Lamoreaux *et al.*, 1998; Buttler *et al.*, 2000; Hughes *et al.*, 2002; Kurtsiefer *et al.*, 2002) over distances of 75 m to 23.4 km suggested improving the signal-to-noise ratio using a combination of detection timing, narrow band filters, and spatial filtering.

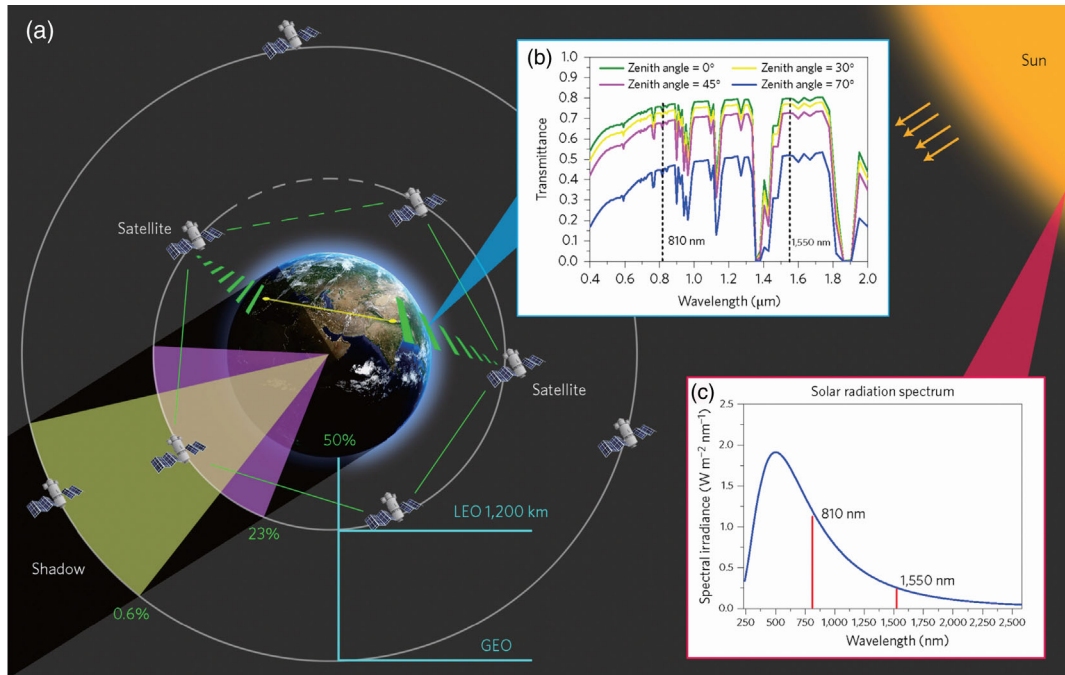


FIG. 41. Satellite-constellation-based global quantum network. (a) A global quantum network needs many LEO satellites or several geosynchronous-orbit satellites to compose a satellite constellation. The time of a satellite in Earth's shadow area is inversely proportional to the orbit height of the satellite. (b) Transmittance spectra from visible to near-infrared light in the atmosphere at selected zenith angles. (c) Solar radiation spectrum from visible to near-infrared light. From Liao *et al.*, 2017c.

Later many research teams employed ultranarrow-bandwidth spectral filtering using multipassed etalon and a Rb vapor filter and improved the time resolution (Rogers *et al.*, 2006; Shan *et al.*, 2006; Höckel *et al.*, 2009; Peloso *et al.*, 2009; Restelli *et al.*, 2010).

A preliminary verification of free-space QKD in daylight under conditions of high channel loss ( $\sim 48$  dB) over 53 km was reported by Liao *et al.* (2017c). First, to increase the signal-to-noise ratio, they chose a working wavelength of 1550 nm. Compared to 800 nm, the telecom-band wavelength has a slightly higher transmission, and Rayleigh scattering has a transmission that is  $\sim 14$  times smaller. Further, the sunlight intensity at 1550 nm is  $\sim 5$  times weaker than that at 800 nm. Second, free-space single-mode fiber coupling was developed with efficiencies of 30% for the indoor test and 5% for the outdoor test. The field of view for the receiving system is reduced below  $10 \mu\text{rad}$  to reduce the background noise. Finally, ultralow-noise up-conversion single-photon detectors were used with a built-in spectral filtering employing volume Bragg grating with a bandwidth of 0.16 nm. Such narrow band filtering reduces noise by a factor of  $\sim 100$  compared to the 3–10 nm filters used in previous experiments at night. A combination of the three key toolboxes enabled a decoy-state QKD with a final key rate of 20–400 bits/s, where the variation was due mainly to the atmospheric environment.

For higher-orbit satellites, especially those working in the daytime, due to the longer distances and the associated diffraction loss, new techniques need to be developed to increase link efficiency in the future, including large telescopes, better APT systems, and wave front correction through adaptive optics (Gruneisen *et al.*, 2015, 2016, 2021; Gruneisen, Flanagan, and Sickmiller, 2017; Gong *et al.*, 2018; Yang *et al.*, 2020).

## B. Satellite-constellation-based quantum networks

A LEO satellite alone is not enough to support the construction of a global-scale quantum communication network. In general, attention should be paid to two aspects: increasing the number of satellites and raising the orbital altitude. It is necessary to build a quantum constellation combining LEO and HEO satellites, as shown in Fig. 41(a).

There is also a need to develop many cheaper satellites in LEO to cover Earth and a few HEO satellites to provide 24-hour service for some important regions, as shown in Fig. 41. On the number of LEO satellites, as shown in Fig. 42, it suggests that about three low-orbit satellites are needed to ensure that all major regions of the world can be covered with enough passages per year. Considering the altitude of LEO satellites, the higher the orbit the more sufficient QKD times can be guaranteed for the ground stations at a specific time. For instance, if there is a three-satellite constellation with an orbit altitude of 800–1000 km, the average number of satellite passes in major regions of the world is about 3.7 times per day, and the average effective QKD time for each ground station at an elevation above  $25^\circ$  is  $\sim 5$  min, which can cover more than 100 ground stations in major areas of the world and guarantee the QKD of each ground station once a week.

Therefore, in future scenarios one of the simplest quantum constellations may include at least three low-orbit satellites

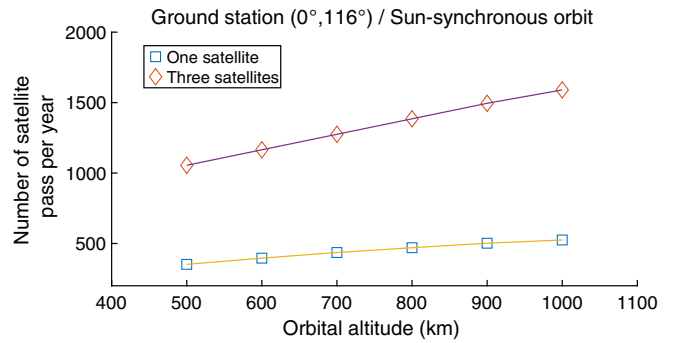


FIG. 42. Simulation of the number of satellite passes through the low latitude region.

and one HEO satellite. In this configuration, the LEO satellites are responsible for the daily needs of numerous ordinary users, for instance,  $\sim 100$  users, and the HEO satellites can provide long-term uninterrupted services for a few important areas and users. According to the Micius data, since LEO satellites have a large margin in channel efficiency, miniaturization and low-cost designs can be considered for both satellite payloads and ground receiving stations. When we consider HEO-satellite-based QKD, because of the high channel loss, we need to prioritize performance in the design of payloads and ground stations.

For LEO satellites, it is economical to consider small and low-cost QKD payloads, which can be assembled on satellites of different sizes, such as microsatsellites and space stations. In this regard, Liao *et al.* (2017b) also made preliminary attempts to develop a small payload for space-to-ground QKD from the Tiangong-2 space laboratory to the Nanshan ground station. The 57.9 kg payload integrates a tracking system, a QKD transmitter along with modules for synchronization, and a laser communication transmitter. In the space laboratory, a 50 MHz vacuum and weak decoy-state optical source was sent through a reflective telescope with an aperture of 200 mm, as shown in Fig. 43. In the experiment, the communication distance was between 388 and 719 km, the QBER was 1.8%, and the final key rate was  $\sim 91$  bits/s when the quantum channel was established.

Compact and low-cost payloads such as those used in Tiangong-2 can be assembled on satellites of various sizes to construct a satellite-constellation-based quantum network, as shown in Fig. 44. The performance of QKD and the size of the payload can still be improved. For instance, the size of the telescope can be reduced to 100 mm, the divergence angle of the source can be narrowed to the diffraction limit, and the decoy-state source rate can be increased to 1 GHz. With such improvements, the weight of the payload is reduced below 20 kg, and the final key rate is increased to  $\sim 10$  kbits/s.

In addition, for the practical space-ground integrated quantum communication network, the number of users is far greater than the QKD payloads in the sky. The typical ground station for Micius satellite is too large and heavy for large-scale applications for more users. The ground station should be redesigned to be smaller, lighter, and cheaper to satisfy the requirements of the practical quantum constellation. Recently the feasibility of performing the satellite-to-ground QKD using the compact ground station (less than

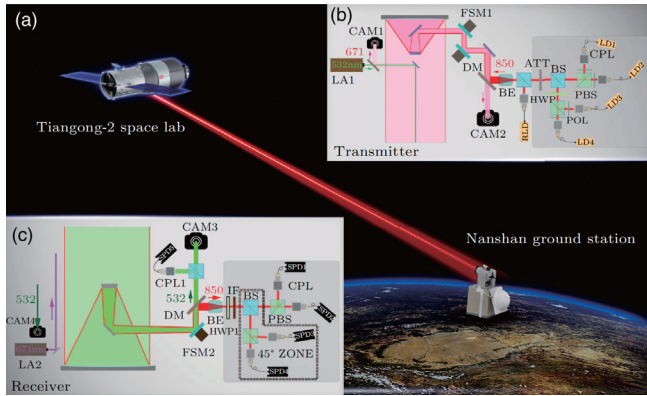


FIG. 43. Schematic diagram of QKD from the Tiangong-2 space laboratory to the ground. (a) Overview of the space-to-ground QKD. (b) Schematic of the decoy-state QKD transmitter. (c) Schematic of the decoy-state QKD decoder in the Nanshan ground station equipped with a 1200-mm-aperture telescope. LA1, green laser (532 nm); CAM1, coarse camera; CAM2, fine camera; LD, laser diode; RLD, reference laser diode; FSM1, fast steering mirror; HWP, half-wave plate; POL, polarizer; PBS, polarization beam splitter; BS, beam splitter; ATT, attenuation; LA2, red laser (671 nm); CAM3, fine camera; CAM4, coarse camera; CPL, coupler; DM, dichroic mirror; IF, interference filter; FSM2, fast steering mirror; BE, beam expander; SPD, single-photon detector. From [Liao \*et al.\*, 2017b](#).

100 kg, 280 mm in diameter) was verified by [Ren \*et al.\* \(2022\)](#) in multiple cities in China, as shown in Fig. 45. A typical sifted key rate can be achieved to 2 kbits/s.

In addition to QKD, quantum teleportation also will play a key role in future quantum networks, and it will require that the long-distance entanglement distribution should be implemented before the Bell-state measurement. For the Micius satellite-based teleportation ([Ren \*et al.\*, 2017](#)), the

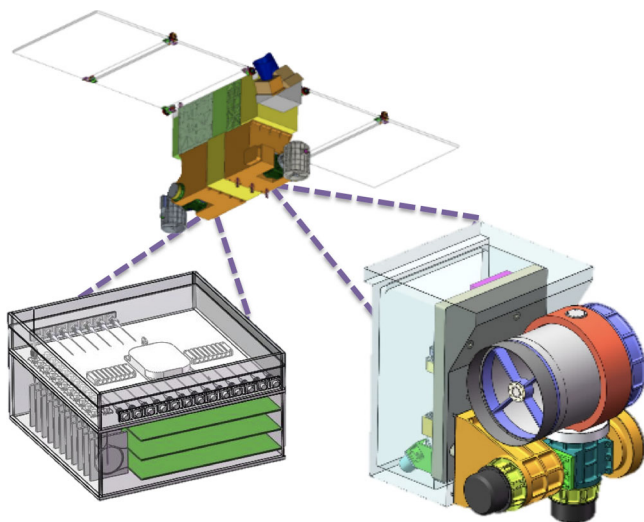


FIG. 44. Preliminary design of small satellites in China. This design will focus on the QKD using downlink channels. The total weight will be less than 100 kg. The orbit height will be 800 km. There will be three or five small quantum satellites for the first step.

entangled-photon source and the Bell-state measurement are performed at the same location on the ground. A next step toward a real network is to develop an entangled-photon source with a long coherence time  $T_c$  and reduce the arrival-time jitter  $T_j$  between independent photons to achieve  $T_c > T_j$ . In this case, semiconductor chip-based sources of deterministic single-photon ([Ding \*et al.\*, 2016](#); [Wang \*et al.\*, 2019a](#)) and entangled-photon sources ([Wang \*et al.\*, 2019b](#)), possessing high purity, indistinguishability, and efficiency simultaneously, have coherence time of the order of a few hundred picoseconds and can offer a more efficient and viable solution. Furthermore, teleportation can be used to transfer the quantum state of a flying single photon to a long-lived matter qubit to realize quantum memory at a distance ([Sherson, Jacob \*et al.\*, 2006](#); [Chen \*et al.\*, 2008](#); [Bussi eres \*et al.\*, 2014](#)). Teleportation can also be employed in entanglement swapping and distributed quantum computing schemes. Using the previously mentioned long-lived quantum memories and efficient light-matter interfaces, more sophisticated space-ground-scale teleportation will soon be realized and will play an important role in a future distributed quantum network.

Through these further efforts, we can envision a global quantum communication infrastructure with quantum constellation and ground-based fiber networks, as shown in Fig. 46. A fiber-based network on the ground provides secure communication services for distance cities. Meanwhile, a quantum constellation with LEO and high-orbit satellites connects key nodes on the fiber networks and movable nodes, even ships in the ocean. Based on our previous analysis, we suggest that the simplest quantum constellation should include at least three low-orbit satellites and one high-orbit satellite. In this configuration, assuming that at least 100 ground stations need to be covered, each ground station needs more than 50 occurrences of QKD links with a satellite per year and can obtain about 2 Mbits for each satellite passage. Each station can then obtain 100 Mbits per year, and the quantum constellation can output about 10 Gbits of keys per year in total, which can support the basic function of voice communication. In addition, HEO satellites can provide 24-hour QKD services at a key rate of 1 kbit/s for some important areas, which can address the basic needs of text communication.

### C. Fundamental test of quantum physics at space scale

The success of the satellite Micius shows not only the feasibility of realizing the global-scale quantum-secure communication network but also a new way for performing fundamental tests in quantum physics at the space scale. With the Micius satellite, the first step toward this space-scale fundamental research has been achieved, for example, a Bell test over 1200 km ([Yin \*et al.\*, 2017a](#)) and satellite testing of a gravitationally induced quantum decoherence model ([Xu \*et al.\*, 2019](#)). Furthermore, many more profound scientific explorations of quantum physics will need higher orbital altitude satellites. In this section, we introduce several space-scale fundamental experiments on quantum physics based on the plan of the HEO satellite of China.

*Further experiments based on an entanglement distribution on a larger space scale.*—According to Einstein’s local

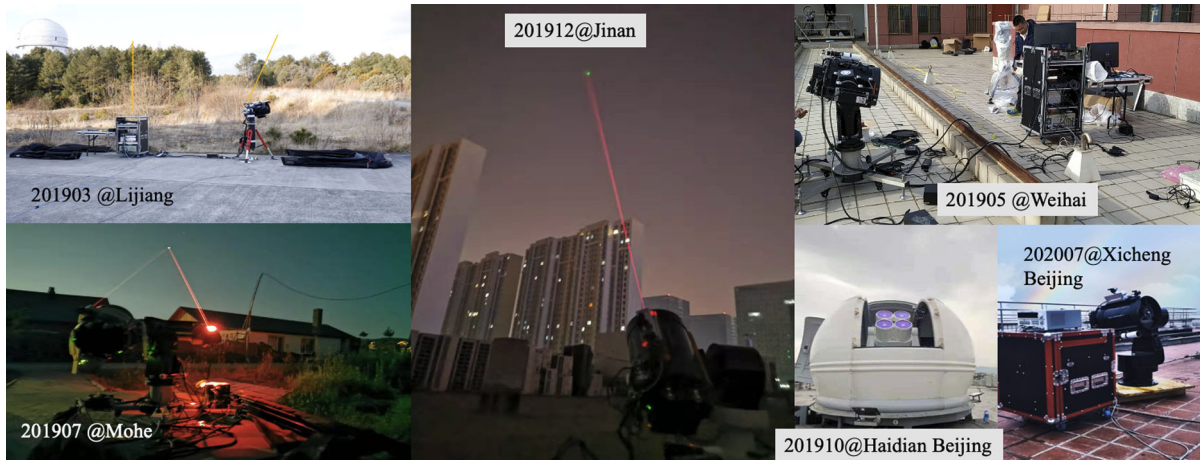


FIG. 45. Experimental demonstration of the feasibility of satellite-to-ground QKD with compact ground stations. By 2020, the QKD with the Micius satellite and the compact ground station had been demonstrated in many Chinese cities, including Beijing, Jinan, Weihai, Lijiang, and Mohe. The typical sifted key rate is  $\sim 2$  kbits/s.

realism, the maximum value of the Bell inequality is 2 (Bell, 1964; Clauser *et al.*, 1969). However, according to quantum mechanics, the maximum value of this quantity can reach  $2\sqrt{2}$ . In recent decades, physicists have performed several experiments, and all of them have confirmed the correctness of quantum mechanics, although some loopholes still exist and should be addressed. One loophole is the freedom-of-choice loophole (Brunner *et al.*, 2014); that is, the random-number generators that determine the choice of measurement bases for the Bell test can be prior correlated, and thus the choice of measurement basis is not truly independent and random. Another loophole is the so-called collapse-locality loophole, or the Schrödinger cat loophole (Kent, 2005). In this case, according to the Schrödinger cat gedanken experiment it is arguable that the measurement outcome, for example, the cat

state in a closed black box, is not defined until it is registered by a human consciousness. This implies that the realized “events” have never been spacelike separated.

A possible solution to these two loopholes is to perform Bell-test experiments with human observers (Bell, 2004). In this way, the measurement basis would be chosen by human free will, and the measurement outcomes could be defined by human consciousness. Since such experiments would require the quantum signal transit time to exceed that of the human reactions, which is typically 100 ms, one must ensure entanglement distribution at a distance of the order of 1 light-second. To address the freedom-of-choice and collapse-locality loopholes, performing an entanglement distribution between Earth and the Moon may be a possible solution, as suggested by Cao *et al.* (2018). The entangled

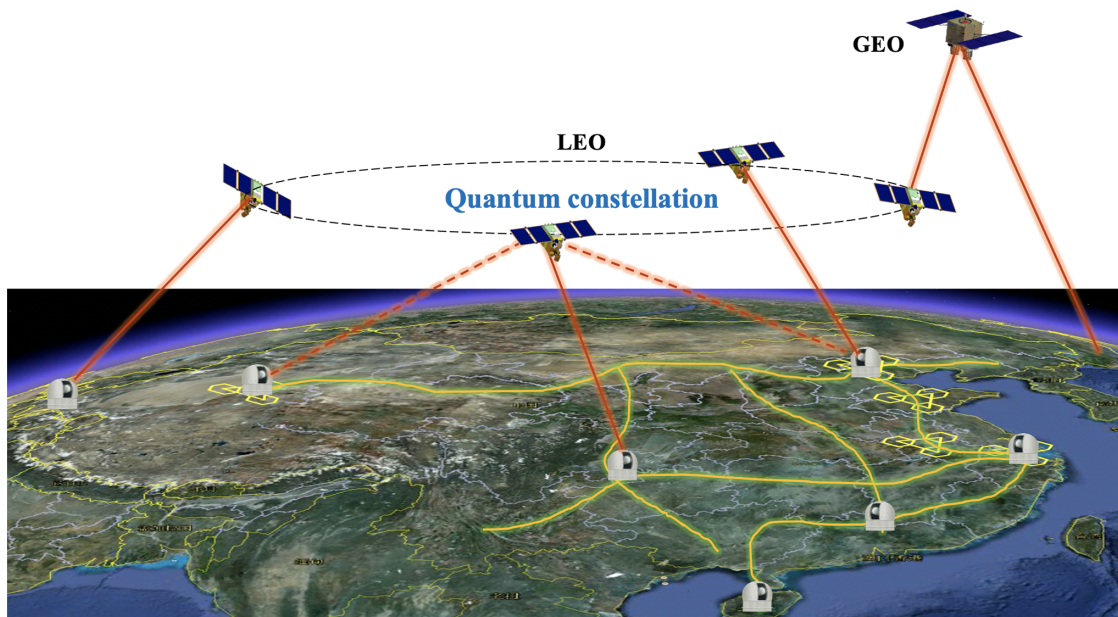


FIG. 46. Road maps for the global quantum communication network. Intracity metropolitan networks will be created using fibers. Quantum repeaters can connect the metropolitan networks. Long-distance and intercontinental quantum communication will be realized via satellite-based quantum channels.

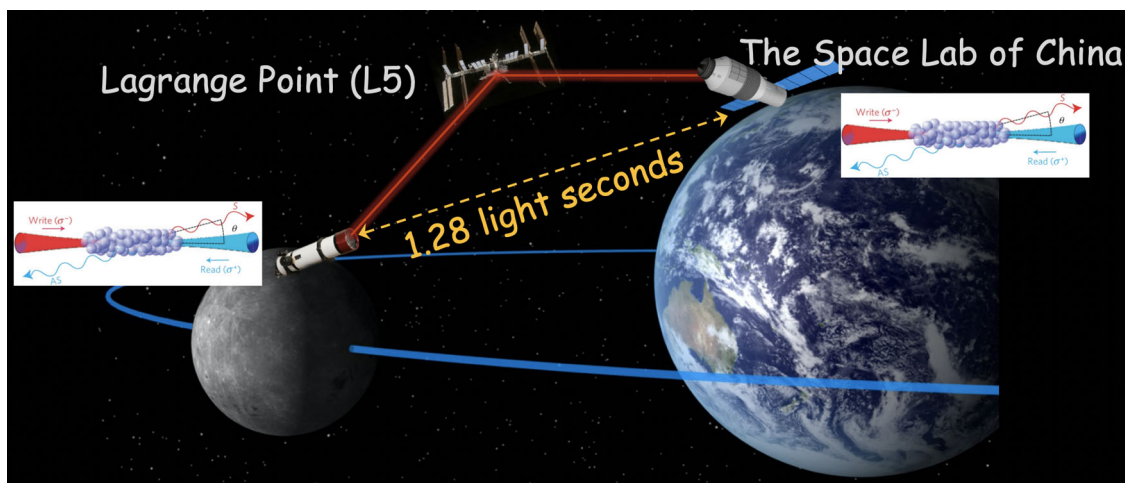


FIG. 47. Scheme for conducting a Bell test between Earth and the Moon. There are five Lagrangian points in the Earth-Moon system, denoted by L1–L5. Since only L4 and L5 are stable and they have the most appropriate space arrangement of the five points, they were chosen for the position of the entanglement source satellite. This satellite contains two telescopes: one is aimed at the Moon and the other at Earth. Two large telescopes must also be built, one on or near the Moon and one on Earth, to create entanglement distribution channels. Human observers and quantum memory combined with an event-ready scheme should be employed to realize a loophole-free Bell test.

photon pairs will then be sent to Earth and the Moon from one of the Earth-Moon Lagrangian points, as shown in Fig. 47. The distance between the two detectors should be greater than 1 light-second, and both loopholes would be closed. Furthermore, using an event-ready scheme (Zukowski *et al.*, 1993; Simon and Irvine, 2003) and a quantum memory technique (Yang *et al.*, 2016) could significantly increase the heralding efficiency, making it possible to introduce human recorders to address the collapse loophole.

*Test the interface of quantum mechanics and general relativity.*—The emergence of quantum mechanics and general relativity has radically changed our understanding of nature. However, any theory that integrates quantum mechanics with general relativity encounters great challenges. Among the four basic interactions currently known, the electromagnetic, weak, and strong interactions have been quantized and unified. Only the question of how to quantize gravitational action is pending. Testing the interplay of quantum mechanics and general relativity will help establish a grand unified theory for the four basic interactions.

The results from a recent work (Xu *et al.*, 2019) are consistent with the descriptions of standard quantum theory and do not support the predictions of event formalism. However, this does not necessarily rule out other approaches, since it may be explained by a weaker decoherence effect. Therefore, this type of experiment can be expanded naturally to the higher-orbit satellite to test other gravity-related models.

Meanwhile, there is another scheme to test the interface of two theories, quantum mechanics and general relativity. It is to probe quantum interference within the frame of general relativity, that is, the optical version of the Colella, Overhauser, and Werner (COW) experiment (Zych *et al.*, 2011, 2012; Rideout *et al.*, 2012). The first experiment measuring the effects of gravity on the quantum wave function of a single particle was achieved by Colella, Overhauser, and Werner (1975) using a neutron beam interferometer.

COW-like experiments were then repeated with an increase in precision over several years (Peters, Chung, and Chu, 1999). However, the phase shifts observed in these interferometric experiments are fully compatible with nonrelativistic quantum mechanics in the presence of the Newtonian gravitational potential. On the other hand, all previous tests of general relativity can be described within the framework of classical physics (Zych *et al.*, 2012). Nevertheless, the quantum interference of photons provides a promising way to probe quantum mechanics in curved spacetime. Single-photon interference is a phenomenon that can prove the wave-particle duality and complementarity in quantum mechanics. In a COW-like experiment with single photons, the Newtonian limit of gravity is insufficient to explain the interference result without the theory of equivalence of mass and energy, which is one conceptual pillar of general relativity. Furthermore, if the concept of the time dilation is introduced to the single-photon COW experiment and the difference in the time dilation of each arm is comparable to the photon's coherence time, the visibility of the quantum interference will drop. This predicted effect of gravitation-induced decoherence would provide the most likely test of the genuine general relativistic notion of proper time in quantum mechanics.

A typical and possible scheme of the single-photon COW experiment can be implemented by combining two identical unbalanced Michelson interferometers and equipping them in the ground station and the high-Earth-orbit satellite, respectively, as shown in Fig. 48. In such an experimental configuration, the effects of gravitationally induced redshift and time dilation can both be tested, depending on the orbit altitude, the length of the unbalance arm  $\sim \Delta l$ , and the measurement accuracy of the interferometer.

*Wide-area quantum-secure and high-precision optical time-frequency transfer.*—Combining quantum communication with time-frequency transmission will lead to the development of meaningful new research interests.

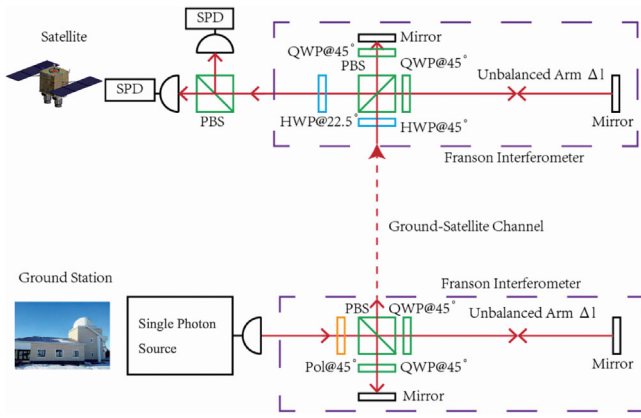


FIG. 48. The scenario of the single-photon COW experiment based on the high-Earth-orbit satellite. Before setting up the Franson interferometer on the ground, a genuine single photon was prepared as the  $|+\rangle$  state. After passing through the interferometer on the ground and the ground-satellite free-space channel, a half-wave plate changes the polarization of the photon, which guarantees that if photons pass through the long arm of the interferometer on the ground, they must pass through the short arm in the satellite, and vice versa. HWP, half-wave plate; QWP, quarter-wave plate; PBS, polarization beam splitter;  $M$ , mirror.

From the perspective of time-frequency transmission, wide-area high-precision time-frequency transfer is an essential component for constructing a physical network of optical timescales. It plays an important role in fundamental science (Kolkowitz *et al.*, 2016; Riehle, 2017; Marra *et al.*, 2018) and real-life applications (Mills, 1991). For instance, it can dramatically improve the precision of navigation and timing (Gill, 2011; Kómar *et al.*, 2014; Ludlow *et al.*, 2015), clock-based geodesy (Ludlow *et al.*, 2015), the testing of the effects of special and general relativity (Müller, Soffel, and Klioner, 2008; Cacciapuoti and Salomon, 2009; Schiller *et al.*, 2009; Ludlow *et al.*, 2015), and even the search for dark matter (Derevianko and Pospelov, 2014). However, security issues, such as man-in-the-middle attacks (Treytl *et al.*, 2007), remain unaddressed. This leads to secure time-frequency transfer evolving as a crucial problem in time-frequency applications. Inspired by the information-theoretic security of QKD, there is a need to extend the application of QKD to time-frequency transmission to improve its security, as shown in Fig. 49. Recently a satellite-based quantum-secure time-transfer scheme based on the two-way quantum key distribution in

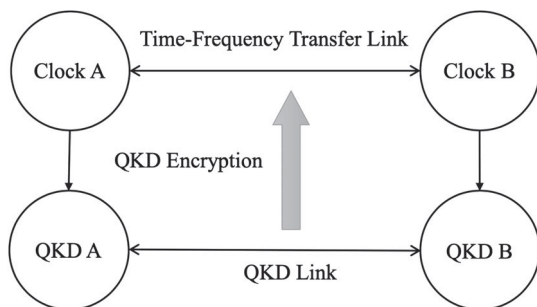


FIG. 49. Diagram of a quantum-secure time-frequency transfer.

a free-space link was experimentally demonstrated, which can be regarded as the first step to an enhanced infrastructure for a time-transfer network (Dai *et al.*, 2020).

The technologies developed from satellite-based quantum communication, such as high-stability and high-efficiency satellite-ground optical links, will promote the development of a satellite-based optical time-frequency transfer. Traditional satellite-based links exhibit an optimum frequency instability of approximately  $1 \times 10^{-15}$  for a day, which is limited mainly by the resolution of the microwave carrier. Optical-based links naturally become an important means of further improving the accuracy of the time-frequency dissemination. Many important works on high-precision and high-stability optical time-frequency transfers with free space and a fiber link have been reported (Smith *et al.*, 2006; Étienne *et al.*, 2008; Predehl *et al.*, 2012; Giorgetta *et al.*, 2013; Sinclair, Laura *et al.*, 2018). Recent experiments have shown that stability on a  $10^{-18}$  level can be achieved at 3000 s with an average loss of 72 dB, which corresponds to the loss of a satellite-ground link (Shen *et al.*, 2021).

A combination of QKD and time-frequency transfer can also further improve the clock synchronization accuracy of QKD, promoting the realization of wide-area quantum repeaters, measurement-device-independent QKD, and twin-field QKD. Thus, for the planning of high-orbit satellites, it would be worthwhile to develop quantum-secure and high-precision optical time-frequency transfer between the satellite and the ground, which would create new possibilities of global-scale quantum time-frequency transfer networks.

*Space-based ultrahigh-precision optical frequency standard.*—Optical atomic frequency references, or optical atomic clocks, have better stability and total uncertainty than the microwave atomic frequency standards and have promise for providing next-generation frequency standards. At the 26th General Conference on Weights and Measures (CGPM), scientists reached an important resolution to define all units in the International System of Units (SI) by nature constants in quantum physics, which opened a new era for quantum metrology. Time is one of the fundamental quantities in SI. It is the most precisely measurable quantity and the most important one. Since the distance can be measured using the propagation time of light, the precision of distance measurements is ultimately limited by the precision of the time measurements.

The unit of time in SI is the second, which is defined based on an atomic hyperfine transition in neutral cesium (Cs) atoms. The primary time standard is currently defined by cold Cs atomic fountains in laboratories, which leads to an inaccuracy of  $10^{16}$  in several parts. This provides the time-frequency signals and the international atomic time, thereby serving as a worldwide time reference. Atomic clocks are now an essential tool in modern society, especially in navigation systems such as GPS, the Global Navigation Satellite System, Galileo, and Beidou.

Although the state-of-the-art technology in atomic clocks already has the lowest inaccuracy by far of any physical unit, optical clocks, which use optical rather than microwave transitions, are being developed in laboratories worldwide

and are at the forefront of frequency metrology. They outperform microwave clocks' instability and inaccuracy by 2 orders of magnitude, prompting discussion concerning a redefinition of the SI second (27th CGPM, 2022). The noteworthy performance of optical atomic clocks paves the way for their applications in fields other than metrology. They cover the fields of time and frequency metrology [comparison of distant clocks (Takano *et al.*, 2016)], quantum communications [synchronization of quantum phases for wide areas (Lucamarini *et al.*, 2018)], geophysics [mapping of the gravitational potential of Earth (Mehlstäubler *et al.*, 2018)], and potential applications in fundamental physics [tests of general relativity and its foundations (Chou *et al.*, 2010; Kolkowitz *et al.*, 2016)].

With the rapidly improving performance of optical clocks, it is possible to take full advantage of it simply by operating the clocks in space (Riehle, 2017; Origlia *et al.*, 2018) since the frequency of the clocks on Earth is influenced by Earth's gravitational potential at the location of the clock, which may cause a drift in time from tidal effects or another cause. Therefore, the standard ultrahigh-precision optical frequency system for space platforms is the key to achieving more precise time reference and ultrahigh-precision time synchronization, which provides support for state-of-art technologies and basic scientific research. At present, a research trend in optical frequency standards is to develop neutral-atom optical clocks for space platforms, and several optical clock plans for low-orbit space platforms have been established. However, optical clocks in the low-orbit space platform are affected by the uneven distribution of Earth's surface and geological activities, which can impede the space optical frequency standard from reaching ultrahigh precision and accuracy (below  $10^{-19}$ ). To develop an ultrahigh-precision optical frequency standard with a stability of  $10^{-21}$  or better, an optical clock plan for high-orbit platforms is desired.

Utilizing a future high-orbit satellite, it will be possible to develop an optical clock to promote the stability to the  $10^{-21}$  level or even better to achieve ultrahigh-precision optical frequency standards, and to establish a new global time reference. Such optical clocks meet ultrahigh-precision time synchronization requirements for wide-area quantum communication. Furthermore, multiple space-based ultrahigh-precision optical clocks are promising devices for detecting gravitational waves and dark matter, which particularly complement existing gravitational-wave-detection techniques by providing efficient detection in the 1–10 Hz frequency band (Kolkowitz *et al.*, 2016).

The work covered in this review represents only the dawn of an emerging field of quantum experiments at space scale. We expect to see in the future both practical applications, such as global-scale quantum communications, and stimulating fundamental research that has otherwise been impossible to conduct on Earth.

#### ACKNOWLEDGMENTS

We thank Xiao-Hui Bao, Han-Ning Dai, Yingqiu Mao, Qi Shen, Ping Xu, and Juan Yin for their helpful discussions and generous assistance. This work is supported by the National

Key R&D Program of China (Grant No. 2017YFA0303900), the National Natural Science Foundation of China (Grants No. U1738201, No. U1738202, No. U1738203, and No. U1738204), the Anhui Initiative in Quantum Information Technologies, and the Chinese Academy of Science.

#### REFERENCES

- Afzelius, M., N. Gisin, and H. de Riedmatten, 2015, "Quantum memory for photons," *Phys. Today* **68**, No. 12, 42–47.
- Andrews, Larry C., and Ronald L. Phillips, 2005, *Laser Beam Propagation through Random Media* (SPIE—International Society for Optical Engineering, Bellingham, WA).
- Armano, M., *et al.*, 2016, "Sub-Femto-*g* Free Fall for Space-Based Gravitational Wave Observatories: LISA Pathfinder Results," *Phys. Rev. Lett.* **116**, 231101.
- Aspect, Alain, Philippe Grangier, and Gérard Roger, 1982, "Experimental Realization of Einstein-Podolsky-Rosen-Bohm Gedankenexperiment: A New Violation of Bell's Inequalities," *Phys. Rev. Lett.* **49**, 91–94.
- Aspelmeyer, M., T. Jennewein, M. Pfennigbauer, W. R. Leeb, and A. Zeilinger, 2003, "Long-distance quantum communication with entangled photons using satellites," *IEEE J. Sel. Top. Quantum Electron.* **9**, 1541–1551.
- Aspelmeyer, M., *et al.*, 2003, "Long-distance free-space distribution of quantum entanglement," *Science* **301**, 621.
- Atatüre, M., D. Englund, N. Vamivakas, S. Y. Lee, and J. Wrachrup, 2018, "Material platforms for spin-based photonic quantum technologies," *Nat. Rev. Mater.* **3**, 38.
- Azuma, Koji, Kiyoshi Tamaki, and Hoi-Kwong Lo, 2015, "All-photonic quantum repeaters," *Nat. Commun.* **6**, 6787.
- Bao, X.-H, A. Reingruber, P. Dietrich, J. Rui, A. Dück, T. Strassel, L. Li, N.-L. Liu, B. Zhao, and J.-W. Pan, 2012, "Efficient and long-lived quantum memory with cold atoms inside a ring cavity," *Nat. Phys.* **8**, 517–521.
- Barrett, M. D., *et al.*, 2004, "Deterministic quantum teleportation of atomic qubits," *Nature (London)* **429**, 737.
- Becker, Dennis, *et al.*, 2018, "Space-borne Bose-Einstein condensation for precision interferometry," *Nature (London)* **562**, 391–395.
- Bedington, Robert, Juan Miguel Arrazola, and Alexander Ling, 2017, "Progress in satellite quantum key distribution," *npj Quantum Inf.* **3**, 30.
- Bell, J., 2004, *Speakable and Unspeakable in Quantum Mechanics* (Cambridge University Press, Cambridge, England).
- Bell, J. S., 1964, "On the Einstein-Podolsky-Rosen paradox," *Physics* **1**, 195.
- Bennett, C. H., 1992, "Quantum Cryptography Using Any Two Nonorthogonal States," *Phys. Rev. Lett.* **68**, 3121.
- Bennett, C. H., F. Bessette, G. Brassard, L. Salvail, and J. Smolin, 1992, "Experimental quantum cryptography," *J. Cryptol.* **5**, 3–28.
- Bennett, C. H., and G. Brassard, 1984, "Quantum cryptography: Public key distribution and coin tossing," in *Proceedings of the IEEE International Conference on Computers, Systems, and Signal Processing, Bangalore, India, 1984*, edited by G. R. Blakley and D. Chaum (IEEE, New York), pp. 175–179.
- Bennett, C. H., G. Brassard, C. Crepeau, R. Jozsa, A. Peres, and W. K. Wootters, 1993, "Teleporting an Unknown Quantum State via Dual Classical and Einstein-Podolsky-Rosen Channels," *Phys. Rev. Lett.* **70**, 1895.
- Bennett, C. H., G. Brassard, and N. D. Mermin, 1992, "Quantum Cryptography without Bell's Theorem," *Phys. Rev. Lett.* **68**, 557–559.

- Bennett, C.H., G. Brassard, S. Popescu, B. Schumacher, J.A. Smolin, and W.K. Wootters, 1996, “Purification of Noisy Entanglement and Faithful Teleportation via Noisy Channels,” *Phys. Rev. Lett.* **76**, 722–725.
- BIG Bell Test Collaboration, 2018, “Challenging local realism with human choices,” *Nature (London)* **557**, 212.
- Boaron, A., *et al.*, 2018, “Secure Quantum Key Distribution over 421 km of Optical Fiber,” *Phys. Rev. Lett.* **121**, 190502.
- Bourgoin, J., *et al.*, 2013, “A comprehensive design and performance analysis of low Earth orbit satellite quantum communication,” *New J. Phys.* **15**, 023006.
- Bourgoin, Jean-Philippe, Brendon L. Higgins, Nikolay Gigov, Catherine Holloway, Christopher J. Pugh, Sarah Kaiser, Miles Cranmer, and Thomas Jennewein, 2015, “Free-space quantum key distribution to a moving receiver,” *Opt. Express* **23**, 33437–33447.
- Bouwmeester, D., J.-W. Pan, K. M., M. Eibl, H. Weinfurter, and A. Zeilinger, 1997, “Experimental quantum teleportation,” *Nature (London)* **390**, 575.
- Brassard, G., 2012, “Brief history of quantum cryptography: A personal perspective,” in *Proceedings of the IEEE Information Theory Workshop on Theory and Practice in Information-Theoretic Security (ICITS 2012), Montreal, 2012*, edited by A. Smith (IEEE, New York).
- Brassard, G., N. Lütkenhaus, T. Mor, and B. C. Sanders, 2000, “Limitations on Practical Quantum Cryptography,” *Phys. Rev. Lett.* **85**, 1330–1333.
- Briegel, H.-J., W. Dür, J. I. Cirac, and P. Zoller, 1998, “Quantum Repeaters: The Role of Imperfect Local Operations in Quantum Communication,” *Phys. Rev. Lett.* **81**, 5932–5935.
- Browne, Daniel E., and T. Rudolph, 2005, “Resource-Efficient Linear Optical Quantum Computation,” *Phys. Rev. Lett.* **95**, 010501.
- Brunner, Nicolas, Daniel Cavalcanti, Stefano Pironio, Valerio Scarani, and Stephanie Wehner, 2014, “Bell nonlocality,” *Rev. Mod. Phys.* **86**, 419–478.
- Bruß, Dagmar, 1998, “Optimal Eavesdropping in Quantum Cryptography with Six States,” *Phys. Rev. Lett.* **81**, 3018–3021.
- Bussi eres, F., *et al.*, 2014, “Quantum teleportation from a telecom-wavelength photon to a solid-state quantum memory,” *Nat. Photonics* **8**, 775–778.
- Buttler, W. T., R. J. Hughes, P. G. Kwiat, S. K. Lamoreaux, G. G. Luther, G. L. Morgan, J. E. Nordholt, C. G. Peterson, and C. M. Simmons, 1998, “Practical Free-Space Quantum Key Distribution over 1 km,” *Phys. Rev. Lett.* **81**, 3283–3286.
- Buttler, W. T., R. J. Hughes, P. G. Kwiat, G. G. Luther, G. L. Morgan, J. E. Nordholt, C. G. Peterson, and C. M. Simmons, 1998, “Free-space quantum-key distribution,” *Phys. Rev. A* **57**, 2379.
- Buttler, W. T., R. J. Hughes, S. K. Lamoreaux, G. L. Morgan, J. E. Nordholt, and C. G. Peterson, 2000, “Daylight Quantum Key Distribution over 1.6 km,” *Phys. Rev. Lett.* **84**, 5652–5655.
- Cacciapuoti, L., and Ch. Salomon, 2009, “Space clocks and fundamental tests: The aces experiment,” *Eur. Phys. J. Special Topics* **172**, 57–68.
- Cao, Y., *et al.*, 2013, “Entanglement-based quantum key distribution with biased basis choice via free space,” *Opt. Express* **21**, 27260–27268.
- Cao, Y., *et al.*, 2018, “Bell Test over Extremely High-Loss Channels: Towards Distributing Entangled Photon Pairs between Earth and the Moon,” *Phys. Rev. Lett.* **120**, 140405.
- Cao, Yuan, *et al.*, 2020, “Long-Distance Free-Space Measurement-Device-Independent Quantum Key Distribution,” *Phys. Rev. Lett.* **125**, 260503.
- Chen, Jiu-Peng, *et al.*, 2020, “Sending-or-Not-Sending with Independent Lasers: Secure Twin-Field Quantum Key Distribution over 509 km,” *Phys. Rev. Lett.* **124**, 070501.
- Chen, Y.-A., S. Chen, Z.-S. Yuan, B. Zhao, C.-S. Chuu, J. Schmiedmayer, and J.-W. Pan, 2008, “Memory-built-in quantum teleportation with photonic and atomic qubits,” *Nat. Phys.* **4**, 103–107.
- Chen, Yu-Ao, *et al.*, 2021, “An integrated space-to-ground quantum communication network over 4,600 kilometres,” *Nature (London)* **589**, 214–219.
- Chou, C. W., D. B. Hume, T. Rosenband, and D. J. Wineland, 2010, “Optical clocks and relativity,” *Science* **329**, 1630.
- Clauser, John F., Michael A. Horne, Abner Shimony, and Richard A. Holt, 1969, “Proposed Experiment to Test Local Hidden-Variable Theories,” *Phys. Rev. Lett.* **23**, 880–884.
- Colella, R., A. W. Overhauser, and S. A. Werner, 1975, “Observation of Gravitationally Induced Quantum Interference,” *Phys. Rev. Lett.* **34**, 1472–1474.
- Dai, Hui, *et al.*, 2020, “Towards satellite-based quantum-secure time transfer,” *Nat. Phys.* **16**, 848–852.
- Dequal, D., G. Vallone, D. Bacco, S. Gaiarin, V. Luceri, G. Bianco, and P. Villoresi, 2016, “Experimental single-photon exchange along a space link of 7000 km,” *Phys. Rev. A* **93**, 010301.
- Derevianko, A., and M. Pospelov, 2014, “Hunting for topological dark matter with atomic clocks,” *Nat. Phys.* **10**, 933–936.
- de Riedmatten, H., I. Marcikic, W. Tittel, H. Zbinden, D. Collins, and N. Gisin, 2004, “Long Distance Quantum Teleportation in a Quantum Relay Configuration,” *Phys. Rev. Lett.* **92**, 047904.
- Deutsch, D., 1991, “Quantum mechanics near closed timelike lines,” *Phys. Rev. D* **44**, 3197.
- Ding, X., *et al.*, 2016, “On-Demand Single Photons with High Extraction Efficiency and Near-Unity Indistinguishability from a Resonantly Driven Quantum Dot in a Micropillar,” *Phys. Rev. Lett.* **116**, 020401.
- Dios, F., J. A. Rubio, A. Rodr guez, and A. Comer n, 2004, “Scintillation and beam-wander analysis in an optical ground station-satellite uplink,” *Appl. Opt.* **43**, 3866.
- Duan, L.-M., M. D. Lukin, J. I. Ciac, and P. Zoller, 2001, “Long-distance quantum communication with atomic ensembles and linear optics,” *Nature (London)* **414**, 413.
- Duan, L.-M., and C. Monroe, 2010, “Colloquium: Quantum networks with trapped ions,” *Rev. Mod. Phys.* **82**, 1209–1224.
- Einstein, A., B. Podolsky, and N. Rosen, 1935, “Can quantum-mechanical description of physical reality be considered complete?,” *Phys. Rev.* **47**, 777.
- Ekert, Artur K., 1991, “Quantum Cryptography Based on Bell’s Theorem,” *Phys. Rev. Lett.* **67**, 661–663.
- ESA, 2018a, “10 new business and research partners join QUARTZ,” <https://artes.esa.int/news/10-new-business-and-research-partners-join-quartz>.
- ESA, 2018b, “D/TIA partners with UK-based ArQit to develop first quantum encryption satellite,” <https://artes.esa.int/news/dtia-partners-ukbased-arqit-develop-first-quantum-encryption-satellite>.
- Ethan, R. Elliott, Markus C. Krutzik, Jason R. Williams, Robert J. Thompson, and David C. Aveline, 2018, “NASA’s Cold Atom Lab (CAL): System development and ground test status,” *npj Microgravity* **4**, 16.
-  tienne, S., J. Weick, P. Vrancken, F. Para, D. Albanese, J. Paris, J. M. Torre, C. Zhao, P. Guillemot, and I. Petitbon, 2008, “Time transfer by laser link—The T2L2 experiment on Jason-2 and further experiments,” *Int. J. Mod. Phys. D* **17**, 1043–1054.

- Fedrizzi, A., T. Herbst, A. Poppe, T. Jennewein, and A. Zeilinger, 2007, “A wavelength-tunable fiber-coupled source of narrowband entangled photons,” *Opt. Express* **15**, 15377–15386.
- Fedrizzi, A., R. Ursin, T. Herbst, M. Nespoli, R. Prevedel, T. Scheidl, F. Tiefenbacher, T. Jennewein, and A. Zeilinger, 2009, “High-fidelity transmission of entanglement over a high-loss free-space channel,” *Nat. Phys.* **5**, 389–392.
- Franson, J. D., and H. Ilves, 1994, “Quantum cryptography using optical fibers,” *Appl. Opt.* **33**, 2949.
- Freedman, Stuart J., and John F. Clauser, 1972, “Experimental Test of Local Hidden-Variable Theories,” *Phys. Rev. Lett.* **28**, 938–941.
- Friedman, J., Michael S. Morris, Igor D. Novikov, F. Echeverria, G. Klinkhammer, Kip S. Thorne, and U. Yurtsever, 1990, “Cauchy problem in spacetimes with closed timelike curves,” *Phys. Rev. D* **42**, 1915.
- Furusawa, A., J. L. Sørensen, S. L. Braunstein, C. A. Fuchs, H. J. Kimble, and E. S. Polzik, 1998, “Unconditional quantum teleportation,” *Science* **282**, 706.
- Gao, W. B., A. Imamoglu, H. Bernien, and R. Hanson, 2015, “Coherent manipulation, measurement and entanglement of individual solid-state spins using optical fields,” *Nat. Photonics* **9**, 363.
- Gasparoni, S., J.-W. Pan, P. Walther, T. Rudolph, and A. Zeilinger, 2004, “Realization of a Photonic Controlled-NOT Gate Sufficient for Quantum Computation,” *Phys. Rev. Lett.* **93**, 020504.
- Gill, P., 2011, “When should we change the definition of the second?,” *Phil. Trans. R. Soc. A* **369**, 4109.
- Gilmore, D. G., 2002, *Spacecraft Thermal Control Handbook, Vol. 1: Fundamental Technologies* (American Institute of Aeronautics and Astronautics, Reston, VA).
- Giorgetta, Fabrizio R., William C. Swann, Laura C. Sinclair, E. Baumann, I. Coddington, and Nathan R. Newbury, 2013, “Optical two-way time and frequency transfer over free space,” *Nat. Photonics* **7**, 434–438.
- Gisin, N., and R. Thew, 2010, “Quantum communication technology,” *Electron. Lett.* **46**, 965–967.
- Gisin, Nicolas, Grégoire Ribordy, Wolfgang Tittel, and Hugo Zbinden, 2002, “Quantum cryptography,” *Rev. Mod. Phys.* **74**, 145–195.
- Gong, Yun-Hong, *et al.*, 2018, “Free-space quantum key distribution in urban daylight with the SPGD algorithm control of a deformable mirror,” *Opt. Express* **26**, 18897–18905.
- Gottesman, D., and Isaac L. Chuang, 1999, “Demonstrating the viability of universal quantum computation using teleportation and single-qubit operations,” *Nature (London)* **402**, 390–393.
- Grieve, James A., Robert Bedington, Z. Tang, R. C. Chandrasekara, and A. Ling, 2018, “SpooQySats: CubeSats to demonstrate quantum key distribution technologies,” *Acta Astronaut.* **151**, 103.
- Gruneisen, Mark T., Michael B. Flanagan, and Brett A. Sickmiller, 2017, “Modeling satellite-Earth quantum channel downlinks with adaptive-optics coupling to single-mode fibers,” *Opt. Eng.* **56**, 126111.
- Gruneisen, Mark T., Michael B. Flanagan, Brett A. Sickmiller, James P. Black, Kurt E. Stoltenberg, and Alexander W. Duchane, 2015, “Modeling daytime sky access for a satellite quantum key distribution downlink,” *Opt. Express* **23**, 23924–23934.
- Gruneisen, Mark T., Brett A. Sickmiller, Michael B. Flanagan, James P. Black, Kurt E. Stoltenberg, and Alexander W. Duchane, 2016, “Adaptive spatial filtering of daytime sky noise in a satellite quantum key distribution downlink receiver,” *Opt. Eng.* **55**, 026104.
- Gruneisen, Mark T., *et al.*, 2021, “Adaptive-Optics-Enabled Quantum Communication: A Technique for Daytime Space-to-Earth Links,” *Phys. Rev. Applied* **16**, 014067.
- Günthner, K., *et al.*, 2017, “Quantum-limited measurements of optical signals from a geostationary satellite,” *Optica* **4**, 611–616.
- Hall, Michael J. W., 2010, “Local Deterministic Model of Singlet State Correlations Based on Relaxing Measurement Independence,” *Phys. Rev. Lett.* **105**, 250404.
- Hartle, James B., 1994, “Unitarity and causality in generalized quantum mechanics for nonchronal spacetimes,” *Phys. Rev. D* **49**, 6543.
- Hawking, Stephen W., 1995, “Quantum coherence and closed timelike curves,” *Phys. Rev. D* **52**, 5681.
- Hensen, B., *et al.*, 2015, “Loophole-free Bell inequality violation using electron spins separated by 1.3 kilometres,” *Nature (London)* **526**, 682.
- Höckel, D., L. Koch, E. Martin, and O. Benson, 2009, “Ultranarrow bandwidth spectral filtering for long-range free-space quantum key distribution at daytime,” *Opt. Lett.* **34**, 3169–3171.
- Horodecki, Ryszard, Paweł Horodecki, Michał Horodecki, and Karol Horodecki, 2009, “Quantum entanglement,” *Rev. Mod. Phys.* **81**, 865–942.
- Hughes, R. J., William T. Buttler, Paul G. Kwiat, Steve K. Lamoreaux, George L. Morgan, Jane E. Nordholt, and C. Glen Peterson, 2000, “Free-space quantum key distribution in daylight,” *J. Mod. Opt.* **47**, 549.
- Hughes, R. J., G. G. Luther, G. L. Morgan, and C. G. Peterson, 1996, “Quantum cryptography over underground optical fibers,” *Lect. Notes Comput. Sci.* **1109**, 329.
- Hughes, R. J., George L. Morgan, and C. Glen Peterson, 2000, “Quantum key distribution over a 48 km optical fibre network,” *J. Mod. Opt.* **47**, 533–547.
- Hughes, Richard J., Jane E. Nordholt, Derek Derkacs, and Charles G. Peterson, 2002, “Practical free-space quantum key distribution over 10 km in daylight and at night,” *New J. Phys.* **4**, 43.
- Hwang, W. Y., 2003, “Quantum Key Distribution with High Loss: Toward Global Secure Communication,” *Phys. Rev. Lett.* **91**, 057901.
- Inagaki, Takahiro, Nobuyuki Matsuda, Osamu Tadanaga, Masaki Asobe, and Hiroki Takesue, 2013, “Entanglement distribution over 300 km of fiber,” *Opt. Express* **21**, 23241–23249.
- Jacobs, B. C., and J. D. Franson, 1996, “Quantum cryptography in free space,” *Opt. Lett.* **21**, 1854.
- Jacobs, B. C., T. B. Pittman, and J. D. Franson, 2002, “Quantum relays and noise suppression using linear optics,” *Phys. Rev. A* **66**, 052307.
- Jennewein, T., J. P. Bourgoin, B. Higgins, C. Holloway, E. Meyer-Scott, C. Erven, B. Heim, Z. Yan, H. Hübel, and G. Weihs, 2014, “QEYSSat: A mission proposal for a quantum receiver in space,” in *Advances in Photonics of Quantum Computing, Memory, and Communication VII*, edited by Z. U. Hasan, P. R. Hemmer, H. Lee, and C. M. Santoria, SPIE Proceedings Vol. 8997 (SPIE—International Society for Optical Engineering, Bellingham, WA), p. 89970A.
- Jennewein, T., C. Simon, G. Weihs, H. Weinfurter, and A. Zeilinger, 2000, “Quantum Cryptography with Entangled Photons,” *Phys. Rev. Lett.* **84**, 4729–4732.
- Jin, X.-M., *et al.*, 2010, “Experimental free-space quantum teleportation,” *Nat. Photonics* **4**, 376–381.
- Joshi, S. K., *et al.* (Space QUEST Topical Team), 2018, “Space QUEST mission proposal: Experimentally testing decoherence due to gravity,” *New J. Phys.* **20**, 063016.
- Kent, Adrian, 2005, “Causal quantum theory and the collapse locality loophole,” *Phys. Rev. A* **72**, 012107.
- Kerstel, Erik, Arnaud Gardelein, Mathieu Barthelemy, Matthias Fink, K. Siddarth Joshi, and Rupert Ursin (CSUG Team), 2018,

- “Nanobob: A CubeSat mission concept for quantum communication experiments in an uplink configuration,” *EPJ Quantum Technol.* **5**, 6.
- Koashi, M., and J. Preskill, 2003, “Secure Quantum Key Distribution with an Uncharacterized Source,” *Phys. Rev. Lett.* **90**, 057902.
- Kolkowitz, S., I. Pikovski, N. Langellier, M. D. Lukin, R. L. Walsworth, and J. Ye, 2016, “Gravitational wave detection with optical lattice atomic clocks,” *Phys. Rev. D* **94**, 124043.
- Kómár, P., E. M. Kessler, M. Bishof, L. Jiang, A. S. Sørensen, J. Ye, and M. D. Lukin, 2014, “A quantum network of clocks,” *Nat. Phys.* **10**, 582–587.
- Kurtsiefer, C., P. Zarda, M. Halder, H. Weinfurter, P. M. Gorman, P. R. Tapster, and J. G. Rarity, 2002, “Quantum cryptography: A step towards global key distribution,” *Nature (London)* **419**, 450.
- Kwiat, P. G., K. Mattle, H. Weinfurter, A. Zeilinger, A. V. Sergienko, and Y. Shih, 1995, “New High-Intensity Source of Polarization-Entangled Photon Pairs,” *Phys. Rev. Lett.* **75**, 4337.
- Li, H.-W., *et al.*, 2011, “Attacking a practical quantum-key-distribution system with wavelength-dependent beam-splitter and multiwavelength sources,” *Phys. Rev. A* **84**, 062308.
- Liao, S.-K., *et al.*, 2017a, “Satellite-to-ground quantum key distribution,” *Nature (London)* **549**, 43.
- Liao, S.-K., *et al.*, 2017b, “Space-to-ground quantum key distribution using a small-sized payload on Tiangong-2 space lab,” *Chin. Phys. Lett.* **34**, 090302.
- Liao, S.-K., *et al.*, 2017c, “Long-distance free-space quantum key distribution in daylight towards inter-satellite communication,” *Nat. Photonics* **11**, 509.
- Liao, S.-K., *et al.*, 2018, “Satellite-Relayed Intercontinental Quantum Network,” *Phys. Rev. Lett.* **120**, 030501.
- Lim, Charles, Ci-Wen, Feihu Xu, Jian-Wei Pan, and Artur Ekert, 2021, “Security Analysis of Quantum Key Distribution with Small Block Length and Its Application to Quantum Space Communications,” *Phys. Rev. Lett.* **126**, 100501.
- Liu, Y., *et al.*, 2013, “Experimental Measurement-Device-Independent Quantum Key Distribution,” *Phys. Rev. Lett.* **111**, 130502.
- Lo, H.-K., and H. F. Chau, 1999, “Unconditional security of quantum key distribution over arbitrarily long distances,” *Science* **283**, 2050–2056.
- Lo, H.-K., M. Curty, and B. Qi, 2012, “Measurement-Device-Independent Quantum Key Distribution,” *Phys. Rev. Lett.* **108**, 130503.
- Lo, H.-K., X. Ma, and K. Chen, 2005, “Decoy State Quantum Key Distribution,” *Phys. Rev. Lett.* **94**, 230504.
- Lucamarini, M., Z. L. Yuan, J. F. Dynes, and A. J. Shields, 2018, “Overcoming the rate-distance limit of quantum key distribution without quantum repeaters,” *Nature (London)* **557**, 400.
- Ludlow, Andrew D., Martin M. Boyd, J. Ye, E. Peik, and P. O. Schmidt, 2015, “Optical atomic clocks,” *Rev. Mod. Phys.* **87**, 637–701.
- Luo, Y.-H., *et al.*, 2019, “Quantum Teleportation in High Dimensions,” *Phys. Rev. Lett.* **123**, 070505.
- Lütkenhaus, Norbert, 2000, “Security against individual attacks for realistic quantum key distribution,” *Phys. Rev. A* **61**, 052304.
- Lvovsky, A. I., B. C. Sanders, and W. Tittel, 2009, “Optical quantum memory,” *Nat. Photonics* **3**, 706–714.
- Lydersen, L., C. Wiechers, C. Wittmann, D. Elser, J. Skaar, and V. Makarov, 2010, “Hacking commercial quantum cryptography systems by tailored bright illumination,” *Nat. Photonics* **4**, 686–689.
- Ma, X., C.-H. F. Fung, and H.-K. Lo, 2007, “Quantum key distribution with entangled photon sources,” *Phys. Rev. A* **76**, 012307.
- Ma, X. S., *et al.*, 2012, “Quantum teleportation over 143 kilometres using active feed-forward,” *Nature (London)* **489**, 269.
- Makarov, V., 2009, “Controlling passively quenched single photon detectors by bright light,” *New J. Phys.* **11**, 065003.
- Marand, C., and P. D. Townsend, 1995, “Quantum key distribution over distances as long as 30 km,” *Opt. Lett.* **20**, 1695.
- Marcikic, I., H. De Riedmatten, W. Tittel, H. Zbinden, and N. Gisin, 2003, “Long-distance teleportation of qubits at telecommunication wavelengths,” *Nature (London)* **421**, 509.
- Marra, G., C. Clivati, R. Lucket, A. Tampellini, J. Kronjäger, L. Wright, A. Mura, F. Levi, S. Robinson, and A. Xuereb, 2018, “Ultrastable laser interferometry for earthquake detection with terrestrial and submarine cables,” *Science* **361**, 486–490.
- Maunz, P., D. L. Moehring, S. Olmschenk, K. C. Younge, D. N. Matsukevich, and C. Monroe, 2007, “Quantum interference of photon pairs from two remote trapped atomic ions,” *Nat. Phys.* **3**, 538–541.
- Mayers, D., 2001, “Unconditional security in quantum cryptography,” *J. ACM* **48**, 351–406.
- Mehlstäubler, Tanja E., G. Grosche, C. Lisdat, P. Schmidt, and H. Denker, 2018, “Atomic clocks for geodesy,” *Rep. Prog. Phys.* **81**, 064401.
- Mills, D. L., 1991, “Internet time synchronization: The network time protocol,” *IEEE Trans. Commun.* **39**, 1482–1493.
- Morris, Michael S., and Kip S. Thorne, 1988, “Wormholes in spacetime and their use for interstellar travel: A tool for teaching general relativity,” *Am. J. Phys.* **56**, 395–412.
- Muller, A., J. Breguet, and N. Gisin, 1993, “Experimental demonstration of quantum cryptography using polarized photons in optical fibre over more than 1 km,” *Europhys. Lett.* **23**, 383.
- Muller, A., H. Zbinden, and N. Gisin, 1996, “Quantum cryptography over 23 km in installed under-lake telecom fibre,” *Europhys. Lett.* **33**, 335.
- Müller, J., M. Soffel, and Sergei A. Klioner, 2008, “Geodesy and relativity,” *J. Geod.* **82**, 133–145.
- Muralidharan, Sreraman, Jungsang Kim, Norbert Lütkenhaus, Mikhail D. Lukin, and Liang Jiang, 2014, “Ultrafast and Fault-Tolerant Quantum Communication across Long Distances,” *Phys. Rev. Lett.* **112**, 250501.
- Naik, D. S., C. G. Peterson, A. G. White, A. J. Berglund, and P. G. Kwiat, 2000, “Entangled State Quantum Cryptography: Eavesdropping on the Ekert Protocol,” *Phys. Rev. Lett.* **84**, 4733–4736.
- Nauerth, S., F. Moll, M. Rau, C. Fuchs, J. Horwath, S. Frick, and H. Weinfurter, 2013, “Air-to-ground quantum communication,” *Nat. Photonics* **7**, 382.
- Nielsen, M. A., E. Knill, and R. Laflamme, 1998, “Complete quantum teleportation using nuclear magnetic resonance,” *Nature (London)* **396**, 52.
- Oberhaus, Daniel, 2020, “NASA’s plan to turn the ISS into a quantum laser lab,” <https://www.wired.com/story/nasas-plan-to-turn-the-iss-into-a-quantum-laser-lab/>.
- O’Brien, J. L., G. J. Pryde, A. G. White, T. C. Ralph, and D. Branning, 2003, “Demonstration of an all-optical quantum controlled-NOT gate,” *Nature (London)* **426**, 264.
- Oi, D. K., A. Ling, G. Vallone, P. Villoresi, S. Greenland, E. Kerr, M. Macdonald, H. Weinfurter, H. Kuiper, and E. Charbon, 2017, “CubeSat quantum communications mission,” *EPJ Quantum Technol.* **4**, 6.

- Olmschenk, S., D. N. Matsukevich, P. Maunz, D. Hayes, L.-M. Duan, and C. Monroe, 2009, “Quantum teleportation between distant matter qubits,” *Science* **323**, 486–489.
- Origlia, S., *et al.*, 2018, “Towards an optical clock for space: Compact, high-performance optical lattice clock based on bosonic atoms,” *Phys. Rev. A* **98**, 053443.
- Pan, J.-W., D. Bouwmeester, M. Daniell, H. Weinfurter, and A. Zeilinger, 2000, “Experimental test of quantum nonlocality in three-photon Greenberger-Horne-Zeilinger entanglement,” *Nature (London)* **403**, 515–519.
- Pan, J.-W., D. Bouwmeester, H. Weinfurter, and A. Zeilinger, 1998, “Experimental Entanglement Swapping: Entangling Photons That Never Interacted,” *Phys. Rev. Lett.* **80**, 3891–3894.
- Pan, J.-W., Z.-B. Chen, C.-Y. Lu, H. Weinfurter, A. Zeilinger, and M. Żukowski, 2012, “Multiphoton entanglement and interferometry,” *Rev. Mod. Phys.* **84**, 777–838.
- Pan, J.-W., S. Gasparoni, M. Aspelmeyer, T. Jennewein, and A. Zeilinger, 2003, “Experimental realization of freely propagating teleported qubits,” *Nature (London)* **421**, 721.
- Pan, J.-W., S. Gasparoni, R. Ursin, G. Weihs, and A. Zeilinger, 2003, “Experimental entanglement purification of arbitrary unknown states,” *Nature (London)* **423**, 417.
- Pan, J.-W., C. Simon, Č. Brukner, and A. Zeilinger, 2001, “Entanglement purification for quantum communication,” *Nature (London)* **410**, 1067.
- Peloso, M. P., I. Gerhardt, C. Ho, A. Lamas-Linares, and C. Kurtsiefer, 2009, “Daylight operation of a free space, entanglement-based quantum key distribution system,” *New J. Phys.* **11**, 045007.
- Peng, C.-Z., J. Zhang, D. Yang, W.-Bo. Gao, H.-X. Ma, H. Yin, H.-P. Zeng, T. Yang, X.-B. Wang, and J.-W. Pan, 2007, “Experimental Long-Distance Decoy-State Quantum Key Distribution Based on Polarization Encoding,” *Phys. Rev. Lett.* **98**, 010505.
- Peng, C.-Z., *et al.*, 2005, “Experimental Free-Space Distribution of Entangled Photon Pairs over 13 km: Towards Satellite-Based Global Quantum Communication,” *Phys. Rev. Lett.* **94**, 150501.
- Peters, A., K. Y. Chung, and S. Chu, 1999, “Measurement of gravitational acceleration by dropping atoms,” *Nature (London)* **400**, 849–852.
- Pfaff, W., *et al.*, 2014, “Unconditional quantum teleportation between distant solid-state quantum bits,” *Science* **345**, 532–535.
- Pirandola, J., J. Eisert, C. Weedbrook, A. Furusawa, and S. L. Braunstein, 2015, “Advances in quantum teleportation,” *Nat. Photonics* **9**, 641.
- Pirandola, S., *et al.*, 2019, “Advances in quantum cryptography,” [arXiv:1906.01645](https://arxiv.org/abs/1906.01645).
- Poe, Edgar Alan, 1841, “A few words on secret writing,” *Graham’s Mag.* **19**, 33–38.
- Politzer, H. David, 1992, “Simple quantum systems in spacetimes with closed timelike curves,” *Phys. Rev. D* **46**, 4470.
- Poppe, A., *et al.*, 2004, “Practical quantum key distribution with polarization entangled photons,” *Opt. Express* **12**, 3865–3871.
- Pratt, S. R., R. A. Raines, C. E. Fossa, and M. A. Temple, 1999, “An operational and performance overview of the iridium low Earth orbit satellite system,” *IEEE Commun. Surv. Tutor.* **2**, 2–10.
- Predehl, K., G. Grosche, S. M. Raupach, S. Droste, O. Terra, J. Alnis, T. Legero, T. W. Hänsch, T. Udem, and R. Holzwarth, 2012, “A 920-kilometer optical fiber link for frequency metrology at the 19th decimal place,” *Science* **336**, 441.
- Pugh, Christopher J., *et al.*, 2017, “Airborne demonstration of a quantum key distribution receiver payload,” *Quantum Sci. Technol.* **2**, 024009.
- Ralph, Timothy C., Gerard J. Milburn, and T. Downes, 2009, “Quantum connectivity of space-time and gravitationally induced decorrelation of entanglement,” *Phys. Rev. A* **79**, 022121.
- Rarity, J. G., P. R. Tapster, P. M. Gorman, and P. Knight, 2002, “Ground to satellite secure key exchange using quantum cryptography,” *New J. Phys.* **4**, 82.
- Reichle, R., D. Leibfried, E. Knill, J. Britton, R. B. Blakestad, J. D. Jost, C. Langer, R. Ozeri, S. Seidelin, and D. J. Wineland, 2006, “Experimental purification of two-atom entanglement,” *Nature (London)* **443**, 838–841.
- Reiserer, Andreas, and Gerhard Rempe, 2015, “Cavity-based quantum networks with single atoms and optical photons,” *Rev. Mod. Phys.* **87**, 1379–1418.
- Ren, J.-G., *et al.*, 2017, “Ground-to-satellite quantum teleportation,” *Nature (London)* **549**, 70.
- Ren, Ji-Gang, *et al.*, 2022, “Portable ground stations based space-to-ground quantum key distribution,” [arXiv:2205.13828](https://arxiv.org/abs/2205.13828).
- Resch, K. J., *et al.*, 2005, “Distributing entanglement and single photons through an intra-city, free-space quantum channel,” *Opt. Express* **13**, 202.
- Restelli, A., J. C. Bienfang, C. W. Clark, I. Rech, I. Labanca, M. Ghioni, and S. Cova, 2010, “Improved timing resolution single-photon detectors in daytime free-space quantum key distribution with 1.25 GHz transmission rate,” *IEEE J. Sel. Top. Quantum Electron.* **16**, 1084–1090.
- Ribordy, G., J. Brendel, J.-D. Gautier, N. Gisin, and H. Zbinden, 2000, “Long-distance entanglement-based quantum key distribution,” *Phys. Rev. A* **63**, 012309.
- Rideout, D., T. Jennewein, G. Amelino-Camelia, Tommaso F. Demarie, Brendon L. Higgins, A. Kempf, A. Kent, R. Laflamme, X. Ma, and Robert B. Mann, 2012, “Fundamental quantum optics experiments conceivable with satellites-reaching relativistic distances and velocities,” *Classical Quantum Gravity* **29**, 224011.
- Riebe, M., *et al.*, 2004, “Deterministic quantum teleportation with atoms,” *Nature (London)* **429**, 734–737.
- Riehle, F., 2017, “Optical clock networks,” *Nat. Photonics* **11**, 25–31.
- Rogers, D. J., J. C. Bienfang, A. Mink, B. J. Hershman, and Charles W. Clark, 2006, “Free-space quantum cryptography in the H-alpha Fraunhofer window,” *Proc. SPIE Int. Soc. Opt. Eng.* **6304**, 630417.
- Rosenberg, D., Jim W. Harrington, P. R. Rice, P. A. Hiskett, C. G. Peterson, R. J. Hughes, A. E. Lita, S. W. Nam, and J. E. Nordholt, 2007, “Long-Distance Decoy-State Quantum Key Distribution in Optical Fiber,” *Phys. Rev. Lett.* **98**, 010503.
- Rozpedek, Filip, Raja Yehia, Kenneth Goodenough, Maximilian Ruf, Peter C. Humphreys, Ronald Hanson, Stephanie Wehner, and David Elkouss, 2019, “Near-term quantum-repeater experiments with nitrogen-vacancy centers: Overcoming the limitations of direct transmission,” *Phys. Rev. A* **99**, 052330.
- Rubenok, A., J. A. Slater, P. Chan, I. Lucio-Martinez, and W. Tittel, 2013, “Real-World Two-Photon Interference and Proof-of-Principle Quantum Key Distribution Immune to Detector Attacks,” *Phys. Rev. Lett.* **111**, 130501.
- Sajeed, S., P. Chaiwongkhot, J.-P. Bourgoin, T. Jennewein, N. Lütkenhaus, and V. Makarov, 2015, “Security loophole in free-space quantum key distribution due to spatial-mode detector-efficiency mismatch,” *Phys. Rev. A* **91**, 062301.
- Sangouard, N., C. Simon, H. de Riedmatten, and N. Gisin, 2011, “Quantum repeaters based on atomic ensembles and linear optics,” *Rev. Mod. Phys.* **83**, 33–80.
- Schiller, S., G. M. Tino, P. Gill, C. Salomon, U. Sterr, E. Peik, A. Nevsky, A. Görlitz, D. Svehla, and G. Ferrari, 2009, “Einstein Gravity Explorer—A medium-class fundamental physics mission,” *Exp. Astron.* **23**, 573–610.

- Schmitt-Manderbach, T., *et al.*, 2007, “Experimental Demonstration of Free-Space Decoy-State Quantum Key Distribution over 144 km,” *Phys. Rev. Lett.* **98**, 010504.
- Schrödinger, E., 1935, “The present situation in quantum mechanics,” *Naturwissenschaften* **23**, 807–812.
- Scudo, Petra F., and Adam M. Lewis, 2021, “Quantum communications infrastructure architecture: Theoretical background, network structure and technologies. A review of recent studies from a European public infrastructure perspective,” [arXiv:2110.06762](https://arxiv.org/abs/2110.06762).
- Shan, X., X. Sun, J. Luo, T. Zheng, and M. Zhan, 2006, “Free-space quantum key distribution with Rb vapor filters,” *Appl. Phys. Lett.* **89**, 191121.
- Shannon, C. E., 1949, “Communication theory of secrecy systems,” *Bell Syst. Tech. J.* **28**, 656–715.
- Shen, Qi, *et al.*, 2021, “Experimental simulation of time and frequency transfer via an optical satellite–ground link at 10–18 instability,” *Optica* **8**, 471–476.
- Sherson, Jacob F., H. Krauter, Rasmus K. Olsson, B. Julsgaard, K. Hammerer, I. Cirac, and Eugene S. Polzik, 2006, “Quantum teleportation between light and matter,” *Nature (London)* **443**, 557–560.
- Shor, Peter W., and J. Preskill, 2000, “Simple Proof of Security of the BB84 Quantum Key Distribution Protocol,” *Phys. Rev. Lett.* **85**, 441–444.
- Simon, C., *et al.*, 2010, “Quantum memories,” *Eur. Phys. J. D* **58**, 1–22.
- Simon, Christoph, and William T. M. Irvine, 2003, “Robust Long-Distance Entanglement and a Loophole-Free Bell Test with Ions and Photons,” *Phys. Rev. Lett.* **91**, 110405.
- Sinclair, Laura, C., H. Bergeron, William C. Swann, E. Baumann, J.-D. Deschênes, and Nathan R. Newbury, 2018, “Comparing Optical Oscillators across the Air to Milliradians in Phase and  $10^{-17}$  in Frequency,” *Phys. Rev. Lett.* **120**, 050801.
- Singh, Manish Kumar, Liang Jiang, David D. Awschalom, and Supratik Guha, 2021, “Key device and materials specifications for a repeater enabled quantum internet,” *IEEE Trans. Quantum Eng.* **2**, 1–9.
- Smith, David E., Maria T. Zuber, X. Sun, Gregory A. Neumann, John F. Cavanaugh, Jan F. McGarry, and Thomas W. Zagwodzki, 2006, “Two-way laser link over interplanetary distance,” *Science* **311**, 53–53.
- Steffen, L., Y. Salathe, M. Oppliger, P. Kurpiers, M. Baur, C. Lang, C. Eichler, G. Puebla-Hellmann, A. Fedorov, and A. Wallraff, 2013, “Deterministic quantum teleportation with feed-forward in a solid state system,” *Nature (London)* **500**, 319–322.
- Stutzman, W. L., and G. A. Thiele, 2012, *Antenna Theory and Design* (John Wiley & Sons, New York).
- Sun, Q.-C., *et al.*, 2017, “Entanglement swapping with independent sources over an optical-fiber network,” *Phys. Rev. A* **95**, 032306.
- Takano, T., M. Takamoto, I. Ushijima, N. Ohmae, T. Akatsuka, A. Yamaguchi, Y. Kuroishi, H. Munekane, B. Miyahara, and H. Katori, 2016, “Geopotential measurements with synchronously linked optical lattice clocks,” *Nat. Photonics* **10**, 662.
- Takeda, S., T. Mizuta, M. Fuwa, P. van Loock, and A. Furusawa, 2013, “Deterministic quantum teleportation of photonic quantum bits by a hybrid technique,” *Nature (London)* **500**, 315–318.
- Takenaka, H., A. Carrascosado, M. Fujiwara, M. Kitamura, M. Sasaki, and M. Toyoshima, 2017, “Satellite-to-ground quantum-limited communication using a 50-kg-class microsatellite,” *Nat. Photonics* **11**, 502–508.
- Tang, Y.-L., *et al.*, 2014, “Measurement-Device-Independent Quantum Key Distribution over 200 km,” *Phys. Rev. Lett.* **113**, 190501.
- Tang, Z., R. Chandrasekara, C. T. Yue, C. Cheng, K. Durak, and A. Ling, 2016, “The photon pair source that survived a rocket explosion,” *Sci. Rep.* **6**, 25603.
- Tang, Zhongkan, Rakhitha Chandrasekara, Yue Chuan Tan, Cliff Cheng, Kadir Dural, and Alexander Ling, 2016, “The photon pair source that survived a rocket explosion,” *Sci. Rep.* **6**, 25603.
- Tino, Guglielmo M., *et al.*, 2019, “SAGE: A proposal for a space atomic gravity explorer,” *Eur. Phys. J. D* **73**, 228.
- Tittel, W., M. Afzelius, T. Chaneliere, Rufus L. Cone, and M. Sellars, 2010, “Photon-echo quantum memory in solid state systems,” *Laser Photonics Rev.* **4**, 244–267.
- Tittel, W., J. Brendel, H. Zbinden, and N. Gisin, 2000, “Quantum Cryptography Using Entangled Photons in Energy-Time Bell States,” *Phys. Rev. Lett.* **84**, 4737–4740.
- Togan, E., Y. Chu, A. Imamoglu, and M. D. Lukin, 2011, “Laser cooling and real-time measurement of the nuclear spin environment of a solid-state qubit,” *Nature (London)* **478**, 497–501.
- Townsend, Paul D., 1994, “Secure key distribution system based on quantum cryptography,” *Electron. Lett.* **30**, 809.
- Townsend, Paul D., J. G. Rarity, and P. R. Tapster, 1993a, “Enhanced single photon fringe visibility in a 10 km long prototype quantum cryptography channel,” *Electron. Lett.* **29**, 1291.
- Townsend, Paul D., J. G. Rarity, and P. R. Tapster, 1993b, “Single photon interference in 10 km long optical fibre interferometer,” *Electron. Lett.* **29**, 634.
- Toyoshima, M., and K. Araki, 1998, “Far-field pattern measurement of an onboard laser transmitter by use of a space-to-ground optical link,” *Appl. Opt.* **37**, 1720.
- Treytl, A., G. Gaderer, B. Hirschler, and R. Cohen, 2007, “Traps and pitfalls in secure clock synchronization,” in *Proceedings of the IEEE International Symposium on Precision Clock Synchronization for Measurement, Vienna, 2007*, edited by D. Latremouille, K. Harper, and R. Subrahmanyam (IEEE, New York).
- Ursin, R., T. Jennewein, M. Aspelmeyer, R. Kaltenbaek, M. Lindenthal, P. Walther, and A. Zeilinger, 2004, “Communications: Quantum teleportation across the Danube,” *Nature (London)* **430**, 849.
- Ursin, R., *et al.*, 2007, “Entanglement-based quantum communication over 144 km,” *Nat. Phys.* **3**, 481.
- Vallone, G., D. Bacco, D. Dequal, S. Gaiarin, V. Luceri, G. Bianco, and P. Villoresi, 2015, “Experimental Satellite Quantum Communications,” *Phys. Rev. Lett.* **115**, 040502.
- Vasylyev, D., A. A. Semenov, and W. Vogel, 2016, “Atmospheric Quantum Channels with Weak and Strong Turbulence,” *Phys. Rev. Lett.* **117**, 090501.
- Vedovato, F., C. Agnesi, M. Schiavon, D. Dequal, L. Calderaro, M. Tomasin, Davide G. Marangon, A. Stanco, V. Luceri, and G. Bianco, 2017, “Extending Wheeler’s delayed-choice experiment to space,” *Sci. Adv.* **3**, e1701180.
- Villar, Aitor, *et al.*, 2020, “Entanglement demonstration on board a nano-satellite,” *Optica* **7**, 734–737.
- Villoresi, P., *et al.*, 2008, “Experimental verification of the feasibility of a quantum channel between space and Earth,” *New J. Phys.* **10**, 033038.
- Waks, E., A. Zeevi, and Y. Yamamoto, 2002, “Security of quantum key distribution with entangled photons against individual attacks,” *Phys. Rev. A* **65**, 052310.
- Walther, P., M. Aspelmeyer, Kevin J. Resch, and A. Zeilinger, 2005, “Experimental Violation of a Cluster State Bell Inequality,” *Phys. Rev. Lett.* **95**, 020403.
- Wang, H., *et al.*, 2019a, “Towards optimal single-photon sources from polarized microcavities,” *Nat. Photonics*, **13**, 770–775.

- Wang, H., *et al.*, 2019b, “On-Demand Semiconductor Source of Entangled Photons Which Simultaneously Has High Fidelity, Efficiency, and Indistinguishability,” *Phys. Rev. Lett.* **122**, 113602.
- Wang, J.-Y., *et al.*, 2013, “Direct and full-scale experimental verifications towards ground-satellite quantum key distribution,” *Nat. Photonics* **7**, 387.
- Wang, X.-L., X.-D. Cai, Z.-E. Su, M.-C. Chen, D. Wu, L. Li, N.-L. Liu, C.-Y. Lu, and J.-W. Pan, 2015, “Quantum teleportation of multiple degrees of freedom of a single photon,” *Nature (London)* **518**, 516.
- Wang, X.-B., 2005, “Beating the Photon-Number-Splitting Attack in Practical Quantum Cryptography,” *Phys. Rev. Lett.* **94**, 230503.
- Weier, H., H. Krauss, M. Rau, M. Fürst, S. Nauerth, and H. Weinfurter, 2011, “Quantum eavesdropping without interception: An attack exploiting the dead time of single-photon detectors,” *New J. Phys.* **13**, 073024.
- Wootters, W. K., and W. H. Zurek, 1982, “A single quantum cannot be cloned,” *Nature (London)* **299**, 802.
- Wu, C. S., and I. Shakhov, 1950, “The angular correlation of scattered annihilation radiation,” *Phys. Rev.* **77**, 136–136.
- Wu, Yufeng, Jianlong Liu, and Christoph Simon, 2020, “Near-term performance of quantum repeaters with imperfect ensemble-based quantum memories,” *Phys. Rev. A* **101**, 042301.
- Xu, Feihu, Xiongfeng Ma, Qiang Zhang, Hoi-Kwong Lo, and Jian-Wei Pan, 2020, “Secure quantum key distribution with realistic devices,” *Rev. Mod. Phys.* **92**, 025002.
- Xu, P., *et al.*, 2019, “Satellite testing of a gravitationally induced quantum decoherence model,” *Science* **366**, 132–135.
- Yang, Kui-Xing, Maimaiti Abulizi, Yu-huai Li, Bo-Yang Zhang, Shuang-Lin Li, Wei-yue Liu, Juan Yin, Yuan Cao, Ji-gang Ren, and Cheng-zhi Peng, 2020, “Single-mode fiber coupling with a M-SPGD algorithm for long-range quantum communications,” *Opt. Express* **28**, 36600–36610.
- Yang, M., *et al.*, 2019, “Spaceborne low-noise single-photon detection for satellite-based quantum communications,” *arXiv:1910.08161*.
- Yang, S. J., X.-J. Wang, X.-H. Bao, and J.-W. Pan, 2016, “An efficient quantum light-matter interface with sub-second lifetime,” *Nat. Photonics* **10**, 381.
- Yao, X. C., *et al.*, 2012, “Experimental demonstration of topological error correction,” *Nature (London)* **482**, 489–494.
- Yin, H.-L., *et al.*, 2016, “Measurement-Device-Independent Quantum Key Distribution over a 404 km Optical Fiber,” *Phys. Rev. Lett.* **117**, 190501.
- Yin, J., *et al.*, 2012, “Quantum teleportation and entanglement distribution over 100-kilometre free-space channels,” *Nature (London)* **488**, 185.
- Yin, J., *et al.*, 2013, “Experimental quasi-single-photon transmission from satellite to Earth,” *Opt. Express* **21**, 20032–20040.
- Yin, J., *et al.*, 2017a, “Satellite-based entanglement distribution over 1200 kilometers,” *Science* **356**, 1140.
- Yin, J., *et al.*, 2017b, “Satellite-to-Ground Entanglement-Based Quantum Key Distribution,” *Phys. Rev. Lett.* **119**, 200501.
- Yin, Juan, *et al.*, 2020, “Entanglement-based secure quantum cryptography over 1,120 kilometres,” *Nature (London)* **582**, 501–505.
- Yu, Y., *et al.*, 2019, “Entanglement of two quantum memories via metropolitan-scale fibers,” *arXiv:1903.11284v1*.
- Yuan, Z.-S., Y.-A. Chen, B. Zhao, S. Chen, J. Schmiedmayer, and J.-W. Pan, 2008, “Experimental demonstration of a BDCZ quantum repeater node,” *Nature (London)* **454**, 1098.
- Zhang, Q., A. Goebel, C. Wagenknecht, Y.-A. Chen, B. Zhao, T. Yang, A. Mair, J. Schmiedmayer, and J.-W. Pan, 2006, “Experimental quantum teleportation of a two-qubit composite system,” *Nat. Phys.* **2**, 678–682.
- Zhao, B., Y.-A. Chen, X.-H. Bao, T. Strassel, C.-S. Chuu, X.-M. Jin, J. Schmiedmayer, Z.-S. Yuan, S. Chen, and J.-W. Pan, 2009, “A millisecond quantum memory for scalable quantum networks,” *Nat. Phys.* **5**, 95–99.
- Zhao, Y., C.-H. Fred Fung, B. Qi, C. Chen, and H.-K. Lo, 2008, “Experimental demonstration of time-shift attack against practical quantum key distribution systems,” *Phys. Rev. A* **78**, 042333.
- Zhao, Z., A.-N. Zhang, Y.-A. Chen, H. Zhang, J.-F. Du, T. Yang, and J.-W. Pan, 2005, “Experimental Demonstration of a Nondestructive Controlled-NOT Quantum Gate for Two Independent Photon Qubits,” *Phys. Rev. Lett.* **94**, 030501.
- Zhong, H.-S., *et al.*, 2018, “12-Photon Entanglement and Scalable Scattershot Boson Sampling with Optimal Entangled-Photon Pairs from Parametric Down-Conversion,” *Phys. Rev. Lett.* **121**, 250505.
- Żukowski, M., Zeilinger, A., M. A. Horne, and A. K. Ekert, 1993, “‘Event-Ready-Detectors’ Bell Experiment via Entanglement Swapping,” *Phys. Rev. Lett.* **71**, 4287–4290.
- Zych, M., F. Costa, I. Pikovski, and B. Časlav, 2011, “Quantum interferometric visibility as a witness of general relativistic proper time,” *Nat. Commun.* **2**, 505.
- Zych, M., F. Costa, I. Pikovski, Timothy C. Ralph, and B. Časlav, 2012, “General relativistic effects in quantum interference of photons,” *Classical Quantum Gravity* **29**, 224010.